



THÈSE

PRÉSENTÉE A

L'UNIVERSITÉ BORDEAUX 1

ÉCOLE DOCTORALE DES SCIENCES CHIMIQUES

Par **Quan GAN**

POUR OBTENIR LE GRADE DE

DOCTEUR

SPÉCIALITÉ : CHIMIE ORGANIQUE

Foldaxanes: Pseudorotaxanes Hélicoïdaux Auto-Assemblés

Structures et Mouvements Moléculaires

Directeur de recherche : Dr. Ivan HUC

Soutenu le 30 novembre 2012

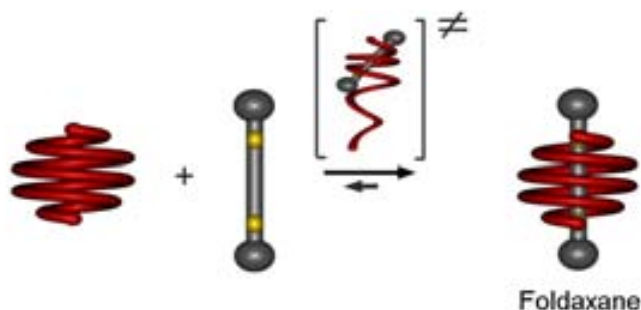
Mme	REINAUD, O.	(Rapporteur)	Professeur, Université Paris Descartes
M.	SEVERIN, K.	(Rapporteur)	Professeur, Ecole Polytechnique Fédérale de Lausanne
<i>Devant la commission d'examen formée de :</i>			
M.	BASSANI, D.	(Rapporteur)	Directeur de recherche, CNRS
Mme	REINAUD, O.	(Rapporteur)	Professeur, Université Paris Descartes
M.	SEVERIN, K.	(Rapporteur)	Professeur, Ecole Polytechnique Fédérale de Lausanne
M.	HUC, I.	(Examineur)	Directeur de recherche, CNRS
M.	FERRAND, Y.	(Membre invité)	Chargé de recherche, CNRS

Résumé de la thèse en français

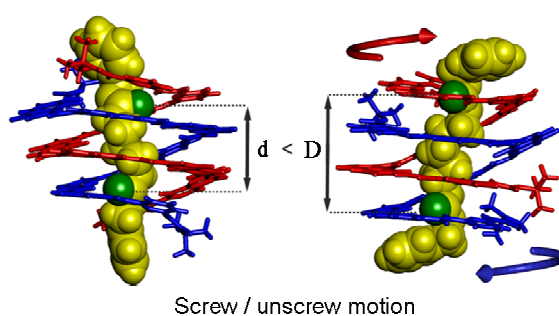
Le design de molécules possédant une propension à l'auto-assemblage est un des domaines les plus fascinants et offrant le plus de challenges que cela soit en chimie supramoléculaire, chimie des matériaux ou encore en biologie. Parmi ces molécules, un domaine tout particulièrement intéressant est le design de molécules artificielles qui peuvent s'auto-assembler en hélices multiples, non seulement dans le but de mimer les structures et fonctions du vivant (e.g. ADN, protéines), d'aider à mieux comprendre certains processus biologiques, mais aussi créer de nouvelles structures codants pour des fonctions originales. Ce manuscrit de thèse traite avant tout du développement de la recherche sur les foldamères (i.e. oligomères artificiels qui peuvent adopter une structure stable et compacte en solution) et notamment d'avancées effectuées sur les oligomères d'amides aromatiques.

Le premier chapitre de ce manuscrit de thèse consiste en une revue non exhaustive traitant de travaux marquants dans le domaine de la reconnaissance de molécules invitées au sein de cavités hélicoïdales. Au cours des deux dernières décades, la communauté des chimistes a investi un effort substantiel sur le développement de la chimie des foldamères. Ces structures qui peuvent être également définies comme des « oligomères artificiels qui se replient de façon ordonnée en solution via un ensemble d'interactions faibles » ont permis d'étendre le registre des structures et fonctions pouvant être obtenues par des molécules non naturelles. Il est possible de subdiviser le domaine entre deux grandes classes de foldamères: aliphatiques et aromatiques. Ce chapitre s'intéresse principalement à cette dernière catégorie et notamment au développement d'oligomères d'amides aromatiques dont le squelette rigide est stabilisé entre autres par des liaisons hydrogènes intramoléculaires et de l'empilement aromatique ce qui leur confèrent des propriétés exceptionnelles telles que: i. la stabilité; ii. la prédictibilité ; iii. la modularité; iv. la facilité de synthèse. Une propriété unique des ces objets est la formation de cavité dès leur repliement secondaire, cavité qui peut être utilisée à des fins de reconnaissance moléculaire. Chaque monomère de la séquence code à la fois pour une propriété structurale (diamètre de l'hélice), et portent également une fonction précise, par exemple pour la reconnaissance moléculaire. Le fait de pouvoir remplacer chaque monomère individuellement sans changer la séquence intégralement confère un haut degré de modularité, propriété indispensable au design de récepteur possédant à la fois affinité et sélectivité en reconnaissance moléculaire.

Le second chapitre traite de la préparation et la caractérisation d'une nouvelle famille de pseudorotaxanes, nommée foldaxane, pour laquelle le macrocycle est remplacé par une hélice. Dans ce système, une hélice (foldamère) peut s'enrouler lentement autour d'une tige en forme d'haltère pour former un complexe hôte-invité stable (foldaxane) dans lequel la molécule réside au sein de la cavité de l'hélice tout en exhibant deux groupes protubérants à chaque extrémité de l'hôte. La formation des foldaxanes est favorisée thermodynamiquement et sa force motrice réside principalement dans la formation de liaisons hydrogènes entre les pinces pyridines (2,6-pyridinedicarboxamide – donneurs de liaisons hydrogènes) et les points d'ancrage sur la tige que sont les carbonyles des fonctions carbamates. Ainsi, il a pu être établi qu'il existait une concordance exacte entre la longueur des foldamères et celles de la tige. Le processus par lequel le foldaxane se forme requiert le déroulement partiel de l'hélice ainsi que son repliement autour de la molécule invitée, ce qui implique un contrôle fin des cinétiques permettant de s'affranchir des liaisons mécaniques « irréversibles » observées dans les architectures de type rotaxanes. De plus, cette barrière cinétique considérable permet la préparation de complexe stable dans le cas d'une dissociation plus lente que l'enroulement. Le mécanisme d'enroulement a également été démontré par comparaison entre des tiges en forme d'haltère et des tiges linéaires sans bouchons stériquement encombrant à chaque extrémité. Enfin, dans ce chapitre il est démontré qu'une fois la tige enroulée sur la tige il est possible de la faire glisser longitudinalement le long de celle-ci tel un piston moléculaire. Ce mouvement moléculaire a notamment été démontré par RMN bidimensionnelle d'échange (EXSY). Enfin, un pas supplémentaire dans la complexité a été franchi, en ce qui concerne le démarrage et l'arrêt du glissement via la protonation ou la déprotonation de la molécule invitée. Cette étude représente un des premiers exemples de l'utilisation de l'auto-assemblage pour le développement de nano-machines.

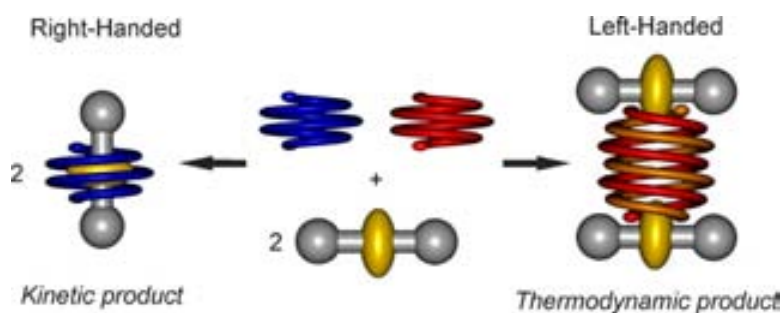


Le troisième chapitre de ce manuscrit de thèse est dédié à la mise en évidence pour la première fois à l'échelle moléculaire d'un mouvement de vissage. Pour ce faire, une double hélice antiparallèle basée sur un squelette d'oligoamides aromatiques a été conçue et préparée. Cette double hélice, à l'instar des simples hélices présentées dans le chapitre précédent peut également s'enrouler autour de molécules invitées en forme d'haltère en utilisant un trimère de pyridines dicarboxamides à une extrémité de chaque brin de la double hélice qui peut ainsi se lier par liaisons hydrogènes aux carbonyles de la tige en configuration antiparallèle. Cependant, à la différence des foldaxanes simple brin, les architectures en double hélice possèdent une plus grande tolérance quant à la longueur des tiges qui peuvent être liées. Cette propriété a été mise en évidence grâce à de multiples titrages en RMN du proton pour lesquelles les constantes d'association pour des tiges de longueur différentes ont été calculées. Les structures cristallines de plusieurs complexes double hélices-tiges ont pu être obtenues et ont mis en évidence une adaptabilité de l'hôte pour la molécule invitée avec un bilan net entre les différentes structures qui s'apparente à un vissage de la double hélice. Afin de réellement mettre en évidence le vissage de deux brins, une tige plus longue comportant deux stations de longueurs différentes (*i.e.* une courte pour l'hélice vissée et une longue complémentaire de l'hélice dévissée) a été préparée. Le mouvement de vissage (glissement et rotation simultanée) entre les deux stations a pu être mis en évidence grâce à l'utilisation de la RMN ROESY qui permet d'identifier les signaux en échange lent entre deux espèces (amides de des tiges vissée et dévissée). Au bilan, cette étude a permis de caractériser un phénomène inhabituel à l'échelle moléculaire et ouvert la porte à l'implémentation du vissage comme nouvelle fonction à l'échelle nanométrique.



Le dernier chapitre de cette thèse traite du piégeage d'un foldaxane comme intermédiaire cinétique supramoléculaire au cours d'un équilibre simple hélice-double hélice. Un oligomère d'amide aromatique a été conçu et préparé afin de former un foldaxane dont la tige est un dérivé

d'acide tartrique fonctionnalisé par des groupements stériquement encombrant et présentant une forme globale en haltère. Le foldamère seul en solution possède une capacité à s'auto-assembler en double hélice à forte concentration et rester en simple hélice à faible concentration. La simple hélice peut s'enrouler autour du dérivé d'acide tartrique grâce notamment à la présence des motifs aminopyridines des naphtyridines qui sont connus pour former de très bonnes liaisons hydrogènes avec les fonctions acides carboxyliques. Le foldaxane a été mis en évidence en utilisant notamment la RMN et le dichroïsme circulaire et il a pu être montré que le complexe existait avec une stœchiométrie 1:1 (simple hélice:tige). Cependant une analyse poussée a permis d'observer la transformation lente de ce complexe en un second complexe plus stable thermodynamiquement. La structure de ce dernier a pu être déterminée grâce à la diffraction des rayons X et par RMN et s'est révélé être un complexe 2:2 (une double hélice et deux acides tartriques à chaque extrémité). La stabilité de ce complexe est révélée par l'existence de huit liaisons hydrogènes entre les unités pyridines des deux brins de l'hélice et les fonctions acides carboxyliques de la molécule invitée. En parallèle il est intéressant de noter que les propriétés chiroptiques sont très affectées par la transition simple hélice-double hélice. En effet, une inversion du signe de l'effet Cotton a été observée lors de la conversion du complexe cinétique vers le complexe thermodynamique. Ce chapitre montre notamment l'importance du contrôle des échelles de temps lors de conversion supramoléculaire.



La Nature démontre une maîtrise inégalée dans l'art d'exploiter les interactions non-covalentes ayant pour but de produire et contrôler des phénomènes complexes, organisés et fonctionnels. Les efforts déployés dans cette thèse ont eu pour objectif de démontrer qu'à l'échelle du chimiste les oligomères d'amides aromatiques peuvent s'avérer de bons candidats pour l'élaboration de machines moléculaires. Il est raisonnable de penser qu'à moyen terme les foldamères d'amides aromatiques puissent être utilisés en routine pour la fabrication d'architectures pourvues de fonctions complexes.

ACKNOWLEDGEMENT

In the past three years, I have not only obtained knowledge in chemistry, but also got a lot of help from many people without whom I could not have finished my project. I feel really grateful to my advisors, because they offer me deeper insights into the field of chemistry, to my friends, because they make the progress of my growth happier and more interesting, to my family members, because they always love me and support me.

First and foremost, I offer my sincerest gratitude to my supervisors, Dr Ivan Huc and Dr Yann Ferrand, who have supported me throughout my thesis with their care, patience and knowledge, providing me with an excellent atmosphere for doing research.

I would like to thank Dr Frédéric Godde, and Dr Victor Maurizot for guiding my research for the past several years and sharing valuable insights in the relevance of the studies.

I would also like to thank Dr Brice Kauffmann who has given me a lot of help for crystallography. Many thanks to Dr Axelle Grélard and Dr Cécile Courreges for their assistance with NMR measurements. My research would not have been possible without their help.

I would also like to thank Mr Yannick Chollet, the engineer of IECB for sharing his valuable time and for giving me helpful information on how to operate instruments.

I would like to thank Michael Singleton, Simon Dawson who as good friends, are always willing to help me and correct my writing. Many thanks to Jone, Zeyuan, Ting, Tracey, Tiny, Stijn, Chandramouli, Krzysztof, Bo, Laure, Guillaume, Christos, Misae and other friends in the laboratory for their help and for the 'happy hours' that we have spent.

I am grateful to the Centre National de la Recherche Scientifique and the Conseil Régional d'Aquitaine. Both offered me the support and equipment I needed to complete my thesis and funded my studies.

Thanks to the staff members of the nearby CNRS restaurant for making so nice French food. It is there that I spent my happy and relaxed moments in dining every noon, and I will not forget it.

I would like to thank my parents for supporting me throughout all my studies at IECB. They always encourage me with their best wishes.

Finally, I would like to thank my wife, Sufang Chen. She is always there cheering me up and stands by me through the good times and bad ones.

List of abbreviations

AcOH : acetic acid

Bn : benzyl

Boc : *tert*-butyloxycarbonyl

Cbz : carbobenzyloxy

CD : circular dichroism

CPK : Corey, Pauling, Koltune space filling

DCM : dichloromethane

DIEA : diisopropylethylamine

DMAP : 4-dimethylaminopyridine

DMF : *N,N*-dimethylformamide

DOSY : diffusion ordered spectroscopy

ESI : electrospray ionization

EXSY : exchange spectroscopy

Ghosez reagent : 1-chloro-*N,N*,2-trimethyl propenylamine

HRMS : high resolution mass spectroscopy

***i*BuOH** : isobutanol

MALDI : matrix-assisted laser desorption/ionization

Me : methyl

MeOH : methanol

MMFFs : Merck molecular force field

NMR : nuclear magnetic resonance

NOESY : nuclear overhauser effect spectroscopy

Piv : pivaloyl

ppm : parts per million

PyBOP : benzotriazol-1-yl-oxytripyrrolidinophosphonium hexafluorophosphate

quant. : quantitative

ROESY : rotating-frame Overhauser spectroscopy

r.t. : room temperature

TEA : triethylamine

TFA : trifluoroacetic acid

THF : tetrahydrofuran

TLC : thin layer chromatography

Abbreviations of the aromatic amino acid building blocks

P : 2,6-diaminopyridine and 2,6-pyridinedicarboxylic acid

Q : 8-amino-2-quinolinecarboxylic acid

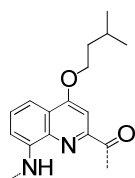
Q^f : 7-amino-8-fluoro-2-quinolinecarboxylic acid

N : 2-amino-1,8-naphthyridine-7-carboxylic acid

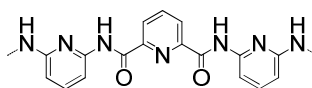
A^f : 1,8-diaza-9-fluoro-2,7-anthracene-dicarboxylic acid

pyr : pyridine

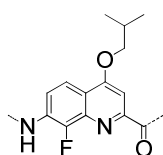
pyz : pyridazine



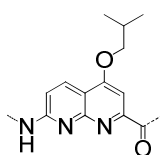
"Q"



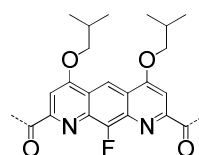
"P₃"



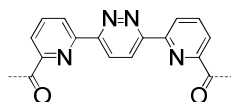
"Q^f"



"N"



"A^f"



"pyr-pyz-pyr"

CONTENTS

INTRODUCTION	1
Chapter 1. Endorecognition in helical foldamers	3
1. Introduction	5
2. Recognition of neutral molecules	7
2.1 Achiral polar guests	7
2.2 Chiral polar guests	10
2.2.1 <i>Carbohydrates</i>	10
2.2.2 <i>Chiral diacids</i>	13
2.3 Apolar guests	14
3. Recognition of cations	16
4. Recognition of anions	21
5. Conclusion	24
6. References	26
Chapter 2. Foldaxanes: aromatic oligoamides around dumbbell-shaped molecules	29
1. Introduction	31
2. Synthesis	33
2.1 Synthesis of helices	33
2.2 Synthesis of guests	33
3. Results and discussion	36
3.1 Hybridization behavior of foldamers 2-4	36
3.2 The thermodynamics of the host-guest complexes	37
3.3 The kinetics of association and dissociation of the host-guest complex	43
3.4 The shuttling motion of foldaxane	45
3.5 Controlling the foldaxane motion	47
4. Conclusion	49

5. Experimental part	50
5.1 Methods for NMR	50
5.2 Methods for X-ray crystallography	51
5.3 Summary of X-Ray crystallographic data	52
5.4 Methods for chemical synthesis	53
5.4.1 <i>Synthesis of helix 2</i>	53
5.4.2 <i>Synthesis of helix 3</i>	54
5.4.3 <i>Synthesis of helix 4</i>	54
5.4.4 <i>Synthesis of guests</i>	55
6. References	61

Chapter 3. Double-helical foldaxanes: template induced screw motions..	63
1. Introduction	65
2. Synthesis	67
2.1 Synthesis of helices	67
2.2 Synthesis of guests	67
3. Results and discussion	69
3.1 The double-helical foldaxane formation	69
3.2 The screw motion of the double-helical foldaxane	71
3.3 The screw motion through the shuttling	74
4. Conclusion	77
5. Experimental part	78
5.1 Methods for NMR	78
5.2 Methods for X-ray crystallography	78
5.3 Summary of X-Ray crystallographic data	80
5.4 Methods for chemical synthesis	81
5.4.1 <i>Synthesis of helix 1</i>	81
5.4.2 <i>Synthesis of guests</i>	81
6. References	84

Chapter 4. Identification of a foldaxane kinetic by-product during guest-induced single to double helix conversion	87
1. Introduction	89
2. Synthesis	91
2.1 Synthesis of helix	91
2.2 Synthesis of guests	91
3. Results and discussion	93
3.1 Hybridization behavior of foldamer 2	93
3.2 The kinetic formation of 1:1 foldaxane	96
3.3 The formation of 2:2 thermodynamic complex	98
4. Conclusion	105
5. Experimental part	107
5.1 Methods for NMR	107
5.2 Methods for Circular Dichroism	108
5.3 Methods for X-ray crystallography	108
5.4 Summary of X-Ray crystallographic data	109
5.5 Methods for chemical synthesis	110
<i>5.5.1 Synthesis of helix 2</i>	110
<i>5.5.2 Synthesis of guests</i>	111
6. References	113
 CONCLUSION AND PERSPECTIVES	 115

INTRODUCTION

Inspired by the amazing structural and functional diversity of biological macromolecules, chemists have been actively engaged in developing synthetic oligomers with well-defined folded structures, termed as foldamers, to improve our understanding of the natural counterparts.

Due to the diversity of sizes and shapes of monomers, a vast number of foldamers have been reported so far, and some significant advances have been achieved, for example catalysis, recognition, and self-assembling materials.

Over the last decade, our group has developed several families of aromatic oligoamides which fold into exceptionally stable helical conformations, and found that their folded structures and properties can be tuned by varying the size of monomers, and/or by changing the relative orientation of the acid and amine groups on each aryl group, and/or by replacing side chains of monomers. For instance: 1) higher-order helical structures (double, triple, quadruple helices) could be obtained with different sequences via spring-like motion; 2) water soluble foldamers have been developed by introducing water soluble side chains on each monomer; 3) helices with a large diameter in the center and narrow diameters at the ends have also been designed by using different monomers, thus creating a cavity able to encapsulate various guests.

Following these earlier studies, in this thesis, we will describe the design, synthesis, and motion properties of a new series of helical foldamers based on aromatic amide backbones, which could be used as modern prototypes of molecular machinery.

Chapter 1 will consist in a short review of several significant achievements on molecular recognition within the cavities of foldamer receptors. The recognition behaviors of foldamers is the common theme of the research, and are based on the design discussed in this chapter.

In chapter 2, a series of aromatic oligoamide helices are proved to wind around rod-like guests to form host-guest complexes. The helices can shuttle along the rods without dissociating, because the timescale of helical unwinding prove to be relatively slow.

In chapter 3, a double helical foldamer is shown to bind to a series of rod-like guests of various lengths upon winding around guests, as a result of a screw motion, an unusual motion that is observed for the first time in artificial architecture.

In chapter 4, an aromatic oligoamide sequence is shown to trap a dumbbell-shaped guest forming a 1:1 host-guest complex. This complex was found to be a long-lived kinetic

supramolecular by-product as it slowly transformed into a thermodynamically favored 2:2 host-guest complex composed of two guests and a double helix.

Chapter 1

Endorecognition in helical foldamers

1. Introduction

Molecular recognition is one of the most fundamental issues in the field of supramolecular chemistry. Supramolecular chemistry originated from the discovery of crown ethers complexed with alkali metal ions.¹ In crown ethers, oxygen and/or sulfur atoms are arranged in a macrocycle to create a binding cavity, that is suitable for recognition of metal ions.

From then on, many macrocyclic compounds acting as receptors have been established, such as cryptands, carcerands or others cyclodextrins.²⁻⁶ Recognition patterns are all based on the spatial organization of arrays of functional groups converging towards a binding site. However, there are several main disadvantages for these receptors: 1) the synthesis of macrocycles presents low efficiency although templated self-assembly may provide some improvement; 2) macrocycles being symmetrical they can mostly complex simple spherical guests; 3) they are very difficult to tune because of the methods used for their preparation. Thus, there has been a continuously growing interest in development of novel high-performance synthetic receptors.

Nature is a good teacher. In biomolecules, folded conformations are ubiquitous, play vital roles and present exquisite biological functions. For example, protein folding is controlled by diverse non-covalent forces, consequently forming binding sites that can effectively recognize substrates and provide complicated functions, such as catalysis, signal transduction or immunity. Inspired by Nature's receptor design, over the last two decades chemists have actively explored the possibility to elicit molecular recognition within the cavities of oligomeric chains folded into helical structures.

These oligomers, termed as foldamers,⁷⁻¹⁶ adopt well-defined helical structures in solution that may act as receptors able to accommodate guest molecules within the helical hollow. In addition, some linear oligomers that are not initially folded can adopt helical structures once complexed with a complementary guest to form guest-induced foldamers.

Compared to conventional macrocyclic receptors, foldamers are more dynamic, i.e., equilibrium in the process of folding and unfolding, and easily tunable: they are based on sequences whose monomers can be changed one at a time and introduced by using the same synthetic methods. Therefore, foldamers represent a novel and important class of hosts for the design of synthetic receptors, and they have been shown to exhibit very efficient and selective abilities for molecular recognition. This chapter will be dedicated to a non-exhaustive review on

several significant achievements based on molecular recognition (e.g. organic chiral and achiral molecules, metals, anions) within the cavities of foldamer receptors.

2. Recognition of neutral molecules

2.1 Achiral polar guests

The Huc group reported that aromatic oligoamide foldamer **1** composed of oligopyridine dicarboxamide units at the center of the sequence and two 8-amino-2-quinolinecarboxylic acid units at each extremity can encapsulate a water molecule in its small cavity as shown in the crystals (Figure 1).¹⁷ These helical structures were driven by intramolecular hydrogen bonding as well as aromatic π - π stacking interactions and electrostatic repulsions between carbonyl and endocyclic nitrogens of the pyridine ring. One of typical features of the architectures is that the diameter of the capsule is large at the center and narrower at both ends. The whole sequence thus shapes like a capsule and can accommodate one water molecule which is completely isolated from the solvent. This was proven by contrastive ^1H NMR experiments, which were performed both in dry and wet CDCl_3 solution. It was found that drying or wetting the solvent had little effect on the chemical shift of the signals of the peripheral amide protons (0.2 ppm). However, large downfield chemical shifting (1.31 ppm) was observed for the signals of most of the central amide protons. The results supported that a water molecule was encapsulated in the cavity, which formed strong hydrogen bonding with these inwardly located amide protons. ^1H - ^1H nuclear Overhauser effect (NOE) experiments were useful in proving the host-guest complementarity. At low temperature ($-50\text{ }^\circ\text{C}$), water signals split and gave rise to two different water peaks, only one of which showed NOE cross peaks with some of the inwardly located amide protons and therefore could be assigned to the encapsulated water. More recently, Zeng et al. prepared some other aromatic oligoamides sequences able to complex water molecules.¹⁸

Furthermore, increasing the number of pyridine units at the central segment from three to seven led to the new helical capsule **2** with larger cavity of which could host two water molecules (Figure 1).¹⁹ Interestingly, ^1H NMR presented distinct signals for the empty, half-full or full

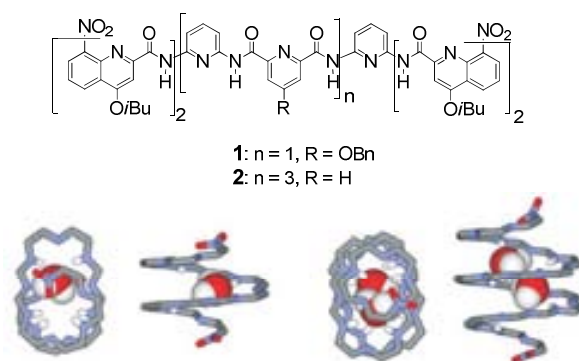


Figure 1. Structures of helical capsule **1** and **2** and crystal structures of helical capsule **1** and **2** with one and two molecules of water trapped in the cavity, respectively.

capsules, which indicated that all these species were in slow exchange on the NMR timescale at low temperature. Additionally, it was found that small polar molecules like hydrazine and hydrogen peroxide can also be encapsulated. However, no encapsulation was observed in the presence of methanol and formic acid. Although the guests were small, one or two water molecules, these findings provide useful hints to synthesize larger capsules, capable of trapping larger guests, by incorporating new monomers coding for lower curvature.

Following this principle, four different aromatic units: 8-amino-2-quinolinecarboxylic acid (Q), 2,6-diaminopyridine and 2,6-pyridinedicarboxylic acid (P), 7-amino-8-fluoro-2-quinolinecarboxylic acid (Q^f), and 1,8-diaza-9-fluoro-2,7-anthracene-dicarboxylic acid (A^f), were assembled together using amide linkages to generate helical capsule **3** (Figure 2).²⁰ In this sequence, the terminal segment Q₃ is known to form a helix too narrow to accommodate any guest and acts as a cap closing each extremity of this capsule.²¹ P₃ is used as cleft able to bind to guests containing hydroxyl and amino groups.¹⁷ Q₂^f and A^f code for a greasy hollow thus providing an ideal environment for an alkyl chain.²² NMR investigations demonstrated that alkane diol and diamine are ideal candidates to be encapsulated. The molecules ranging in size from ethylene glycol to 1,4-butanediol were incorporated in the close shell with affinities in the range from 500 to 5000 M⁻¹ in chloroform. X-ray analyses provided direct proof for the encapsulations (Figure 2).

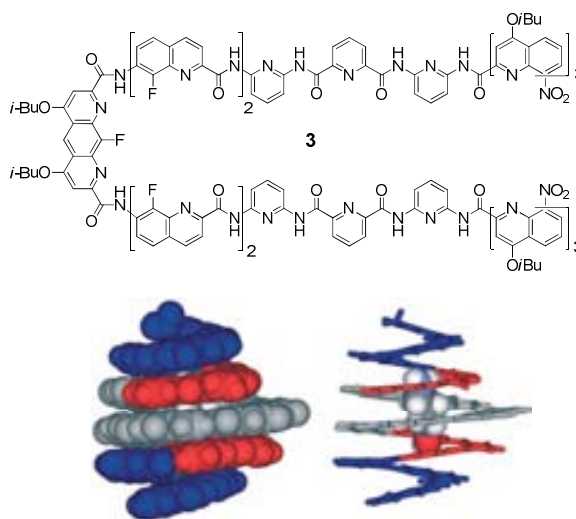


Figure 2. Structure of foldamer **3** and X-ray crystal structures of **3** containing 4-amino-1-butanol.

Encapsulating an elongated guest in a helical capsule, requires a long and close space. For this regard, self-assembly which is usually based on small and accessible building blocks provides an efficient approach to produce large supramolecular containers. Along this line, Huc and coworkers have designed oligomer **4** comprised of three different segments: Q_8^f , which can

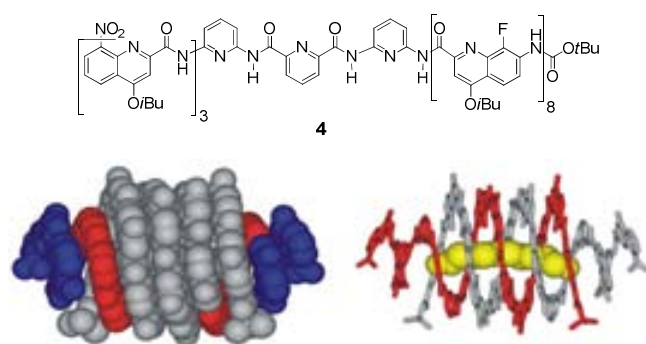


Figure 3. Structure of foldamer **4** and crystal structures of foldamer **4** with a 1,10-decanediol molecule trapped

form very stable double helices,²² Q_3 and P_3 , whose functions are similar to that in oligomer **3**. Thus, the foldamer **4** was envisaged to possess all features required to form an antiparallel double helical capsule twice as long as its single helical precursor. With the distinct character in the structure, the double helical capsule provides an unprecedented opportunity to investigate the binding properties of

long linear guest molecules in confined space. As expected, the crystal structure of **4** showed that in the center two Q_8^f segments entwined one another to form a duplex section, while the two narrow peripheral single Q_3 subunits capped the cavity of the duplex. The double helical capsule had a dimerization constant calculated to be 250 M^{-1} . Long guests like nonanediol, decanediol and undecanediol tended to reside in the close hollow of the double helical capsule. Among the different guests, decanediol showed the better complementarity to the cavity as observed in solution and in the solid phase (Figure 3).²³

All of the above aromatic amide oligomers are formed by intramolecular hydrogen bonds to adopt a well ordered helical conformation for binding guests. In principle, the

sequences may adopt random coil conformations due to the flexible rotation of the amide bonds without intramolecular hydrogen bonding. Nevertheless, they can fold into helical structures by

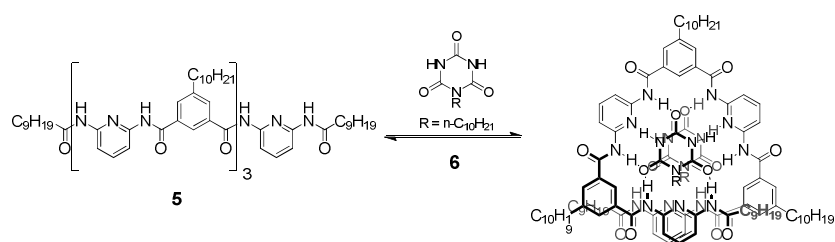


Figure 4. Hydrogen bonding of complementary guest **6** to foldamer **5** results in a helical host-guest complex

induction of guest. One such example is linear oligomer **5**, which was reported by Lehn et al. (Figure 4).²⁴ Upon adding 2 equiv. of monosubstituted cyanurate **6** to the solution of **5** in chloroform, ¹H NMR spectra showed that the signals of heptamer were sharpened, indicating the ability of the oligomer to form specific conformations. Results showed that a 1:2 complex formed depending on the rotation of the central aryl–CO bonds and enforced by was the six intermolecular DAD/ADA hydrogen bonds. The helical strand could stack to disklike architectures, which could further self-assemble to supramolecular fibers of several μm of length, as revealed by electron microscopy.

2.2 Chiral polar guests

2.2.1 Carbohydrates

Hydrogen bonding-driven aromatic foldamers normally have relatively rigid helical structures. Specific binding sites, such as hydrogen bonding donors and acceptors, thus can be selectively arranged inside of the cavities. In this way, saccharides, which play very important roles in biological processes, could be recognized by aromatic foldamers. Li and coworkers reported a series of hydrazide-based foldamers **7a-c** possessing a rigid cavity of ca. 1 nm in diameter and with half of the hydrazide carbonyl groups orientated toward the center of the cavity, creating a hydrogen bond-accepting environment inside (Figure 5).²⁵ ¹H NMR, fluorescent and CD experiments confirmed that alkylated saccharides **8a-d** could be entrapped inside to form a 1:1 complexes in chloroform through the formation of multiple intermolecular C=O...H–O hydrogen bonds. The highest binding constant displayed by complex **7c-8d** in chloroform was determined to be $6.9 \times 10^6 \text{ M}^{-1}$, which was about 10-fold higher than that of the complexes of the monosaccharides, suggesting that the increasing the length of the sequence has helped to raise the binding ability.

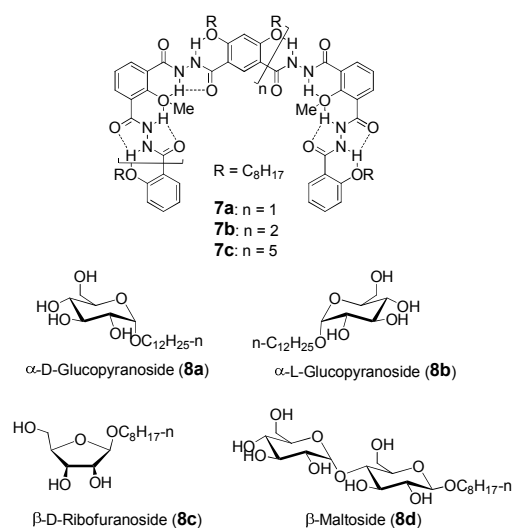


Figure 5. Structures of foldamers **7a-c** and the guests **8a-d**

In continuing investigations, a similar series of foldamers but with long decyl side chains and two large aromatic units, such as naphthalene, anthracene and pyrene, at the terminals of

their backbones, was found to strongly gelate organic solvents of varying polarity.²⁶ Addition of chiral guests **8a** or **8b** could further enhance the capacity of the foldamers to gelate through complexation. As a consequence, chiral induction occurred in the gel phase, as evidenced by formation of induced circular dichroism. Afterwards, Li and coworkers appended chiral proline moieties at the terminal units of aromatic hydrazide foldamers to generate chiral foldamers having a preferred handedness defined by the stereochemistry of proline. This chiral foldamer was shown to achieve diastereoselective recognition of glucose by CD experiments.²⁷ These results demonstrated that handedness could be induced in order to form a chiral cavity for selective complexation of chiral guests by introducing rationally designed chiral groups.

Similar amide-based foldamers **9a** and **9b** have also been developed by the same group (Figure 6).²⁸ Molecular modeling showed that the cavity of the helical conformations was less than 1 nm in diameter. Their binding for saccharides **8** in chloroform was proven by the ¹H NMR, fluorescent and CD spectroscopy, which were shown to be in a 1:1 stoichiometry. The binding constants (550-7800 M⁻¹ in chloroform) obtained by fluorescent experiments were lower than those of their hydrazide analogues **7** that had the same number of benzene units.

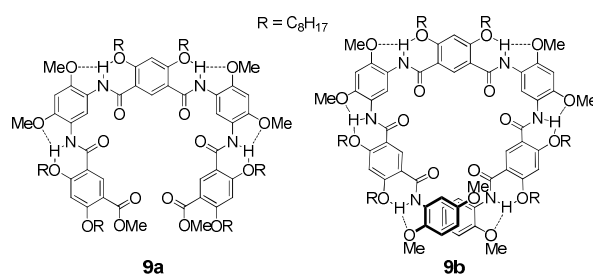


Figure 6. Structures of foldamers **9a** and **9b**

Conversely, saccharides could be used as templates to induce flexible oligomers to fold. Inouye and coworkers have reported the synthesis of oligo-(pyridine-ethynylene)s **10** having alkoxy side chains (Figure 7).²⁹ These oligomers adopted a linear extended conformation in dichloromethane due to the dipole-dipole repulsion between the adjacent pyridine units. However, upon addition of *n*-octyl β -pyranoside, long oligomers ($n = 18, 24$) folded into compact helical structures driven by intermolecular multiple hydrogen bonds between the pyridine nitrogen atoms and hydroxyl groups of the saccharides enclosed inwardly. The chirality was transferred from the bound saccharides to the helices, as evidenced by the formation of induced CD signals. The binding was in a 1:1 stoichiometry and the binding constant of the complex ($n = 24$) was determined to be 1200 M⁻¹ in dichloromethane.

Recent research found that ICD signals of the saccharide complex **10** ($n = 18$) was enhanced through addition of copper(II) triflate. It was expected that the copper(II) could coordinate with the pyridine nitrogens, thus stabilized the resulting helical complex with a saccharide guest by interlinking the pyridine nitrogens and the hydroxy groups inside the helix. After subsequent addition of *o*-phenanthroline, a strong ligand for copper compared to saccharide, the saccharide was replaced by *o*-phenanthroline and was thus kicked out of the helix cavity. The new helical structure and chirality of the complex was further stabilized as a result of the cooperativity of copper and achiral ligand *o*-phenanthroline inside. This phenomenon suggested that the helix could memorize its biased helicity even after the removal of the initial chiral source (saccharide).³⁰

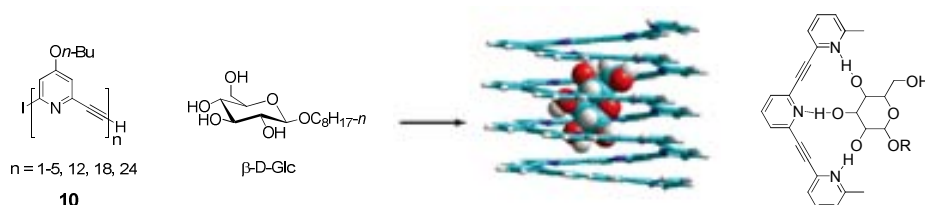


Figure 7. Helical structure of **10** induced by the saccharide complexation

At the same time, to further explore the saccharide-binding ability of these oligomers in aqueous solution, the same group developed water-soluble polymers by replacing alkoxy side chains with hydrophilic ethylene glycol side chains.³¹ ¹H NMR, UV/Vis and CD spectroscopy consistently demonstrated that these polymers spontaneously collapse into stable helical structures in protic media as a result of the solvophobic effect. The helices could also bind saccharides with helical cavities, as reflected by the formation of ICD signals in the absorptive region of the polymers. Most interestingly, when pure α - and β anomers of D-glucoside were used, the preferred helical sense of the complex could be inverted by mutarotation of the saccharides.³²

In addition, the oligomeric and polymeric pyridine-ethynylenes can be further modified in different ways. For example, polymers with dialkylamino side chains have been prepared. The protonation of the dialkylamino pyridines allows one to reversibly modulate saccharide binding and thus folding.³³

A series of saccharide-linked oligomers **11** have also been designed (Figure 8).³⁴ The oligomers and glycoside moieties self-assembled into unique intramolecular helical complexes, due to intramolecular hydrogen bonds, which were studied with CD and ¹H

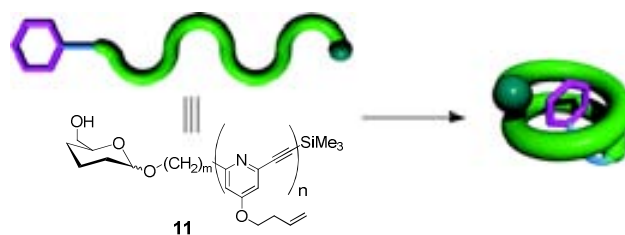


Figure 8. Helical structure of **11** formed by autophagy

NMR experiments. The sign and strength of the ICD signals were found to depend strongly on the length of pyridine-ethynylene segments and the types of the glycosides, indicating that the primary structures of oligomers encoded their further self-assembled architectures.

2.2.2 Chiral diacids

Recently, the Huc group introduced an aromatic oligoamide foldamer **12** that can

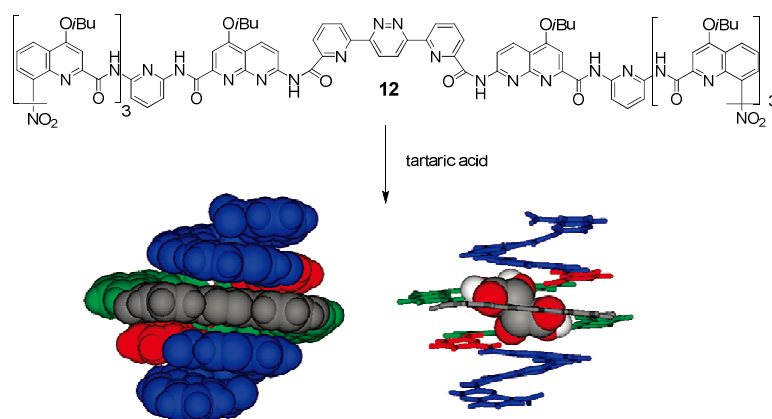


Figure 9. Structure of foldamer **12** and its crystal structures containing tartaric acid

encapsulate tartaric acid with high affinity, selectivity and diastereoselectivity (Figure 9).^{35,36} Its design is based on amino-acid units coding for a large helix cavity in the center of the sequence and a narrow helix diameter at the ends, as mentioned above, thus creating a binding site completely surrounded by the helix

backbone. Upon addition of 1 equiv of a single enantiomer of tartaric acid as a guest, ¹H NMR showed that all the signals of the free helix completely disappeared, indicating very high binding constant ($> 10^6 \text{ M}^{-1}$) of the complex in chloroform; a new single set of sharp signals emerged, suggesting that it existed in a single diastereomeric form (de $> 99\%$). A mirror imaged CD spectrum was observed upon adding each enantiomeric guest. The induced CD signals are the consequence of the foldamer association with tartaric acid in a diastereoselective manner, resulting in a helix-preferred handedness. The crystal structure showed an unambiguous attribution of the

matching stereochemistry: the natural *L*-tartaric acid is bound by the M helix of **12** and *D*-tartaric acid by the P helix.

2.3 Apolar guests

In 2000, Moore et al. reported a series of oligomers of *m*-phenylene-ethynylenes (*m*PE) **13** that presented an extended conformation in chloroform and folded into a compact helical conformation by solvophobic interactions in polar medium, such as acetonitrile.³⁷ Upon folding, a cavity was formed, which could hold the chiral pinene **14** inside (Figure 10).³⁸ The binding strictly adhered to a 1:1 stoichiometry and the binding constant was determined to be 6830 M⁻¹ in water/acetonitrile (40:60 vol/vol). With the increase of the water content in the solvent, the binding constant was increased linearly, showing that the binding was a solvophobic driven process.³⁹ Other similar chiral hydrophobic molecules **15-19** were also found to bind to the foldamer *m*PE (n = 12) in a 1:1 stoichiometry under identical conditions, albeit with lower binding constants. When methyl groups were introduced at the 4-positions of the benzenes of foldamers, the binding capacity of the corresponding foldamer toward pinene was decreased dramatically. The methyl groups thus disfavored the binding of small molecules, supporting that binding takes place within the tubular cavity.

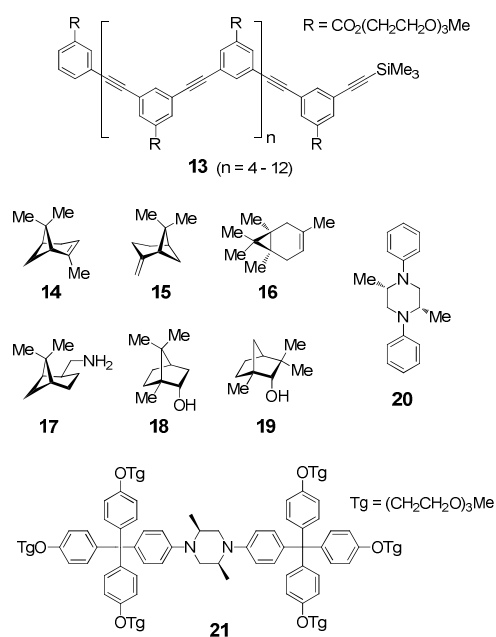
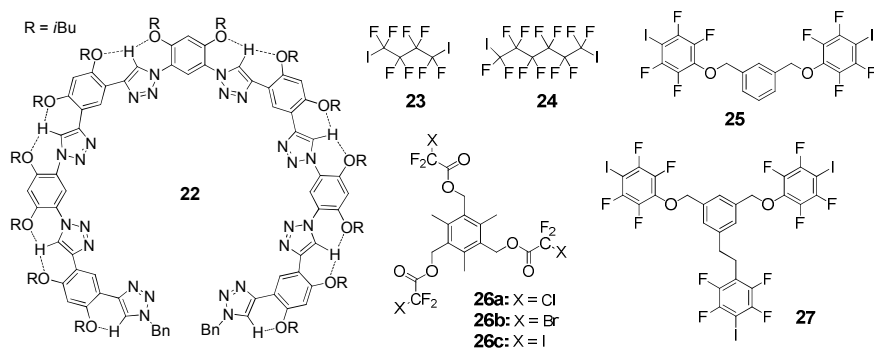


Figure 10. Structures of foldamers **13** and the guests **14-21**

When elongating the backbones, the cavity depth of the foldamers **13** was also increased. This may maximize their binding strength for rodlike chain guests of appropriate diameter. The Moore group showed that the complexes of *m*PE foldamers (n = 10, 12, 14, 16, 18, 20, 22, 24) and rigid straight guest diphenyl-piperidine **20** were still in a 1:1 stoichiometry, but binding affinities were remarkably dependent on oligomer length.⁴⁰ The binding constant of foldamer n = 10 was smaller than that of foldamer n = 12, and binding constants in water/acetonitrile (40:60 vol/vol) were dramatically enhanced by increasing oligomer length to reach a maximum when n

= 20 and 22, and then dropped for $n = 24$. The decrease in the binding affinity for $n = 24$ was ascribed to the volume mismatch between the foldamer cavity and the guest as shown by models. This result stimulated the researchers to propose two possible mechanisms of guest binding by helices. The first is the chiral ligand threading into the helical cavity of a rigid oligomer, and the second involves a transiently unfolded oligomer winding around the chiral ligand. To further clarify the binding mechanisms, Moore et al. synthesized a dumbbell-shaped guest **21** with bulky termini. Kinetic studies showed that the oligomers were able to bind the dumbbell-shaped guest, suggesting that a second mechanism was plausible.⁴¹ However, a simple threading appears to be more likely for thin guests, even though partial unfolding could not be ruled out.

Most recently, Li and coworkers demonstrated that intramolecular C–H···O hydrogen bonding can be utilized to



induce alternative diphenyl-triazole oligomer **22** to form helical structure.⁴² In the structure, all the nitrogen atoms of triazole units were positioned inward to form a cavity with ca. 1.8 nm in diameter (Figure 11). It

Figure 11. Structures of foldamer **22** and the guests **23-27**

was proven that this foldamer was capable of binding bidentate and tridentate organohalogen **23-27** through multiple N···X (X = Cl, Br and I) halogen bonds to form stable 1:1 complexes. The binding affinity of the complexes increased from organobromine to organochlorine and then to organoiodine, which was consistent with the order of halogen donor ability. These results revealed that halogen bonding may be used for recognition in macromolecular system.

3. Recognition of cations

The formation of helical structures with six units per turn could be obtained from alternating sequences of pyridine–pyrimidine units by adopting the transoid conformational preference of ortho-linked aromatic azaheterocycles, as demonstrated by Lehn et al.⁴³ However, the cavity of the helices are too small to host any metallic or organic guest. Replacement of the pyridine units by the 1,8-naphthyridine units provided a larger cavity of about 3.5 Å in diameter for the resulting helix **28**.⁴⁴

Naphthyridines possess large electric dipoles (~ 4.1 D), which point into the interior cavity formed upon helical folding. Hence, **28** was suitable to bind to cations such as K⁺, Cs⁺, hydronium, and guanidinium through ion-dipole or dipole-dipole interactions (Figure 12). Titrations of **28** with the metal salts in a mixture of CDCl₃ and CD₃CN showed a strong broadening and upfield shift of all the aromatic resonances, indicating that aggregation behavior occurred.

The formation of cylindrical aggregates was further confirmed by ES-MS experiments, X-ray powder diffraction and transmission electron microscopy.

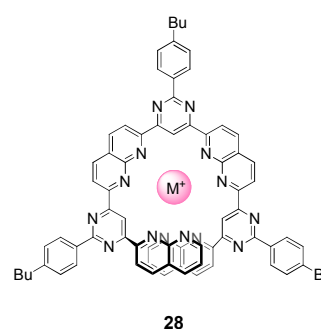


Figure 12. Structure of azaheterocycle oligomer **28** with a cavity suit for cations

The same group described a pyridine-hydrazone oligomer **29** that bound to Pb²⁺ ions in

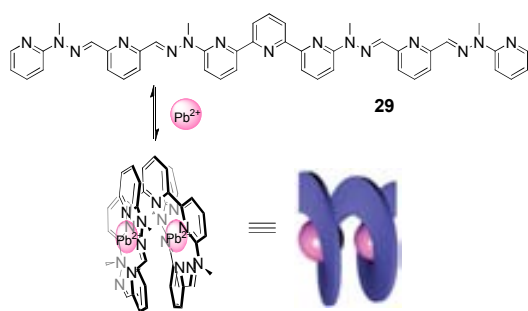


Figure 13. Structure of oligomer **29** binding to 2 eq. of Pb²⁺ ions could be controlled by pH and the structure of strand will thus reversibly transform from linear to helical shape.

acetoneitrile and subsequently formed a two-turn, helically folded complex (Figure 13).⁴⁵ The X-ray structure definitely showed a dinuclear complex consisting of a helically folded strand wrapped around two Pb²⁺ ions. ¹H NMR experiments also proved the formation of the complex; the aromatic resonances shifted to high field in accordance with the π-π stacking upon folded strand.

The

Moore and coworkers have shown that the *m*PE oligomers with cyano groups could tightly and selectively bind silver ions in the internal cavity of a helical structure by a combination of solvophobic and metal-coordination interactions (Figure 14).⁴⁶ These oligomers all adopted a random coil conformation in tetrahydrofuran.

However, upon addition of silver triflate, complex of **30** with silver ions resulted in a well-defined helical structure in the same solvent. Therefore, the formation of the helix is entirely dependant on metal coordination. UV-Vis, ¹H NMR titrations and ESI-MS experiments indicated that **30** complexed AgO₃SCF₃ in a 1:2 stoichiometry, and the binding constant of the complex K_1K_2 , was more than 10^{12} M^{-2} . In comparison to **30**, oligomer **31** with the same length but half cyano groups formed a 1:1 complex with AgO₃SCF₃, and the binding constant was calculated to be $2 \times 10^4 \text{ M}^{-1}$. The result suggested that $K_2 \gg K_1$ and the binding of 2 equiv of AgO₃SCF₃ to **30** was a cooperative process. In another experiment, it was also found that short hexamer **32** did not complex AgO₃SCF₃ at all. Comparing **31** with **32**, the addition of phenylacetylene segments that cannot bind metals to **32** but allowed for metal-ligand coordination to **31**, showing that solvophobic interactions played an important role in the metal-induced formation of the helical structure.

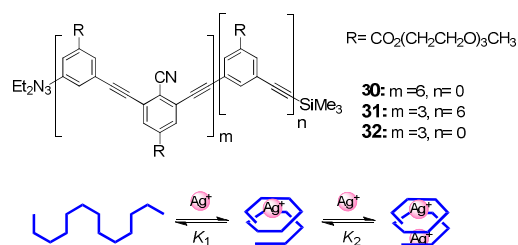


Figure 14. Structures of oligomers **30-32** and the schem of binding to Ag²⁺

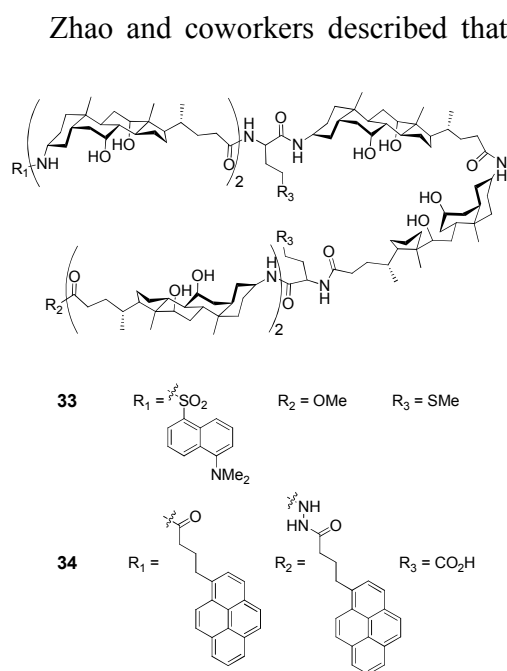


Figure 15. Structures of oligocholates **33**, **34**

(Figure 15).⁴⁸ The fluorescent emission of **33** was quenched due to the recognition processes. The selectivity for Hg^{2+} was very high in comparison to other divalent cations including Mg^{2+} , Zn^{2+} , Cu^{2+} , Co^{2+} , Ni^{2+} , and Pb^{2+} , and was attributed to the great binding affinity of Hg^{2+} for the orthionine sulfur. When two glutamic acid units were incorporated into the center, the two free carboxylic acid groups of the resulting oligocholate **34** could also chelate with a divalent metal ion (Figure 15).⁴⁹ The enhancement of an intramolecular pyrene excimer was most evident for both folding and binding processes. Specific binding for Zn^{2+} was observed, which was most sensitive in 15% MeOH/ethyl acetate, a little of polar environment, because the foldamer sensed the metal ion by going from the unfolded to the folded conformation.

Zhao and coworkers described that amino functionalized cholic acid could be used as a useful building block for the construction of amphiphilic foldamers. The native cholic acid is very rigid, with four fused rings that have a distinctive shape and facial amphiphilicity. These cholate oligomers could fold into helical structures with nanometer-sized hydrophilic internal cavities in mostly nonpolar solvents such as carbon tetrachloride or hexane/ethyl acetate, which was driven by the solvophobic interaction.⁴⁷ An oligocholate **33** decorated with two methionine units as bidentate ligands in the middle and with fluorescent dansyl groups at the chain end could bind Hg^{2+} ($K_a > 10^7 \text{ M}^{-1}$) ions in 5% MeOH in hexane–ethyl acetate (2:1 vol/vol)

A double helix could be obtained by consisting of two *ortho*-linked oligophenol strands bridged by two boron atoms via the formation of two spiroborate ($-\text{BO}_4$) moieties, as demonstrated by Yashima and Furusho groups.⁵⁰ Subsequently, researchers optimized the sequence and prepared a new double helix **35** in which the central sodium cation is coordinated to the spiroborate moieties (Figure 16).⁵¹ Upon adding cryptand [2.2.1] **36** to the solution, the sodium ions are removed from the double helix. A detailed analysis of the structure by X-ray crystallography revealed that the helix approximately doubled its length, from 6 to 13 Å. This noticeably large extension is most likely attributable to the enhanced electrostatic repulsion between the two anionic spiroborate moieties due to the absence of the central Na^+ ion. After adding NaPF_6 subsequently, the initial double helix with Na^+ inside was completely recovered through a contraction and winding motion.

This extension-contraction cycle can be repeated

several times by the sequential addition of cryptand **36** and NaPF_6 in an alternating manner. Most importantly, helix chirality was maintained during the contraction and extension processes by CD studies, that is, the helix underwent a unidirectional rotary motion.

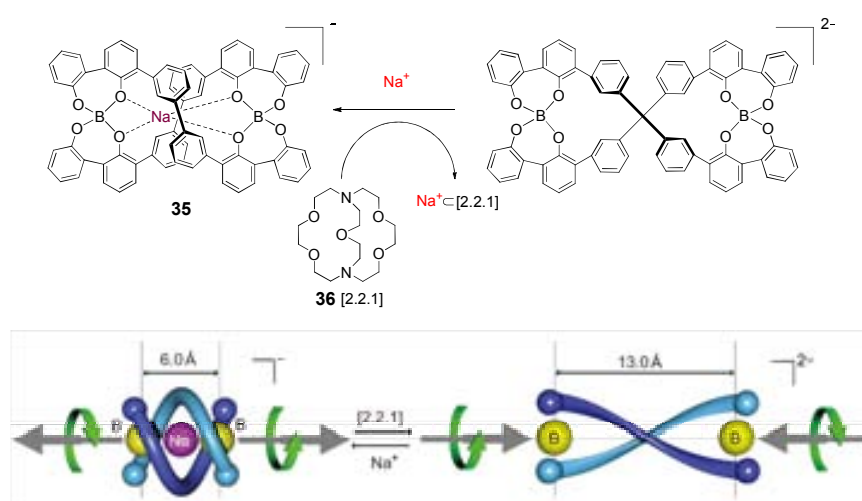


Figure 16. Structures of double helix **35** and cryptand **36** and schematic representation of the contraction and extension of a double helix by trigger with a cryptand and sodium

Besides metal ions, organic cations can also be recognized by foldamers. Li, Chen and coworkers developed novel oligomer **37** consisted of naphthalene units linked by ethylene glycols,

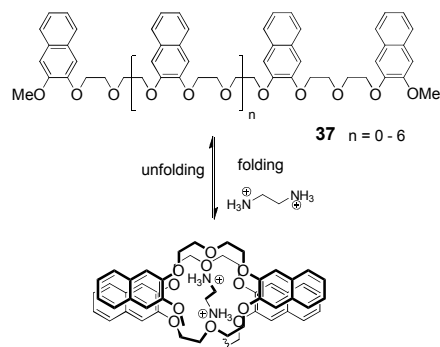


Figure 17. Binding of naphthylene derivatized oligo(ethylene glycol) **37** to ammonium within a helical cavity stabilized by solvophobic driven

stochiometry and the binding constants were determined to be in the range of 10^3 - 10^4 M^{-1} in acetonitrile. UV/Vis experiments in a chloroform–acetonitrile mixture showed hypochromic shifts due to intramolecular aromatic π -stacking effects, indicating the helical conformation of the oligomers became even more compact and rigid upon complexation.

Aromatic fluoro foldamer **38** was established by Li et al.⁵³ It revealed that N–H...F bond was strong enough to form stable intramolecular five- or six-membered and even three-centered continuous hydrogen bonds, inducing the whole sequence to form a rigid helical structure (Figure 18). ¹H NMR, mass, fluorescent experiments indicated that foldamer **38** could bind dialkyl ammonium ions **39** in a 1:1 stoichiometry with high binding affinity ($K_a = 8 \times 10^6$ M^{-1}) in chloroform, which is considerably higher than those of the complexes between dibenzo[24]crown-8 and dialkylammonium ions in chloroform (ca. 2.7×10^4 M^{-1}).⁵⁴ Furthermore, chiral induction could also be achieved by complexation of **38** with chiral L-tyrosine-derived ammonium ion **40**.

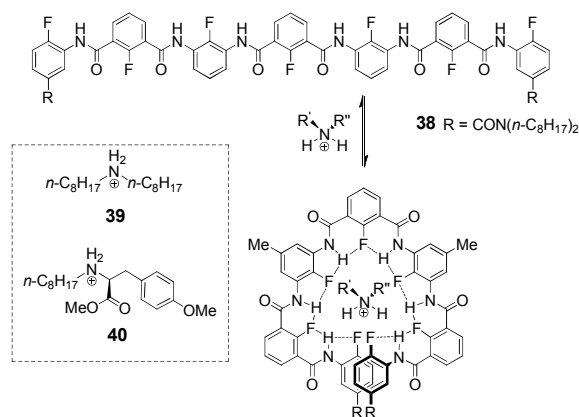


Figure 18. Binding of fluoro foldamer **38** to ammonium within a helical cavity stabilized by N–H...F hydrogen bonds

4. Recognition of anions

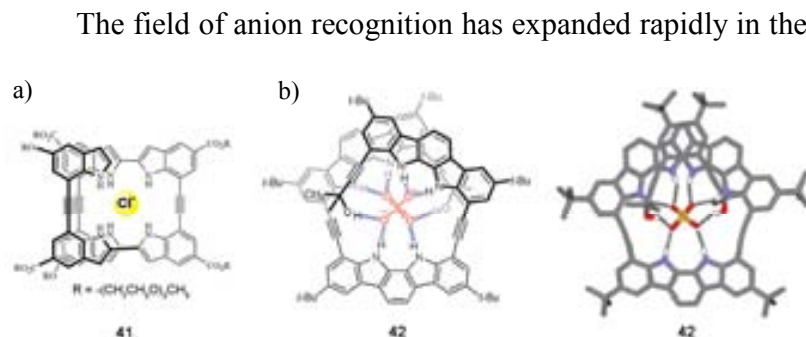


Figure 19. a) Structure of oligomer **41** binding to the chloride anion. b) Structure and crystal structure of oligomer **42** binding to the sulfate anion.

play important roles in biology, medicine, and the environment.⁵⁵ Recent research has shown that anions could be used to template the formation of a series of helical oligomers. One original example is the oligoindoles **41**, which was developed by Jeong and coworkers in 2005.⁵⁶ These oligoindoles containing four, six and eight indole rings connected by ethynyl linker adopted an expanded conformation due to the *transoid* preference of ortho-linked aromatic azaheterocycles, but fold into helical structures in the presence of chloride (Figure 19a). This was demonstrated by ¹H NMR and ROESY experiments. When chloride was added, ¹H NMR showed that the *NH* signals of the indoles shifted downfield as a result of hydrogen bond formation, and that aromatic signals shifted upfield because of aromatic stacking between indole moieties. The induced helical conformation was further proved by ROESY experiments where NOE cross peaks have been observed between protons located at adjacent aromatic units. It was evidenced that oligoindoles form 1:1 complexes with chloride; association constants were determined to be 1.3×10^5 , 1.2×10^6 , and $>10^7 \text{ M}^{-1}$ in acetonitrile for oligomers having four, six, and eight indole rings, respectively. In order to recognize larger anions, indolocarbazole units instead of indoles had been used to construct oligomer **42**, which contained six indole NHs and two aliphatic OHs at each terminus (Figure 19b).⁵⁷ ¹H NMR and ROESY experiments proved that this oligomer could form a helical structure induced by sulfate ion. The X-ray structure directly revealed that the tetrahedral sulfate ion was encapsulated in a helical cavity by a total of eight hydrogen bonds, with each oxygen forming two hydrogen bonds. Oligomer **42** displayed a high binding strength and selectivity towards sulfate ($K_a = 6.4 \times 10^5 \text{ M}^{-1}$ in 10% $\text{CH}_3\text{OH}/\text{CH}_3\text{CN}$ (vol/vol) compared to other anions, such as Cl^- , Br^- , I^- , AcO^- , CN^- , N_3^- and H_2PO_4^- .

When connected with chiral amide groups at terminal units, the similar oligomer **43** could fold into a helical conformation with *M*-handed preference via intramolecular hydrogen bonds between amide oxygens with NH protons of the indolocarbazole rings (Figure 20).⁵⁸ Most interestingly, when sulfate ions were added, the preferred chirality of the helix inverted into *P*-handedness upon the anion binding, as demonstrated by CD spectra and in the X-ray structure. This behavior is unique in that the foldamer interaction with an achiral anion leads to an opposite helical preference.

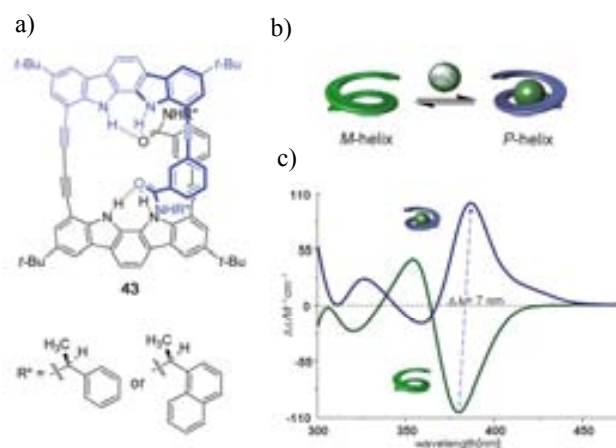


Figure 20. a) Structure of oligomer **43**. b) Scheme of the handedness inversion based on anion binding. c) CD spectra showing the handedness inversion.

Thanks to the highly efficient formation of triazoles by click reactions, oligotriazoles could be used as anion receptors exploiting hydrogen bonds between the electropositive CH side of the

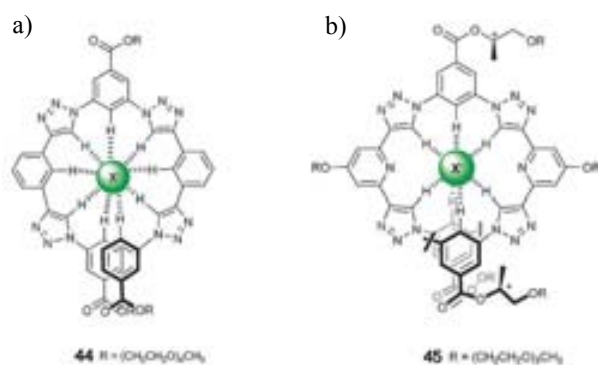


Figure 21. a) Folded structure of oligomer **44** induced by anion binding. b) Folded Structure of oligomer **45** induced by anion binding.

1,4-substituted 1,2,3-triazole ring and electron-rich guests such as anions. In 2008, Craig reported a series of novel 1,4-diaryl-triazole oligomers **44** with ester-solubilizing side chains, which was used as a chloride receptor.⁵⁹ It was shown that the oligomer **44** was in a random coil conformation due to the flexibility of aryl-triazole single bond. However, the C-H chloride bond could induce the oligomer to fold into a helical structure (Figure 21a). The complex was evidenced by the downfield shift of the 1,2,3-triazole protons, and an upfield shift of the aryl protons due to aromatic stacking. The complexation was further proven by ROESY experiments where NOE cross peaks had been observed between the protons converging toward the helix cavity in the presence of chloride. It was evidenced that the oligomer forms 1:1 complexes with chloride; association constants in acetone

were determined to be $1.7 \times 10^4 \text{ M}^{-1}$. Hecht and coworkers independently synthesized oligomer **45** with chiral side-chains by alternating pyridine and aryl-1,2,3-triazole moieties (Figure 21b).⁶⁰ Dipole–dipole repulsion between the heterocycles enables **45** to adopt a two-turn helical conformation in water–acetonitrile mixture that is further stabilized by π -stacking of the overlapped strand and solvophobic effects. The presence of the chiral side chains induced the foldamer **45** to generate CD signals. Interestingly, the addition of HCl did not result in denaturation of the helical conformation, but rather an inversion of the CD signals. At neutral pH, such an inversion could also be realized by adding KCl or KBr, even the intensity caused by KCl was not so high. Instead, KF did not cause the inversion. It was hypothesized that the halide interaction with the chiral ethylene glycol side chains of **45** transferred helicity to the aromatic backbone, thus resulting in an inversion between left- and right-handed helicity.

Using similar design principles of alternating meta-phenyl groups with 1,2,3-triazoles, Flood and Jiang independently have reported the oligotriazole **46** and **47** coupled with photoswitchable azobenzene groups (Figure 22).^{61,62} These oligomers adopted helical conformations with a cavity suited for anions in polar solvents via solvophobic effect. The behavior of binding anions could be controlled by light. From these reports it is clear that 1,2,3-triazoles are useful building blocks for foldamers as anion receptors due to their ease of synthesis, and also due to their inherent electronic (strong dipole, electropositive CH), and structural (planar, π -rich) properties.

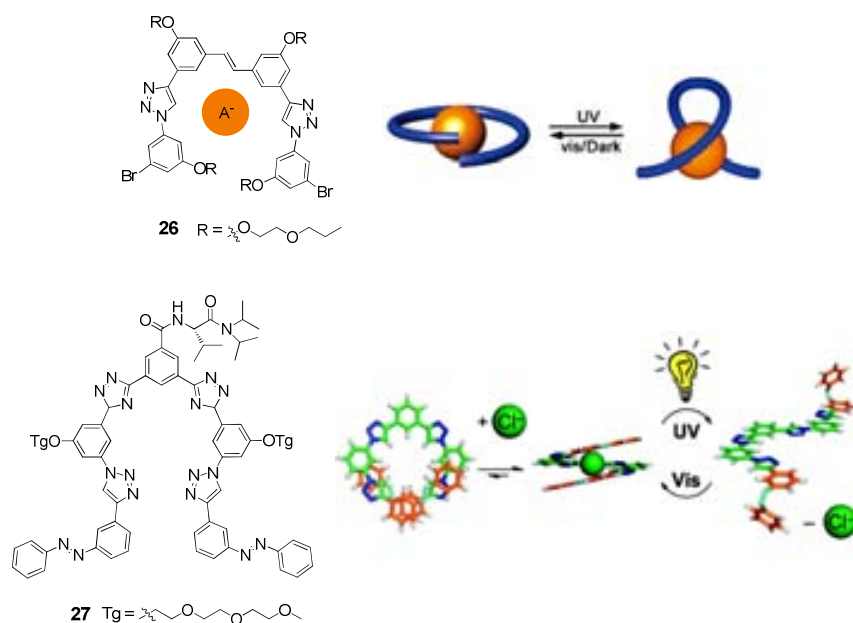


Figure 22. Structures and schemes of oligomers **46** and **47** binding anions by using light as a trigger

Besides inorganic anions, organic anions can also be recognized by foldamers. Li et al. designed a class of oligomers **48a-d**, which consisted of alternate benzene and naphthalene segments (Figure 23).⁶³ Modeling studied suggested that **48c** formed a folded structure with a cavity that was large enough to host a 1,3,5-tricarboxylate anion **49**. The long oligomer **48d** did not adopt defined conformations in DMSO, even though the large stacking naphthalene units were available. However, these oligomers could fold into compact helical structures completely in the presence of **49**, as evidenced by ¹H NMR, fluorescence and UV-Vis experiments. ¹H NMR studies showed that a new set of signals of low field was exhibited, while the signals of the free oligomers themselves disappeared completely upon addition of ca. one equivalent of **49**. The bindings for **49** were shown to be in a 1:1 stoichiometry for all the complexes by ¹H NMR and UV-Vis experiments, and the binding constants were determined to be in the range of 10⁴-10⁶ M⁻¹ in DMSO. The complexes were further proven by the NOESY experiments, in which relative multiple intermolecular NOE cross-peaks were observed. It was thus revealed that the folded conformations were induced by intermolecular N-H...O⁻ and C-H...O⁻ hydrogen bonds or electrostatic interactions between the amide and aromatic hydrogen atoms of the oligomers and the oxygen atoms of the anion.

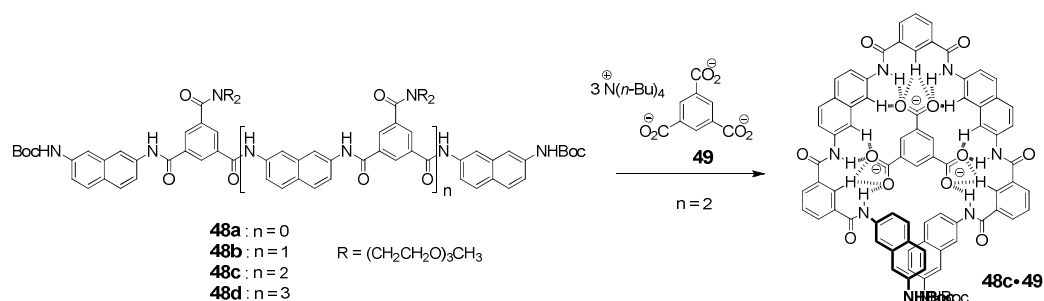


Figure 23. The structure of oligomers **48** and guest **49** stabilized by hydrogen bond

5. Conclusion

In the last decade, a large number of synthetic foldamers with recognition behaviours have been researched. The tunable versatility and flexibility of these structures make them suitable models for accommodating guests, as well as accompanying corresponding functions.

Despite the progress made so far, the research field is still in its early stages. We suggest several aspects that we think are worthy to receive more attention or to be addressed in the future: 1) new families of backbones, and structures of larger size and complexity will certainly be continued; 2) development of selective recognition in a series of guests by exchanging certain units in the foldamer receptor are also worth researching; 3) the broader applications in supramolecular devices, such as catalysis, sensors, and drug-delivery, are also expected.

6. References

- 1 C. J. Pedersen, Cyclic polyethers and their complexes with metal salts. *J. Am. Chem. Soc.*, **1967**, *89*, 7017–7036.
- 2 J. W. Lee, S. Samal, N. Selvapalam, H.-J. Kim, K. Kim, Cucurbituril homologues and derivatives: new opportunities in supramolecular chemistry. *Acc. Chem. Res.*, **2003**, *36*, 621–630.
- 3 M.-X. Wang, Heterocalixaromatics, new generation macrocyclic host molecules in supramolecular chemistry. *Chem. Commun.*, **2008**, 4541–4551.
- 4 M. Xue, Y. Yang, X. Chi, Z. Zhang, F. Huang, Pillararenes, a new class of macrocycles for supramolecular chemistry. *Acc. Chem. Res.*, **2012**, *45*, 1294–1308.
- 5 L. Isaacs, Cucurbit[n]urils: from mechanism to structure and function. *Chem. Commun.*, **2009**, 619–629.
- 6 J. F. Stoddart, The chemistry of the mechanical bond. *Chem. Soc. Rev.*, **2009**, *38*, 1802–1820.
- 7 S. Hecht, I. Huc, Foldamers: structure, properties and applications, Wiley-VCH, Weinheim, **2007**.
- 8 R. P. Cheng, S. H. Gellman, W. F. DeGrado, α -Peptides: from structure to function. *Chem. Rev.*, **2001**, *101*, 3219–3232.
- 9 A. R. Sanford, B. Gong, Evolution of helical foldamers. *Curr. Org. Chem.*, **2003**, *7*, 1649–1659.
- 10 I. Huc, Aromatic oligoamide foldamers. *Eur. J. Org. Chem.*, **2004**, 17–29.
- 11 Z.-T. Li, J.-L. Hou, C. Li, Peptide mimics by linear arylamides: a structural and functional diversity test. *Acc. Chem. Res.*, **2008**, *41*, 1343–1353.
- 12 B. Gong, Hollow crescents, helices, and macrocycles from enforced folding and folding-assisted macrocyclization. *Acc. Chem. Res.*, **2008**, *41*, 1376–1386.
- 13 W. S. Horne, S. H. Gellman, Foldamers with heterogeneous backbones. *Acc. Chem. Res.*, **2008**, *41*, 1399–1408.
- 14 I. Saraogi, A. D. Hamilton, Recent advances in the development of aryl-based foldamers. *Chem. Soc. Rev.*, **2009**, *38*, 1726–1743.
- 15 C. M. Goodman, S. Choi, S. Shandler, W. F. DeGrado, Foldamers as versatile frameworks for the design and evolution of function. *Nature Chem. Biol.*, **2007**, *3*, 252–262.
- 16 H. Juwarker, J.-M. Suk, K.-S. Jeong, Foldamers with helical cavities for binding complementary guests. *Chem. Soc. Rev.*, **2009**, *38*, 3316–3325.
- 17 J. Garric, J. M. Leger, I. Huc, Molecular apple peels. *Angew. Chem. Int. Ed.*, **2005**, *44*, 1954–1958.
- 18 W. Q. Ong, H. Zhao, X. Fang, S. Woen, F. Zhou, W. Yap, H. Su, Sam F. Y. Li, H. Zeng, Encapsulation of conventional and unconventional water dimers by water-binding foldamers. *Org. Lett.*, **2011**, *13*, 3194–3197.
- 19 J. Garric, J.-M. Leger, I. Huc, Encapsulation of small polar guests in molecular apple peels. *Chem. Eur. J.*, **2007**, *13*, 8454–8462.
- 20 C. Bao, B. Kauffmann, Q. Gan, K. Srinivas, H. Jiang, I. Huc, Converting sequences of aromatic amino acid monomers into function: second generation helical capsules. *Angew. Chem. Int. Ed.*, **2008**, *47*, 4153–4156.
- 21 H. Jiang, J.-M. Léger, I. Huc, Aromatic δ -peptides. *J. Am. Chem. Soc.*, **2003**, *125*, 3448–3449.
- 22 Q. Gan, C. Bao, B. Kauffmann, A. Grélard, J. Xiang, S. Liu, I. Huc, H. Jiang, Quadruple and double helices of 8-fluoroquinoline oligoamides. *Angew. Chem. Int. Ed.*, **2008**, *47*, 1715–1718.
- 23 C. Bao, Q. Gan, B. Kauffmann, H. Jiang, I. Huc, Self-assembled foldamer capsule: combining single and double helical segments in one aromatic amide sequence. *Chem. Eur. J.*, **2009**, *15*, 11530–11536.
- 24 V. Berl, M. J. Krische, I. Huc, J.-M. Lehn, M. Schmutz, Template-induced and molecular recognition directed hierarchical generation of supramolecular assemblies from molecular strands. *Chem. Eur. J.*, **2000**, *6*,

1938–1946.

- 25 J.-L. Hou, X.-B. Shao, G.-J. Chen, Y.-X. Zhou, X.-K. Jiang, Z.-T. Li, Hydrogen bonded oligohydrazide foldamers and their recognition for saccharides. *J. Am. Chem. Soc.*, **2004**, *126*, 12386–12394.
- 26 W. Cai, G.-T. Wang, P. Du, R.-X. Wang, X.-K. Jiang, Z.-T. Li, Foldamer organogels: a circular dichroism study of glucose-mediated dynamic helicity induction and amplification. *J. Am. Chem. Soc.*, **2008**, *130*, 13450–13459.
- 27 C. Li, G.-T. Wang, H.-P. Yi, X.-K. Jiang, Z.-T. Li, R.-X. Wang, Diastereomeric recognition of chiral foldamer receptors for chiral glucoses. *Org. Lett.*, **2007**, *9*, 1797–1800.
- 28 H.-P. Yi, X.-B. Shao, J.-L. Hou, C. Li, X.-K. Jiang, Z.-T. Li, Hydrogen-bonding-mediated oligoanthranilamide foldamer receptors that efficiently bind a triol and saccharides in chloroform. *New J. Chem.*, **2005**, *29*, 1213–1218.
- 29 M. Inouye, M. Waki, H. Abe, Saccharide-dependent induction of chiral helicity in achiral synthetic hydrogen-bonding oligomers. *J. Am. Chem. Soc.*, **2004**, *126*, 2022–2027.
- 30 S. Takashima, H. Abe and M. Inouye. Copper(II)/phenanthroline-mediated CD-enhancement and chiral memory effect on a meta-ethynylpyridine oligomer. *Chem. Commun.*, **2012**, *48*, 3330–3332.
- 31 M. Waki, H. Abe, M. Inouye, Helix formation in synthetic polymers by hydrogen bonding with native saccharides in protic media. *Chem. Eur. J.*, **2006**, *12*, 7839–7847.
- 32 M. Waki, H. Abe, M. Inouye, Translation of mutarotation into induced circular dichroism signals through helix inversion of host polymers. *Angew. Chem. Int. Ed.*, **2007**, *46*, 3059–3061.
- 33 H. Abe, N. Masuda, M. Waki, M. Inouye, Regulation of saccharide binding with basic poly(ethynylpyridine)s by H⁺-induced helix formation. *J. Am. Chem. Soc.*, **2005**, *127*, 16189–16196.
- 34 H. Abe, D. Murayama, F. Kayamori, M. Inouye, Saccharide-linked ethynylpyridine oligomers: primary structures encode chiral helices. *Macromolecules*, **2008**, *41*, 6903–6909.
- 35 Y. Ferrand, A. M. Kendhale, B. Kauffmann, A. Grélard, C. Marie, V. Blot, M. Pipelier, D. Dubreuil, I. Huc, Diastereoselective encapsulation of tartaric acid by a helical aromatic oligoamide, *J. Am. Chem. Soc.* **2010**, *132*, 7858–7859.
- 36 Y. Ferrand, N. Chandramouli, A. M. Kendhale, C. Aube, B. Kauffmann, A. Grélard, M. Laguerre, D. Dubreuil, I. Huc, Long-range effects on the capture and release of a chiral guest by a helical molecular capsule. *J. Am. Chem. Soc.*, **2012**, *134*, 11282–11288.
- 37 J. C. Nelson, J.G. Saven, J.S. Moore, P.G. Wolynes, Solvophobic driven folding of nonbiological oligomers. *Science*, **1997**, *277*, 1793–1796
- 38 R. B. Prince, S. A. Barnes, J. S. Moore, Foldamer-based molecular recognition. *J. Am. Chem. Soc.*, **2000**, *122*, 2758–2762.
- 39 M. T. Stone, J. S. Moore, A water-soluble *m*-phenylene ethynylene foldamer. *Org. Lett.*, **2004**, *6*, 469–4712.
- 40 A. Tanatani, M. J. Mio, J. S. Moore, Chain length-dependent affinity of helical foldamers for a rodlike guest. *J. Am. Chem. Soc.*, **2001**, *123*, 1792–1793.
- 41 A. Tanatani, T. S. Hughes, J. S. Moore, Foldamers as dynamic receptors: probing the mechanism of molecular association between helical oligomers and rodlike ligands. *Angew. Chem. Int. Ed.*, **2002**, *41*, 325–328.
- 42 L.-Y. You, S.-G. Chen, X. Zhao, Y. Liu, W.-X. Lan, Y. Zhang, H.-J. Lu, C.-Y. Cao, Z.-T. Li, C–H···O Hydrogen bonding induced triazole foldamers: efficient halogen bonding receptors for organohalogens. *Angew. Chem. Int. Ed.*, **2012**, *57*, 1657–1661.
- 43 D. M. Bassani, J.-M. Lehn, Gerhard Baum, Dieter. Fenske, Designed self-generation of an extended helical structure from an achiral polyheterocyclic strand. *Angew. Chem. Int. Ed.*, **1997**, *36*, 1845–1847.
- 44 A. Petitjean, L.A. Cuccia, J.-M. Lehn, H. Nierengarten, M. Schmutz, Cation-promoted hierarchical formation of supramolecular assemblies of self-organized helical molecular components. *Angew. Chem. Int. Ed.*, **2002**, *41*, 1195–1198.

- 45 A.-M. Stadler, N. Kyritsakas and J.-M. Lehn, Reversible folding/unfolding of linear molecular strands into helical channel-like complexes upon proton-modulated binding and release of metal ions. *Chem. Commun.*, **2004**, 2024–2025.
- 46 R. B. Prince, T. Okada and J. S. Moore, Controlling the secondary structure of nonbiological oligomers with solvophobic and coordination interactions. *Angew. Chem., Int. Ed.*, **1999**, 38, 233–236.
- 47 Y. Zhao, Z. Zhong, Oligomeric cholates: amphiphilic foldamers with nanometer-sized hydrophilic cavities. *J. Am. Chem. Soc.*, **2005**, 127, 17894–17901.
- 48 Y. Zhao, Z. Zhong, Tuning the sensitivity of a foldamer-based mercury sensor by its folding energy. *J. Am. Chem. Soc.*, **2006**, 128, 9988–9989.
- 49 Z. Zhong, Y. Zhao, Cholate-glutamic acid hybrid foldamer and its fluorescent detection of Zn^{2+} . *Org. Lett.*, **2007**, 9, 2891–2894.
- 50 H. Katagiri, T. Miyagawa, Y. Furusho, E. Yashima, Synthesis and optical resolution of a double helicate consisting of ortho-linked hexaphenol strands bridged by spiroborates. *Angew. Chem. Int. Ed.*, **2006**, 45, 1741–1744.
- 51 K. Miwa, Y. Furusho, E. Yashima, Ion-triggered spring-like motion of a double helicate accompanied by anisotropic twisting. *Nature chemistry*, **2010**, 2, 444–449.
- 52 J.-L. Hou, M.-X. Jia, X.-K. Jiang, Z.-T. Li, G.-J. Chen, Solvophobic-driven oligo(Ethylene glycol) helical foldamers. synthesis, characterization, and complexation with ethylene diammonium. *J. Org. Chem.*, **2004**, 69, 6228–6237.
- 53 C. Li, S.-F. Ren, J.-L. Hou, H.-P. Yi, S.-Z. Zhu, X.-K. Jiang, Z.-T. Li, F··H–N hydrogen bonding driven foldamers: efficient receptors for dialkylammonium ions. *Angew. Chem. Int. Ed.*, **2005**, 44, 5725–5729.
- 54 P. R. Ashton, P. J. Campbell, E. J. T. Chrystal, P. T. Glink, P. S. Menzer, D. Philip, N. Spencer, J. F. Stoddart, P. A. Tasker, D. J. Williams, Dialkylammonium ion/crown ether complexes: the forerunners of a new family of interlocked molecules. *Angew. Chem. Int. Ed.*, **1995**, 34, 1865–1869.
- 55 J.-M. Lehn, *Supramolecular chemistry: concepts and perspectives*, VCH, Weinheim, **1995**.
- 56 K.-J. Chang, B.-N. Kang, M.-H. Lee, K.-S. Jeong, Oligoindole-based foldamers with a helical conformation induced by chloride. *J. Am. Chem. Soc.*, **2005**, 127, 12214–12215.
- 57 J.-i. Kim, H. Juwarker, X. Liu, M. S. Lah, K.-S. Jeong, Selective sulfate binding induces helical folding of an indolocarbazole oligomer in solution and solid state. *Chem. Commun.*, **2010**, 764–766.
- 58 J.-m. Suk, V. R. Naidu, X. Liu, M. S. Lah, K.-S. Jeong, A foldamer-based chiroptical molecular switch that displays complete inversion of the helical sense upon anion binding. *J. Am. Chem. Soc.*, **2011**, 133, 13938–13941.
- 59 H. Juwarker, J. M. Lenhardt, D. M. Pham, S. L. Craig, 1,2,3-Triazole $CH\cdots Cl$ contacts guide anion binding and concomitant folding in 1,4-diaryl triazole oligomers. *Angew. Chem. Int. Ed.*, **2008**, 47, 3740–3743.
- 60 R. M. Meudtner, S. Hecht, Helicity inversion in responsive foldamers induced by achiral halide ion guests. *Angew. Chem. Int. Ed.*, **2008**, 47, 4926–4930.
- 61 Y. Wang, F. Bie, H. Jiang, Controlling binding affinities for anions by a photoswitchable foldamer. *Org. Lett.* **2010**, 12, 3630–3633.
- 62 Y. Hua, A. H. Flood, Flipping the switch on chloride concentrations with a light-active foldamer. *J. Am. Chem. Soc.*, **2010**, 132, 12838–12840.
- 63 Xu, Y.-X.; Zhao, X.; Jiang, X.-K.; Li, Z.-T. Helical folding of aromatic amide-based oligomers induced by 1,3,5-benzenetricarboxylate anion in DMSO. *J. Org. Chem.*, **2009**, 74, 7267–7273.

Chapter 2

Foldaxanes: helically folded aromatic oligoamides around dumbbell-shaped molecules

1. Introduction

Biological ‘machines’ play an important role in nature, in that they are clearly indispensable to cellular functions. Two prominent examples are myosin, which moderates muscle contraction, and kinesin, which moves cargo inside cells away from the nucleus along microtubules.¹ All these remarkable behaviours fascinate and inspire scientists to construct artificial compounds that can mimic the functions of their natural counterparts. Over the decades, a wide variety of ingenious molecular machines have been synthesized, including switches, motors, shuttles, “molecular muscles”.²⁻⁸ Most of them are constructed from mechanically-interlocked molecular architectures, such as rotaxanes and catenanes. In rotaxanes, rings are irreversibly locked around rods along which they may slide. In catenanes, interlocked rings may rotate around each another (Figure 1). An important improvement to these designs would use a reversible assembly method to avoid the difficulty of mechanically interlocking molecular components, meanwhile the machines can still work long enough to perform their task, just as biological molecular machines self-assemble and disassemble slowly while their work regime is rapid.



Figure 1. Cartoon representation of a rotaxane and a catenane

Helical architecture is one of the most significant structural motifs observed in biomolecules.⁹ Thus, much effort has recently focused on foldamers, synthetic molecules that can fold into a stable ordered (helical) conformation in solution, to mimic protein-like structures and their distinctive functions. As an example, Moore et al. reported a series of oligomers of *m*-phenylene-ethynylene (*m*PE) that could wind around a dumbbell-shaped guest by solvophobic interactions in a polar medium.¹⁰ These structures resemble rotaxanes in which macrocycles are replaced by helices. It has thus triggered us to design new molecular machines based on aromatic oligoamide foldamers. The following pages describe details this concept.

We have previously shown that the aromatic oligoamide sequence **1** composed of four different monomers (see below) can fold into a robust helical structure which possesses a hollow large enough to bind a linear alkyldiol or diamine such as 1,4-butanediol or 1,4-butanediamine (Figure 2).¹¹ Such constructs proved to completely surround their guests, especially because of

quinoline units present at both extremities of the capsule. The quinoline units act as ‘stoppers’, closing the molecular shell, but also preventing the single helix assembling into a double helix. Without quinoline units, we thus anticipated that the sequence **3** would not only hybridize to the double helix, but also give a chance to open the ‘mouth’ of the helix at each end and thus bind longer guests, typically dumbbell molecules with hydrogen bond acceptor groups.

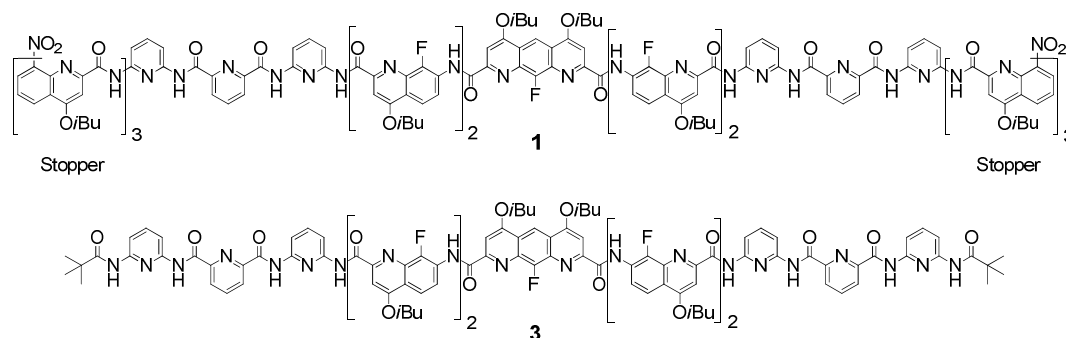


Figure 2. Structures of sequences **1** and **3**

A series of aromatic oligoamide sequences like **3** were designed. It was revealed that they could slowly wind around rod-like guests (Figure 3). The winding process requires helix unfolding and refolding, as well as a strict match between helix length and anchor points (golden balls, figure 3) on the rods. Because the timescale of helical unwinding is relatively slow, the helix can shuttle along the guest without dissociating. This modular design and dynamic assembly open up promising capabilities in molecular machinery.

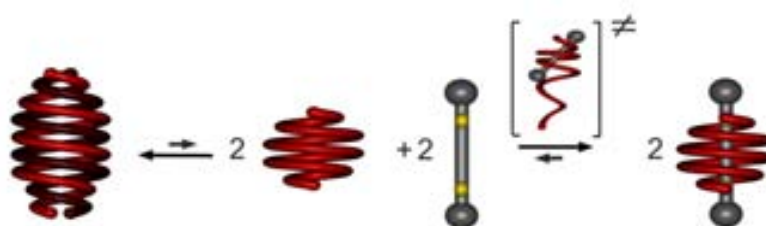


Figure 3. Cartoon representation of the formation of foldaxane: double helix dissociate to single helix, and then single helix winds around rod-like guest via unfolding and refolding mechanism.

2. Synthesis

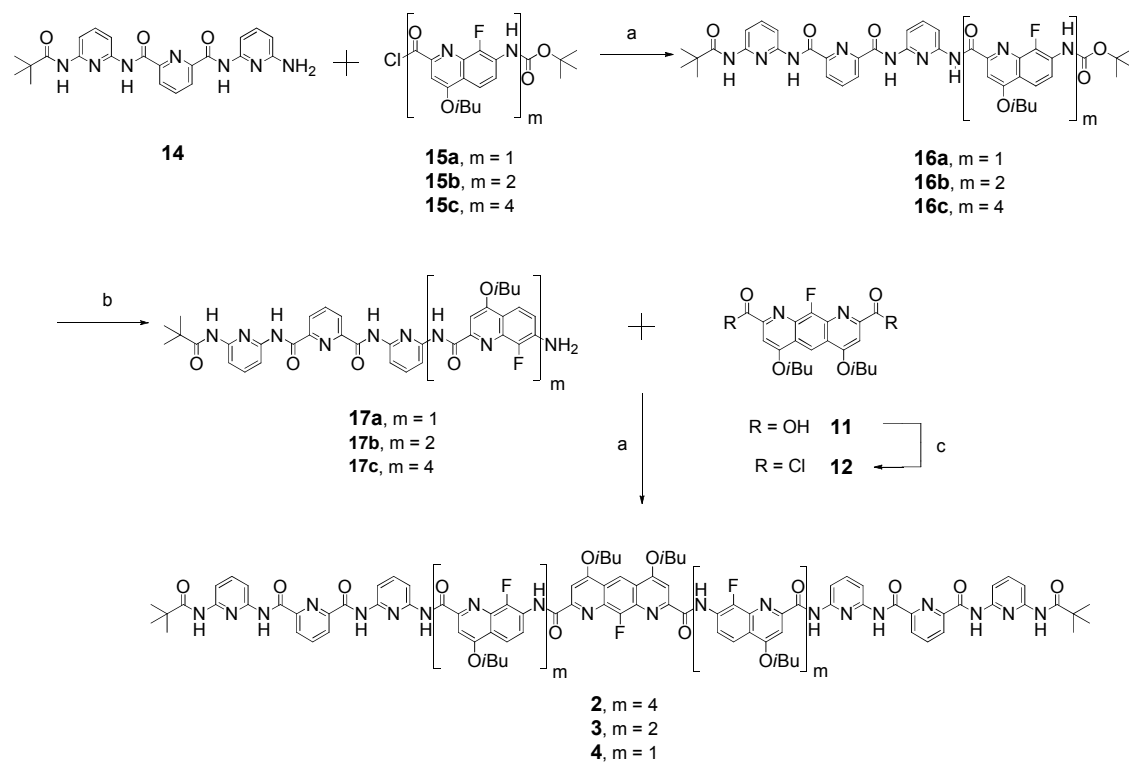
2.1 Synthesis of helices

Aromatic oligoamides **2-4** were designed according to well-established rules^{12,13} to fold into helical structures stabilized by local preferential conformations at aryl-amide linkages and intramolecular interactions between aromatic groups (Scheme 1). They were composed of three different units that have all been characterized: 2,6-diaminopyridine and 2,6-pyridinedicarboxylic acid (**P**),¹⁴⁻¹⁶ 7-amino-8-fluoro-2-quinolinecarboxylic acid (**Q^f**),¹⁷ and 1,8-diaza-9-fluoro-2,7-anthracene-dicarboxylic acid (**A^f**).¹¹ Based on studies of related compounds,^{11,18,19} it was predicted that the fluoroaromatic units in the center of the sequence would form a helix wide enough to accommodate an alkyl chain but nothing much larger, whilst each peripheral 2,6-pyridinedicarboxamide units are hydrogen bond donors and may thus act as anchor points to bind a guest at a defined position in the helix cavity.

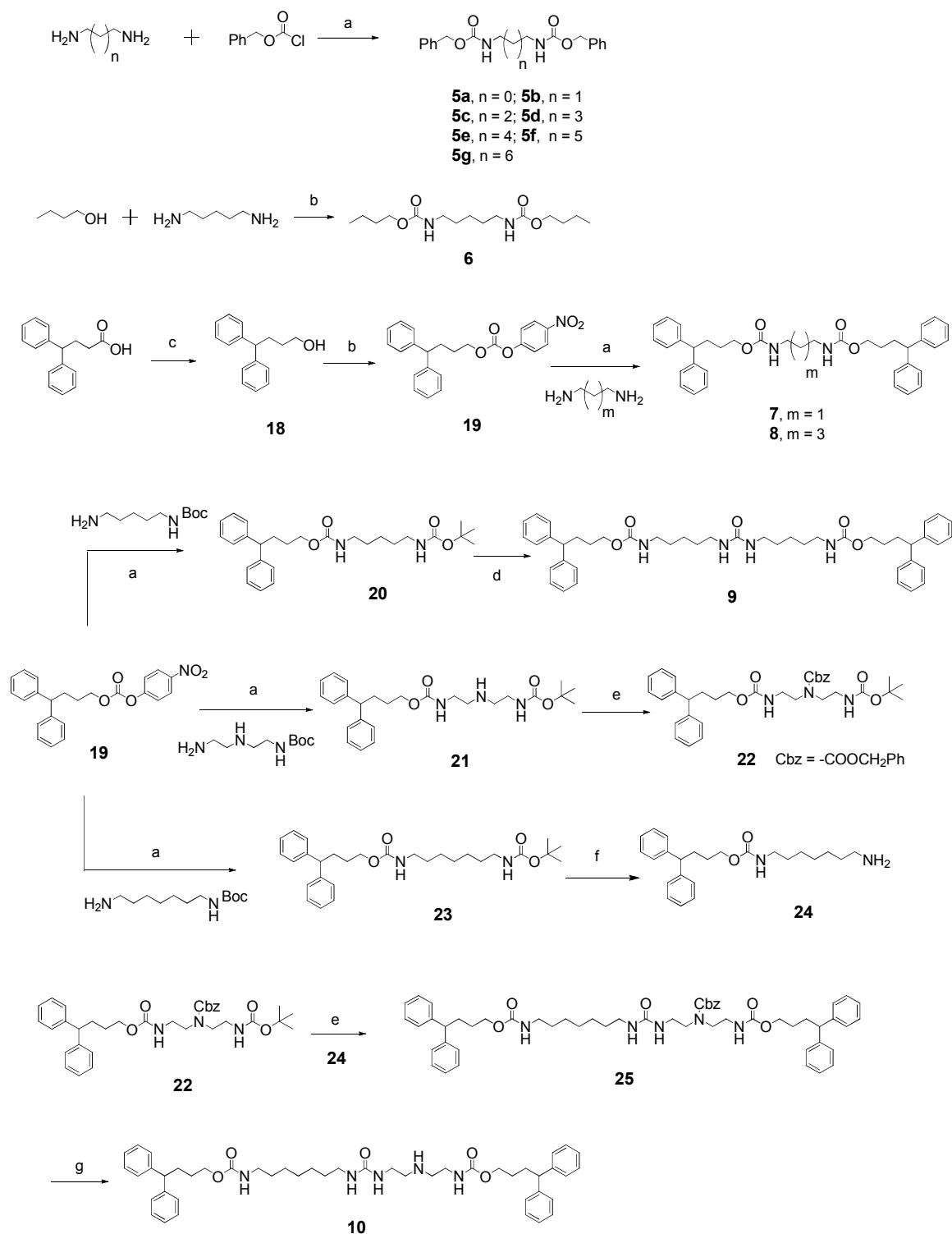
The procedures for the synthesis of aromatic oligoamides **2-4** via a convergent approach are depicted in Scheme 1. There is one criterion for the synthesis of these capsule-shaped sequences: in order to avoid the aggregation of early synthetic segments, which may reduce their reactivity in subsequent steps, the order of coupling units should be carried out from the sequence termini to its center, that is, from **P** monomer to **A^f** monomer. Precursor **16** was obtained by coupling the trimer **P₃** **14** and **Q^f** segments of different length. The Boc group was subsequently cleaved using TFA, affording the corresponding amine **17**. In a final step, the activation of diacid **11** was carried out in the presence of Ghosez reagent to generate diacid chloride **12** which was directly coupled with monoamine **17** to generate the target products **2-4**.

2.2 Synthesis of guests

The dumbbell-shaped guests **5a-5g** were synthesized through the reaction of benzyl chloroformate with the corresponding diamines. The guest **6** with non-bulky groups at the end was obtained via activation of *n*-butanol with 4-nitrophenyl chloroformate, and subsequent coupling to 1,5-diaminopentane. The synthetic procedures for guests **7-10** were similar to that of guest **6**: first activation of the alcohol to get the carbonate intermediate, and then reaction with the corresponding amine. Details are shown in Scheme 2.



Scheme 1. The synthesis of foldamers **2-4**: a) DIEA, DCM, r.t.; b) TFA, DCM, r.t.; c) 1-chloro-*N,N,2*-trimethylpropenylamine, CHCl_3 , r.t., 2 h.



Scheme 2. The synthesis of guests **5-10**: a) DIEA, DCM, r.t.; b) 4-nitrophenyl chloroformate, TEA, DCM, r.t.; c) LiAlH₄, THF, r.t.; d) TFA, DCM, r.t., then, 4-nitrophenyl chloroformate, TEA, DCM, r.t.; e) benzyl chloroformate, DCM, r.t.; f) TFA, DCM, r.t.; g) Pd/C, H₂, EtOAc.

3. Results and discussion

3.1 Hybridization behavior of foldamers 2-4

The foldamers **2-4** have very similar structures: they are all made up of the four different monomer units, and their sequence only differs in the number of Q^f units (Figure 4). Increasing strand length (from **4** to **2**) allows one to adjust the distance between the binding anchor points (P_3) along the helix axis and their relative orientation in a plane perpendicular to the helix axis. It also determines the timescale of helix unfolding and refolding dynamics, which may range from fractions of seconds, to minutes, to hours or even days for multiturn helices.²⁰

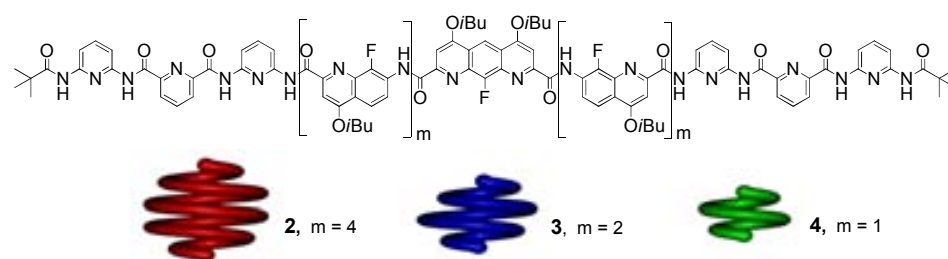


Figure 4. Structures of foldamers **2-4**

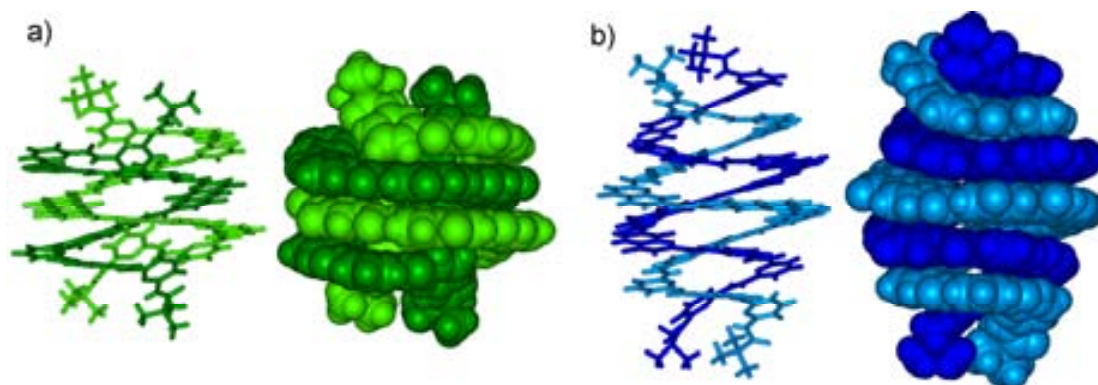


Figure 5. Crystal structures of a) double helix (**4**)₂ and b) double helix (**3**)₂ in tube and CPK representation. Isobutyl side chains and solvent molecules have been omitted for clarity.

As mentioned above, without quinoline units (Q) at the extremities, the foldamers **2-4** fold into single helical conformers which then aggregate to form helical duplexes.²¹ The structures of the double helices (**3**)₂ and (**4**)₂ have been characterized in the solid state by x-ray crystallography (Figure 5). In solution, there is only one set of broad peaks that can be detected at equilibrium at 25°C by Nuclear Magnetic Resonance (NMR), even at low concentration. We deduced that only double helical conformations of **2-4** exist in these conditions. However, heating to 80 °C in

CD_2Cl_4 , some new signals appear at low field, indicating that some duplexes have dissociated into single helices (Figure 6).¹³ Under these conditions, integration signals of the single and double helix gives a measure of the dimerization constants K_{dim} : 2.8×10^5 , 6.4×10^5 and $>10^6 \text{ L}\cdot\text{mol}^{-1}$ for **2**, **3**, and **4**, respectively (Figure 7).

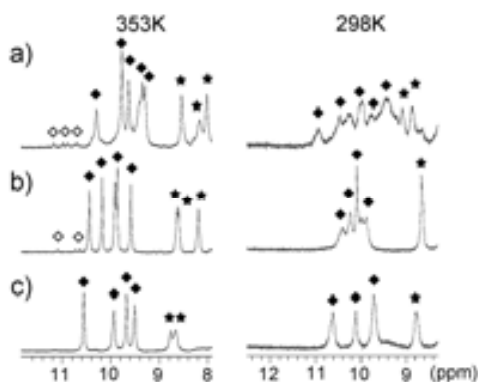
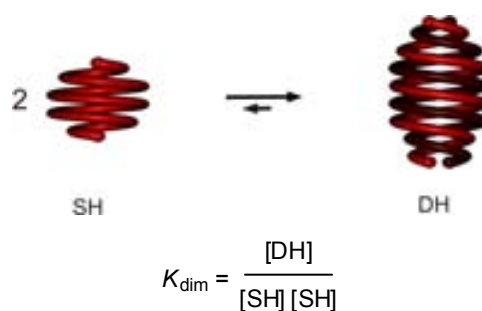


Figure 6. Excerpts of the ^1H NMR spectra of a) 15-mer **2**; b) 11-mer **3**; c) 9-mer **4** at 2 mM in $\text{C}_2\text{D}_2\text{Cl}_4$ at 80°C (left) and 25°C (right). Amide signals of the double helix are marked with black diamonds whereas those of the single helix which are in slow exchange on the NMR timescale are represented with white diamonds. A few aromatic resonances are marked with stars.



[SH] = single helix concentration
[DH] = double helix concentration

Figure 7. Scheme of calculation of the dimerization constant K_{dim}

3.2 The thermodynamics of the host-guest complexes

The foldamers **2-4** have different lengths (i.e., different number of Q^f units), but the same recognition site (P units). Thus, the length of guests should also be different to match helix length. Anticipating this, we prepared a range of rod-shaped guests, **5a** to **5g**, incorporating a successive number of methylene units. Each guest has two carbamate groups on both sides, which could act as hydrogen bond acceptors to anchor the pyridine dicarboxamide units of the foldamers.

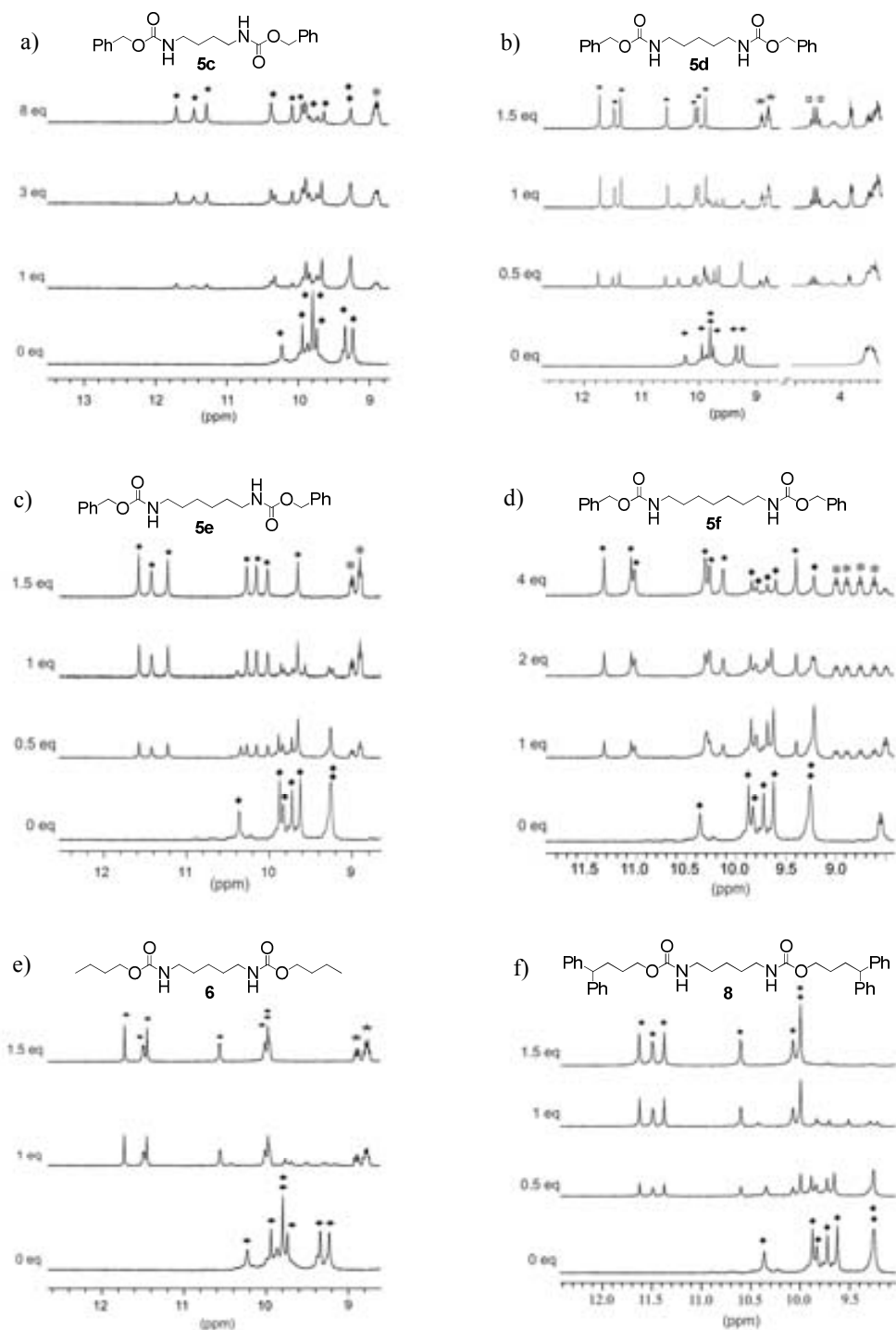


Figure 8. Representative 400 MHz NMR spectra of **2** (2 mM) in CDCl_3 at 318K titrated with various guests. Amide signals of the double helix and foldaxane are marked with black diamonds and black circles, respectively. Aromatic proton resonances are marked with stars. At higher field (~ 4.3 ppm), one can see a diastereotopic pattern (due to the chiral environment of the helix) corresponding to benzylic $-\text{CH}_2$ of the guest (white squares).

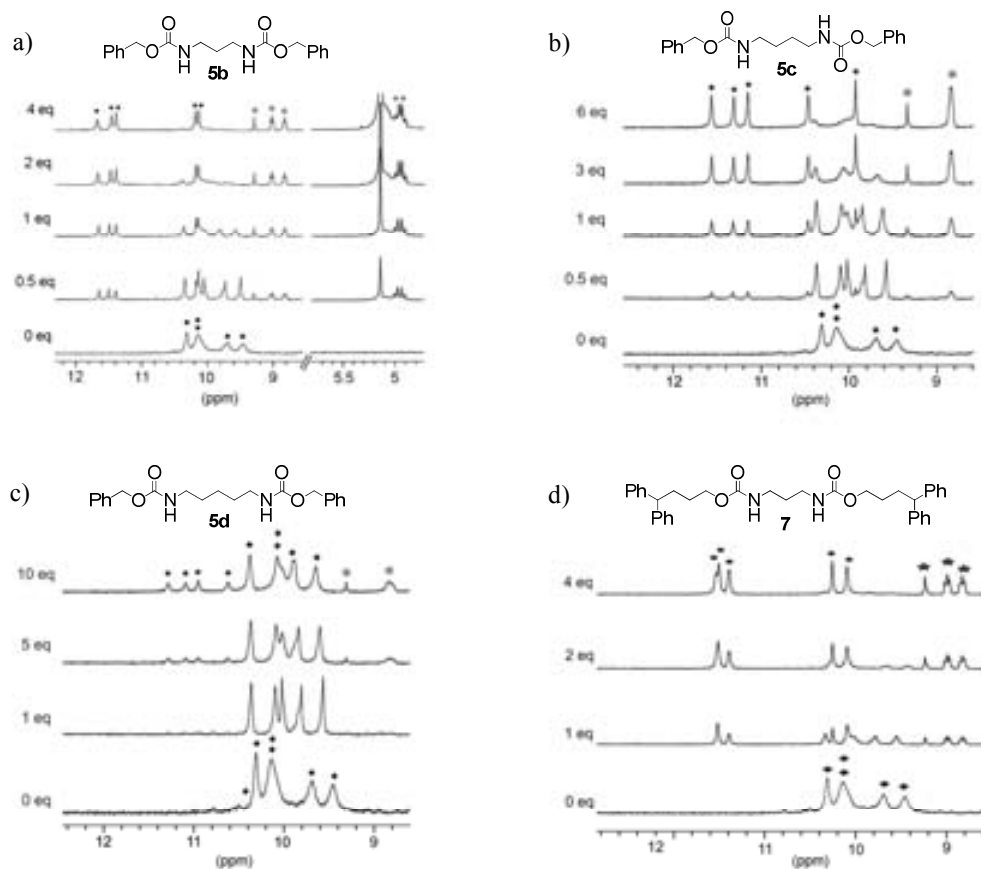


Figure 9. Representative 400 MHz NMR spectra of **3** (2 mM) in CDCl_3 at 318K titrated with various guests. Amide signals of the double helix and foldaxane are marked with black diamond and black circles, respectively. Aromatic proton resonances are marked with stars. At higher field (~ 4.9 ppm), one can see a diastereotopic pattern (due to the chiral environment of the helix) corresponding to benzylic $-\text{CH}_2-$ of the guest (white squares).

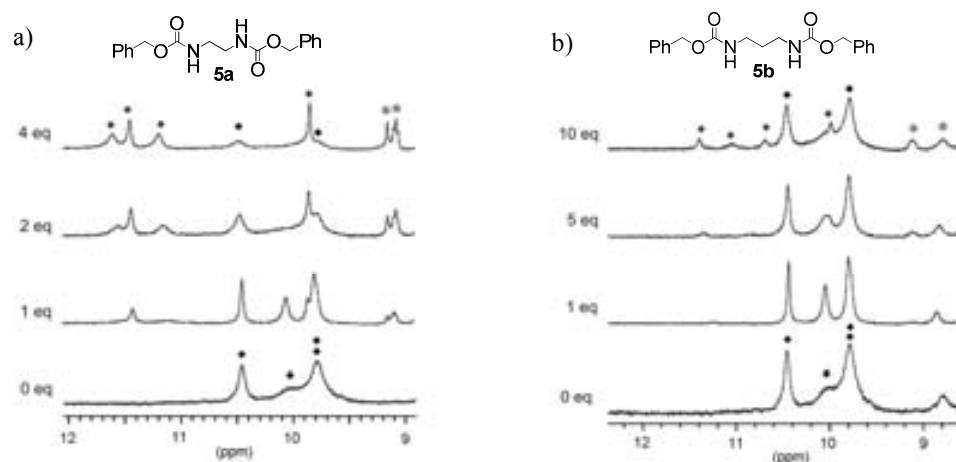


Figure 10. Representative 400 MHz NMR spectra of **4** (2 mM) in CDCl_3 at 318K titrated with various guests. Amide signals of the double helix and foldaxane are marked with black diamonds and black circles, respectively. Aromatic proton resonances are marked with stars.

Upon adding each rod-like molecule **5a-g** to a solution of **2**, **3** or **4**, the NMR signals of the duplexes in some cases disappeared and a new species emerged corresponding to a complex in which a single helix is wound around a rod-like guest (Figure 3). Aromatic signals of the complexes are shifted downfield compared to those of the double helices, indicating weaker ring current effects and thus less extensive π -stacking to that expected in the single helix. In addition, some of the guest protons become diastereotopic in complexes due to the chiral environment of the helix (Figure 8-10). Because the kinetics of host-guest complex formation can be extremely slow at room temperature (see below), all titrations were carried out at 45°C, and the spectra are showed in Figure 8-10. The binding constants K_a , listed in table 1, could be calculated between double helix and host-guest complex by integration of the corresponding signals (Figure 11).

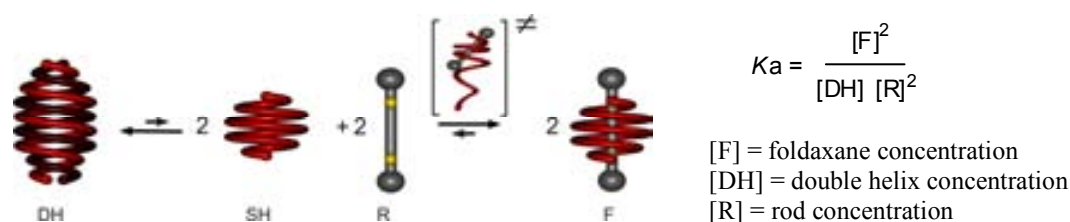


Figure 11. Schematic representation of foldaxane formation and the equation used for the calculation of the association constant K_a

Table 1. Titration of oligomers **2**, **3** and **4** by different dumbbell molecules monitored by Nuclear Magnetic Resonance (400 MHz) in $CDCl_3$ at 318K. Dashes reflect no measurable affinity of the oligomers for the rods. All experimental errors < 5%.

	5a	5b	5c	5d	5e	5f	5g	6	7	8
2	-	nd	45 (± 2)	31000 (± 1000)	22000 (± 300)	140 (± 5)	nd	33000 (± 1300)	-	30000 (± 1400)
3	nd	1000 (± 40)	90 (± 3)	nd	-	-	-	-	1000 (± 35)	-
4	150 (± 20)	< 1	-	-	-	-	-	-	-	-

The stoichiometry and structure of these complexes can also be assessed by other techniques, such as nuclear Overhauser effect (NOE) and Diffusion Ordered Spectroscopy (DOSY) NMR,²² mass spectrometry and X-ray crystallography, i.e., in solution, in the gas phase, and the solid state, respectively. In solution, multiple intermolecular nuclear Overhauser effect (NOE) correlations are observed between aromatic amide protons of the helices and aliphatic

alkyl protons of the guests (Figure 12); and Diffusion Ordered Spectroscopy (DOSY) shows that the diffusion coefficient of the complex of **2**⊃**6** is similar to (but slightly higher than) that of the double helix; these were calculated to be $5.61 \times 10^{-10} \text{ m}^2 \text{ s}^{-1}$ for complex of **2**⊃**6** and $4.86 \times 10^{-10} \text{ m}^2 \text{ s}^{-1}$ for the double helix (Figure 13). This means the structure of the complex is smaller than that of the double helix, according to the Stokes-Einstein equation.

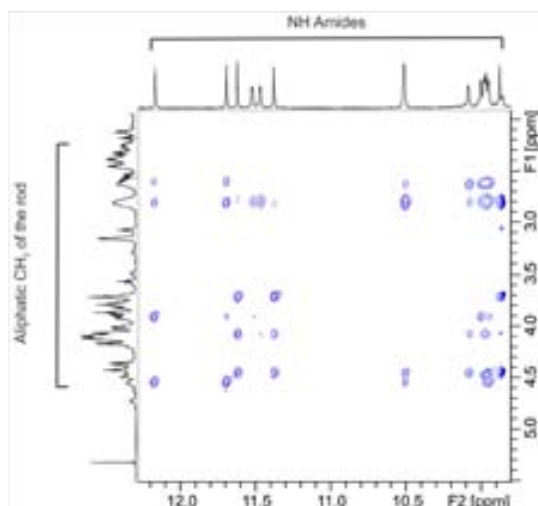


Figure 12. Expansion from the ^1H - ^1H ROESY spectrum (700 MHz) of **2**⊃**9** (4 mM each) in CDCl_3 , showing intermolecular correlations. These cross peaks correlate between aromatic amide protons of the helix and aliphatic alkyl protons of the guests.

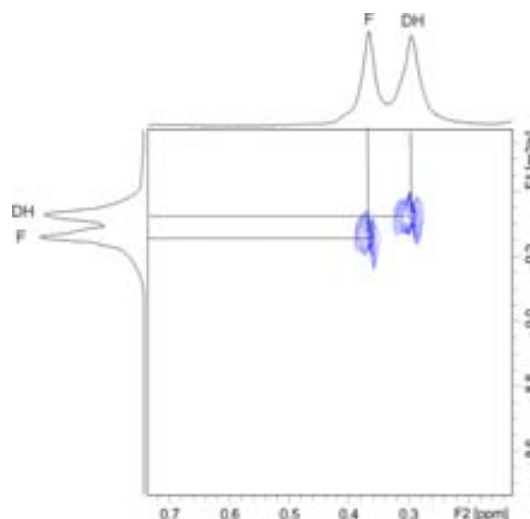


Figure 13. Zoom of ^1H DOSY NMR spectrum (400 MHz) of a mixture of **2** and **6** at 4 mM in CDCl_3 (298K) showing the terminal pivaloyl groups of both double helix (**1**)₂ (DH) and foldaxane **2**⊃**6** (F).

Both mass spectrometry and thin layer chromatography (TLC) confirmed that the complexes had been generated (Figure 14 and 15).

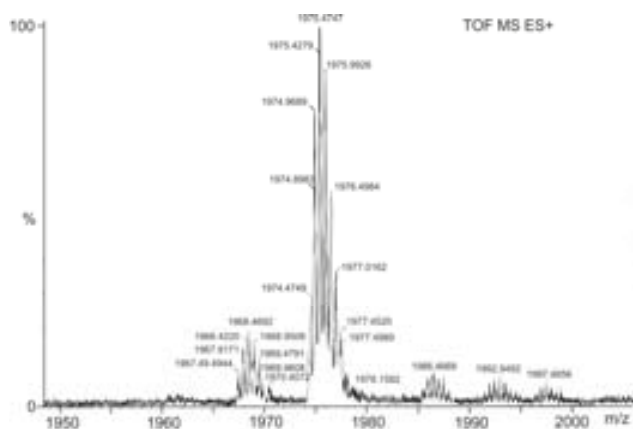


Figure 14. Electrospray mass spectrum of foldaxane **2D8**. MS (ES⁺): m/z calcd for $C_{217}H_{221}F_9N_{34}O_3$ [**2D8**+2H]²⁺ 1976.8334 found 1975.5; m/z calcd for [**2D8**+H+Na]²⁺ $C_{217}H_{220}F_9N_{34}O_3Na$ 1987.8244 found 1986.5.

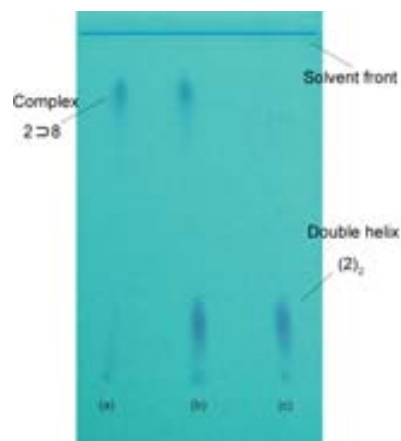


Figure 15. Photograph of a thin layer chromatography (EtOAc/CH₂Cl₂:10/90) of: a) foldaxane **2D8** (R_f = 0.79); b) a co-spot of foldaxane **2D8** and double helix (**2**)₂; c) double helix (**2**)₂ (R_f = 0.11).

In the solid state, crystal structures of **3D7**, **2D8**, **2D6** all show that a single helix winds around a guest, and the 2,6-pyridinedicarboxamide units of the helix hydrogen bond to the carbonyl groups of the guest (Figure 16). It follows that the complexes form only when the helix and the guest match in length with a tolerance of, at most, one CH₂ unit of the guest (table 1). This trend may be extended to even longer helices, demonstrating a high modularity in space of this system. Remarkably, the affinity of the single helices for their guests is clearly high enough to overcome their strong propensity to form double helices. In fact, the dimerization constant K_{dim} and equilibrium constant K_a of host-guest formation (estimated as mentioned above actually) are comparable. However, the overall equilibrium shows that the helix dimerization constant K_{dim} is in balance with the square of the rod-helix equilibrium constant K from the single helix (Figure 17). This is facilitated by the fact that it takes two strands to form a duplex and only one to form a host-guest complex. Therefore, the equilibrium constant K_a of host-guest formation largely prevails even though thermodynamic parameters do not differ so much from dimerization constant K_{dim} .

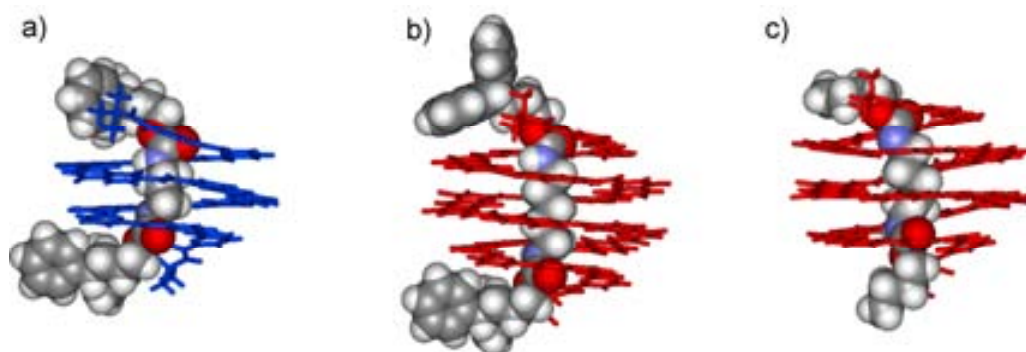


Figure 16. Crystal structures of a) complex 3⊃7; b) complex 2⊃8; c) complex 2⊃6. Isobutyl side chains and solvent molecules have been omitted for clarity.

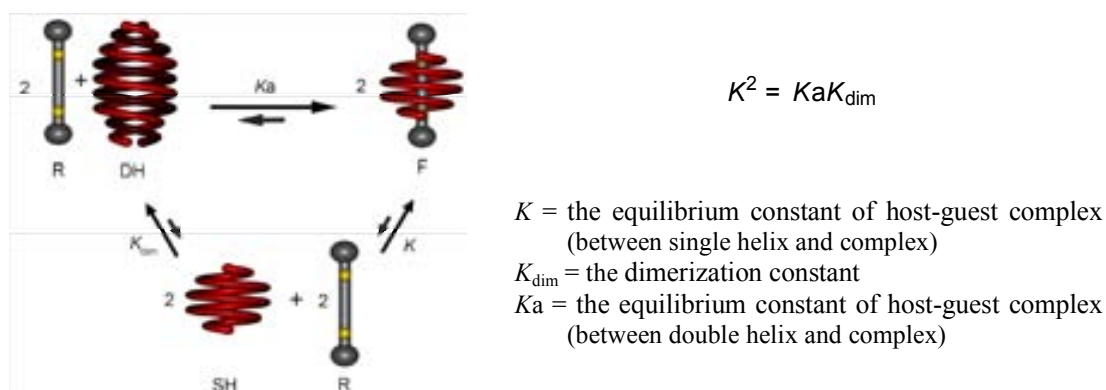


Figure 17. Schematic representation of the overall equilibrium between the single, double helix and the complex.

3.3 The kinetics of association and dissociation of the host-guest complex

The complexes between the shortest oligomers **3** and **4** and their respective guests form readily at 25 °C. However, complexes involving **2** do not form even after days unless the mixture undergoes a heating-cooling cycle. The reasons lie in slow kinetics of complex formation from the single helix and in very slow kinetics of double helix dissociation into single helices.²¹ The pure single helical conformer of **2** could be fortuitously isolated by selective precipitation from methanol even though it constitutes a minor component in solution. Upon dissolving it again in CDCl₃, the double helix slowly forms over 24 h at 2 mM concentration if no guest is present (Figure 18). However, in the presence of **8**, which possesses bulky end groups, the complex 2⊃8 forms at 25 °C over the course of 30 min, which allowed us to estimate a kinetic second order rate constant k_1 of host-guest complex formation of about 2.25 M⁻¹s⁻¹ (Figure 19).

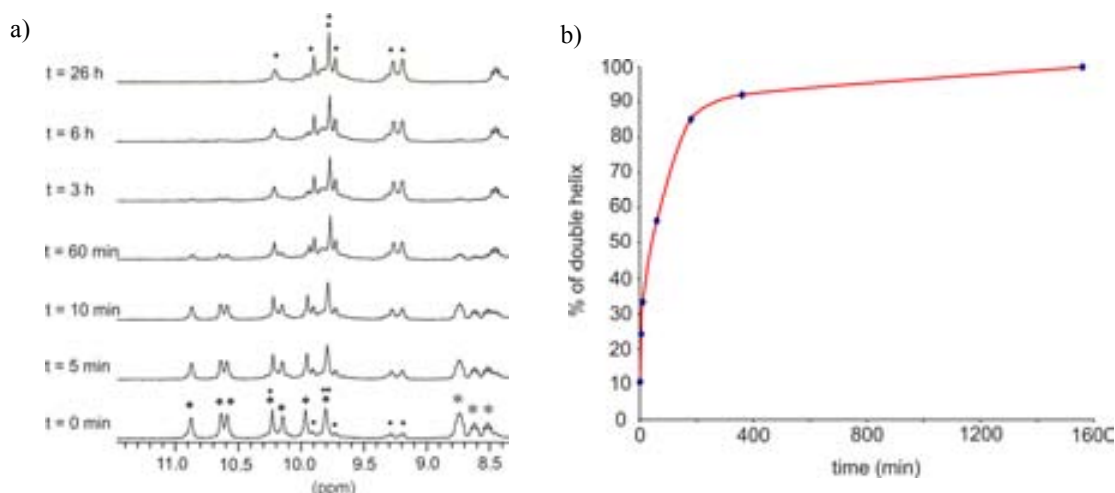


Figure 18. a) Excerpts of the ¹H NMR spectra (300 MHz) showing the formation of double helix from a 2 mM solution of single helix **2**. The selected window presents the amide resonances as a function of time (t). Single helix of **2** was dissolved in CDCl₃ then spectra were instantaneously recorded at 298K. Amide signals of the double helix are marked with black diamonds whereas those of the single helix (which are in slow exchange on the NMR timescale) are represented with white diamonds. A few aromatic resonances are marked with stars. b) Time trace of duplex hybridization of a 2 mM solution of **2** in CDCl₃ monitored by ¹H NMR at 298K.

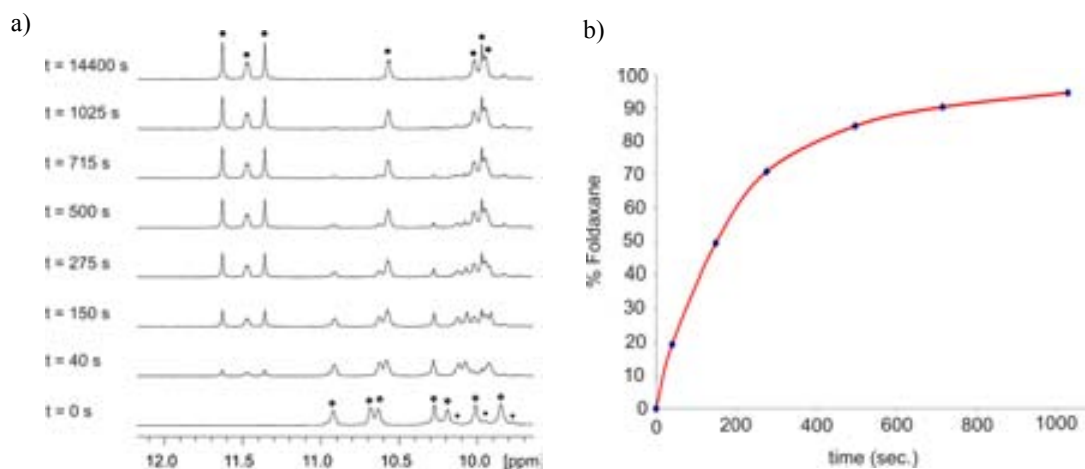


Figure 19. a) Excerpts of the ¹H NMR spectra (300 MHz) showing the formation of foldaxane **2-8** from a mixture of single helical **2** (2 mM) and **8** (2mM) in CDCl₃. Host and guest were dissolved in CDCl₃ then spectra were instantaneously recorded at 298K. Amide signals of foldaxane **2-8** are marked with black circles where double and single helices of **2** are marked with black and white diamonds respectively. b) Time trace of the formation of **2-8** from single stranded oligomer **2** (2 mM) and rod **8** in CDCl₃ monitored by ¹H NMR at 298K.

We also estimated that the rod-helix equilibrium constant K of **2-8** was over 92000 M^{-1} from the overall equilibrium as discussed above (Figure 17). We can conclude the rate constant of host-guest complex dissociation k_{-1} is slower than $2.5 \times 10^{-5} \text{ s}^{-1}$ (about twice per day) (Figure

20). Because helical dissociation is relatively slow compared to complex formation (they differ by 5 orders of magnitude), once the complex is formed the helix does not dissociate from the rod.

$$K = \frac{k_1}{k_{-1}}$$

K = the equilibrium constant of host-guest complex (between single helix and complex)
 k_1 = the rate constant of host-guest complex formation
 k_{-1} = the rate constant of host-guest complex dissociation

Figure 20. Schematic representation of calculation of the rate constant of host-guest complex

In contrast, **6** does not possess any bulky groups and forms the complex **2**⊃**6** at rates too fast to monitor. These results indicate that complexes such as **2**⊃**6** may form by a simple threading of the guest into the helix cavity, whereas the formation of **2**⊃**8** requires an unwinding and rewinding of the helix around the guest (Figure 3).^{10,23,24} The crystal structures of **2**⊃**8** and **2**⊃**6**, shown in Figure 17, illustrate that **6** is thin enough to thread itself into the helix of **2**, whereas **8** is much too bulky to do so.

These complexes relate to some structurally labile rotaxane structures in which molecular rings are closed by noncovalent bonds^{25,26} or by reversible covalent attachments.^{27,28} Due to their mechanism of formation, i.e., unfolding/refolding, we thus propose to term the architectures described here “foldaxanes”.

3.4 The shuttling motion of foldaxane

High foldaxane stability and slow kinetics of foldaxane formation in the case of **2** hint at even slower kinetics of foldaxane dissociation. Indeed, complexes such as **2**⊃**8** can be eluted on a silica gel thin layer chromatography support without any observable dissociation (Figure 15). We thus endeavoured to explore the extent to which helices of **2** wrapped around guests could undergo sliding motions much faster than they dissociate. Rod-like guest **9** possesses three hydrogen bond acceptors and thus two degenerate stations which, because of their proximity, can bind only one helix at a time (Scheme 2). Both solution and solid state (Figure 21) data confirm that it forms a 1:1 complex with oligomer **2**.

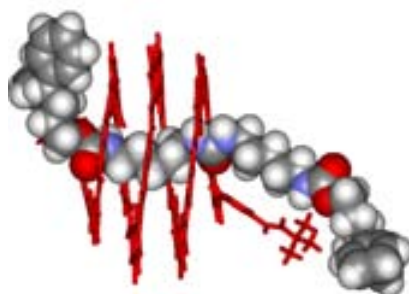


Figure 21. Crystal structure of complex **2**⊃**9**. Isobutyl side chains and solvent molecules have been omitted for clarity.

The single helix of **9** is C_2 symmetrical but this symmetry is broken in **2**⊃**9**, because one extremity of **2** lies near the central urea function of **9**, whereas the other extremity is bound to one of the two carbamate functions. This loss of symmetry is seen in the ^1H and ^{19}F NMR spectra of **2**⊃**9** which feature twice as many signals as symmetrical complexes (Figure 22).

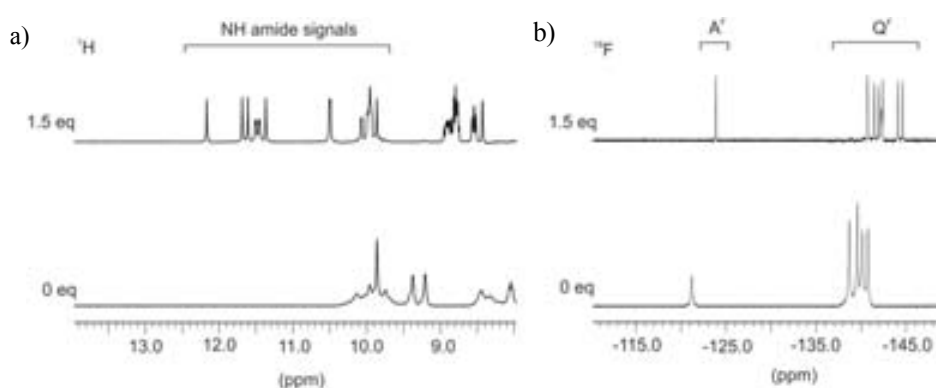


Figure 22. a) Representative 300 MHz ^1H NMR spectra of **2** (2 mM) in CDCl_3 at 298K titrated with **9**. b) 282 MHz ^{19}F NMR spectra of **2** (2 mM) in CDCl_3 titrated with **9**.

The two extremities of **2** should exchange their environments when **2** goes from one binding station of **9** to the other. Exchange spectroscopy (EXSY) NMR²⁹ experiments were carried out on solutions of **2**⊃**9** and showed clear correlation resulting from the motion of **2** between the two stations of **8** (Figure 23). This motion can be calculated to take place at rates between 2 and 4 min^{-1} , a time scale considerably smaller than that of foldaxane formation and dissociation, implying that **2** exchanges between the two stations of **9** via a sliding (shuttling) process and not via a dissociation (unfolding)–association (refolding) mechanism. Other kinetic parameters for

the shuttling process of the foldaxane could be calculated according to the EXSY experiments, such as the Gibb's free energy showed in Figure 24.

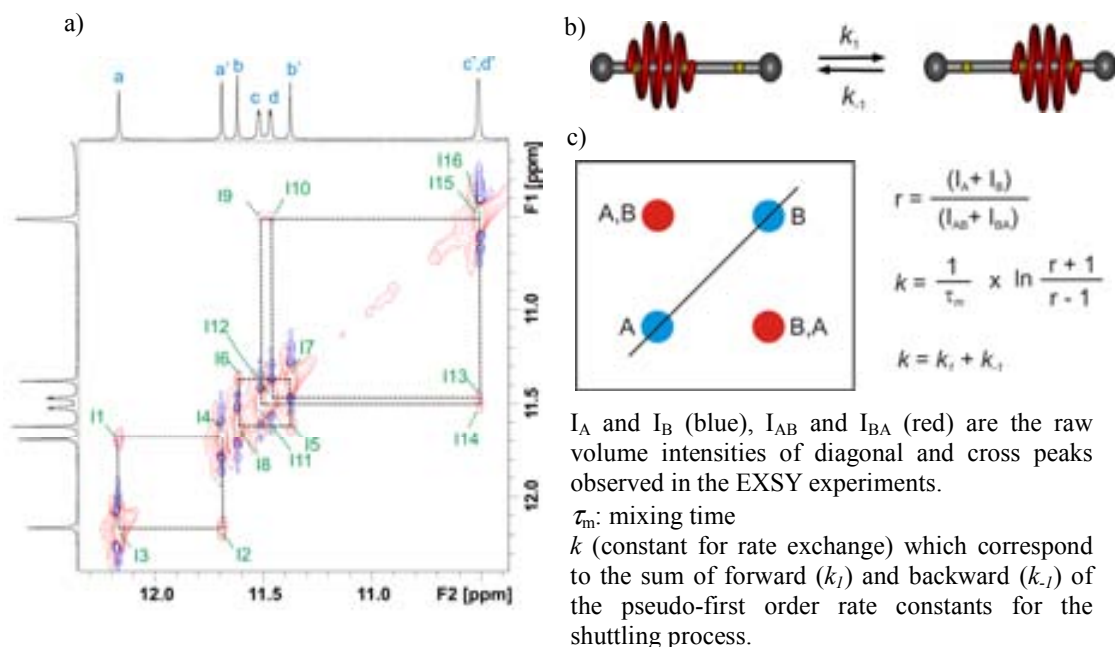


Figure 23. a) Part of 2D-EXSY spectrum of **2D9** (4 mM, 700 MHz, CDCl_3 , 298 K, $\tau_m = 300\text{ms}$). b) Schematic representation of shuttling of foldaxane. c) Scheme of calculation of the exchange rate constant of shuttling.

a)
$$\Delta G^\ddagger = -RT \ln \frac{k_{\text{obs}} h}{k_B T}$$

ΔG^\ddagger : the Gibbs energy of activation
 R : gas constant ($1.9872 \text{ cal.K}^{-1}.\text{mol}^{-1}$)
 k_B : Boltzmann's constant ($3.3 \times 10^{-24} \text{ cal.K}^{-1}$)
 h : Planck's constant ($1.58 \times 10^{-34} \text{ cal.s}$)
 T : absolute temperature (298 K)
 $k_{\text{obs}} = k_1 = k_{-1}$

b)

	I_A	I_B	I_{AB}	I_{BA}	k_{obs} (s^{-1})	ΔG^\ddagger (kcal.mol^{-1})
a-a'	0.749	0.773	0.017	0.017	0.074	18.99
b-b'	0.739	0.742	0.013	0.015	0.064	19.07
cd-c'd'	1.771	1.580	0.012	0.015	0.028	19.56

Figure 24. a) Schematic representation of calculation the Gibbs energy using Eyring equation. b) The results of the Exchange Rate Matrix (Figure 23).

3.5 Controlling the foldaxane motion

A step beyond a random sliding consists in triggering motion so that all molecules would undergo the same change within a given time window. To reach this objective, guest **10** was designed with two different binding stations, one with a heptyl segment, the other with a

diethylamine segment (Scheme 2), with the expectation that a foldaxane would form on the neutral amine segment, but not on the corresponding ammonium. As with **9**, only a 1:1 complex forms between **2** and **10**, as confirmed by integrating the ^1H NMR signals belonging to **2** and to **10** in **2**⊃**10**. However, **2** may not reside equally at the two different stations of **10**. Indeed, ^1H and ^{19}F NMR spectra of **2**⊃**10** feature two sets of signals in slightly different (58/42) proportions corresponding to a slight bias in favour of one station. Upon titrating **2**⊃**10** with an acid, the smaller NMR signals disappear without any measurable delay during the measurement of a ^1H NMR spectrum (*ca.* 2 min) and only one set of signals remains after adding excess acid (Figure 25). This is consistent with the trapping of **2** on a single station of **10**, as it is repelled by the ammonium function of the other station. Adding a base instantly reverses the process. Again the timescale of this controlled motion is much faster than the rates of unfolding and refolding of **2** around **10**, implying that motion is mediated by the rapid sliding of **2** along **10**.

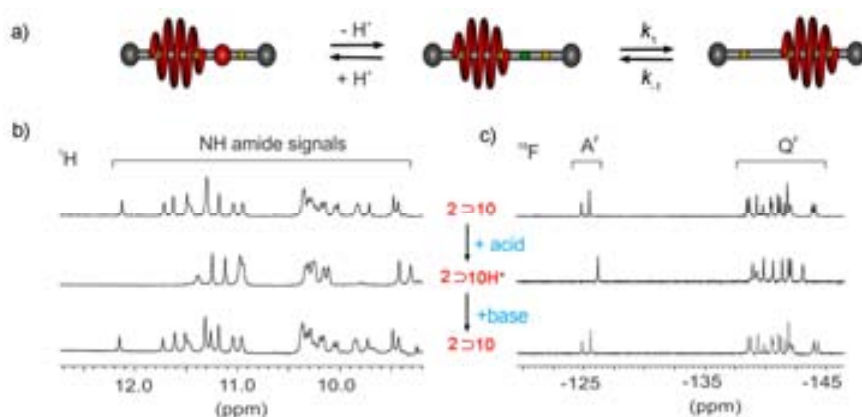


Figure 25. a) Schematic representation of helix sliding along a non-degenerate guest possessing a station which can be blocked or unblocked upon protonation or deprotonation, respectively. The green dot symbolizes the amine function of **10** which can be included in the helix cavity. The back dot is the corresponding ammonium which is not included in the helix cavity. b) and c) Part of the ^1H and ^{19}F NMR spectra of **2**⊃**10** in CDCl_3 at equilibrium, after adding excess of an organic acid (2,4-dinitrophenol), and after neutralizing with a base (Et_3N). A^{F} and Q^{F} stand for fluoro-anthracene and fluoro-quinoline, respectively.

4. Conclusion

In conclusion, upon controlling the length of the helically folded oligomers and the matching length of their rod-like guests, one may generate specific foldaxanes of controlled kinetic and thermodynamic stability. One may thus fully segregate the timescale of foldaxane assembly and that of sliding motions of the helix along the rod. Using long helices will expectedly result in slower sliding but also in much slower foldaxane dissociation. It can thus be predicted that combining rods with multiple distinct stations with mixtures of foldamers of different lengths will allow several controlled motions to proceed at different rates within a single supramolecular construct. It can be envisaged that foldamer-based molecular shuttles via a reversible assembly method will give a new chance for constructing molecular nanotechnological devices.

5. Experimental part

5.1 Methods for NMR

NMR spectra were recorded on 3 different NMR spectrometers: (1) an Avance II NMR spectrometer (Bruker Biospin) with a vertical 7.05T narrow-bore/ultrashield magnet operating at 300 MHz for ^1H observation, 282 MHz for ^{19}F observation and 75 MHz for ^{13}C observation by means of a 5-mm direct BBO H/X probe with Z gradient capabilities; (2) a DPX-400 NMR spectrometer (Bruker Biospin) with a vertical 9.4T narrow-bore/ultrashield magnet operating at 400 MHz for ^1H observation by means of a 5-mm direct QNP $^1\text{H}/^{13}\text{C}/^{31}\text{P}/^{19}\text{F}$ probe with gradient capabilities; (3) an Avance III NMR spectrometer (Bruker Biospin) with a vertical 16.45T narrow-bore/ultrashield magnet operating at 700 MHz for ^1H observation by means of a 5-mm TXI $^1\text{H}/^{13}\text{C}/^{15}\text{N}$ probe with Z gradient capabilities. Chemical shifts are reported in parts per million (ppm, δ) relative to the ^1H residual signal of the deuterated solvent used. ^1H NMR splitting patterns with observed first-order coupling are designated as singlet (s), doublet (d), triplet (t), or quartet (q). Coupling constants (J) are reported in hertz. Samples were not degassed. Data processing was performed with Topspin 2.0 software.

ROESY. Rotating-frame Overhauser spectroscopy (ROESY) experiments were recorded at 700 MHz and were used to observe dipolar interactions between NH amides from the helices pointing towards the methylene groups of the rods with the following acquisition parameters: the acquisition was performed with $2048(t_2) \times 256(t_1)$ data points, in States-TPPI mode with Z gradients selection and with CW-spinlock for mixing, relaxation delay of 2 s, and 64 scans per increment; sweep width of 14000 Hz in both dimensions; mixing time of 300 ms. Processing was done after a sine-bell multiplication in both dimensions and Fourier transformation in $1K \times 1K$ real points.

DOSY. Diffusion Ordered spectroscopy (DOSY) experiments were recorded at 400 MHz and were used to study diffusion coefficients of the double helices and host-guest complexes with the following parameters: longitudinal eddy current delay (LED) using sine-shaped gradient of 2 ms (δ), Δ of 100 ms, a relaxation delay of 2 s and 32 scans for each gradient intensity (2 to 95%, 10A gradient unit).

EXSY. Exchange spectroscopy (EXSY) experiments were recorded at 700 MHz and were used to study helix motions along rods with the following parameters: the acquisition was performed with $2048(t_2) \times 512(t_1)$ data points, in States-TPPI mode with Z gradients selection, relaxation

delay of 1.5 s, and 45 scans per increment; sweep width of 14000 Hz in both dimensions. Processing was done after a Sine Square multiplication in F1, Gaussian multiplication in F2 and Fourier transformation in $1K \times 1K$ real points.

5.2 Methods for X-ray crystallography

The data for crystal structures of compounds **(3)₂**, **(4)₂**, **3⇨7**, have been collected at the European Institute for Chemistry and Biology X-ray facility (UMS 3033) on a Bruker X8 proteum rotating anode at the $\text{CuK}\alpha$ wavelength. The system features the microstar micro-focus x-ray source with the PLATINUM135 CCD detector combined with the 4-circle KAPPA goniometer and the Helios multilayer graded optics. The system is driven by the PROTEUM2 software.³⁰ The unit cell determinations have been performed using a combination of Fast Fourier and Difference Vector techniques, the data were integrated using SAINT and scaled and corrected for absorption with SADABS. The data for crystal structures of compounds **2⇨6** and **2⇨8** and **2⇨9** were collected at the European Synchrotron Radiation facility (ESRF) in Grenoble on ID29 Beamline at three different wavelength (0.77492, 0.87260 and 0.80000 Å). The data were processed using the XDS package.³¹ All the structures except **2⇨8** have been solved by direct methods with SHELXD and refined by full-matrix least-squares methods using SHELXL.³² **2⇨8** was solved by the charge flipping algorithm implemented in the program Superflip.³³ The SQUEEZE procedure from PLATON³⁴ was used for solvent flattening at the end of the refinement of structures **2⇨9**, **3⇨7** and **2⇨8**. The WinGX-software³⁵ was used for modelling. It has to be noticed that all the crystals described below contain a large percentage of disordered solvent molecules and very few of them could be modeled in the Fourier difference density maps. High flux X-ray Beams on small crystals with high solvent contents can explain the modest quality of the refinement statistics reported in this study.

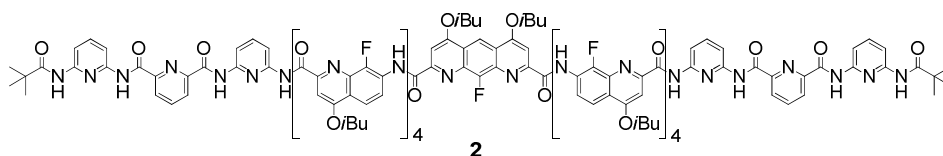
5.3 Summary of X-Ray crystallographic data

Name	Double helix (3) ₂	Double helix (4) ₂	Foldaxane 3⇨7	Foldaxane 2⇨8	Foldaxane 2⇨6	Foldaxane 2⇨9
Formula	C ₂₅₅ H ₂₄₉ Cl ₁₃ F ₁₀ N ₄₈ O _{46.50}	C ₉₅ H ₉₄ Cl ₃ F ₃ N ₂₀ O ₁₅	C ₁₆₃ H ₁₆₃ Cl _{11.54} F ₅ N ₂₆ O ₂₂	C ₂₄₂ H ₂₂₃ Cl _{2.54} F ₉ N ₃₄ O ₃₅	C ₂₂₉ H ₂₄₃ Cl ₆ F ₉ N ₃₄ O ₃₀	C ₄₅₂ H ₄₅₆ Cl ₁₁ F ₁₈ N ₇₂ O ₁₀₀
M	5380.87	1919.25	3342.33	4428.49	4335.27	9228.86
Crystal system	Triclinic	Monoclinic	Triclinic	Triclinic	Orthorhombic	Monoclinic
Space group	P-1	C2/c	P-1	P-1	Pna2(1)	C2/c
<i>a</i> /Å	19.757(4)	35.415(7)	18.372(4)	15.820(3)	39.021(8)	40.797(8)
<i>b</i> /Å	22.968(3)	22.130(4)	19.185(4)	26.120(5)	16.630(3)	32.399(7)
<i>c</i> /Å	31.494(6)	25.416(5)	24.904(5)	30.170(6)	32.270(7)	42.089(8)
<i>α</i> /o	92.40(3)	90.00	81.34(3)	81.06(3)	90.00	90.00
<i>β</i> /o	103.25(3)	111.62(3)	70.43(3)	84.39(3)	90.00	114.82(3)
<i>γ</i> /o	99.67(3)	90.00	85.92(3)	78.08(3)	90.00	90.00
U/Å ³	13665.1	18519(6)	8174(3)	12022(4)	20941(7)	50494(18)
T /K	213	213	100	100	100	100
Z	2	8	2	2	4	4
ρ/g cm ⁻¹	1.308	1.377	1.358	1.223	1.375	1.214
size (mm)	0.05 x 0.05 x 0.05	0.1 x 0.1 x 0.1	0.05 x 0.05 x 0.05	0.1 x 0.05 x 0.05	0.1 x 0.1 x 0.1	0.05 x 0.01 x 0.01
λ / Å	1.54178	1.54178	1.54178	1.54178	0.77492	0.87260
μ/mm ⁻¹	1.926	1.591	2.458	0.100	0.171	0
Absorption correction	none	none	none	none	none	none
unique data	23608	11267	24316	27262	42152	33446
parameters/restraints	3384/22	1240/7	2075/7	2874/16	2757/23	2799/22
R1, wR2	0.1577, 0.3725	0.0908, 0.2387	0.1256, 0.4206	0.1557, 0.4253	0.0992, 0.2781	0.1744, 0.4877
goodness of fit	1.512	0.959	2.149	2.076	1.259	2.311
CCDC#	797911	797906	797907	797908	797910	797909

5.4 Methods for chemical synthesis

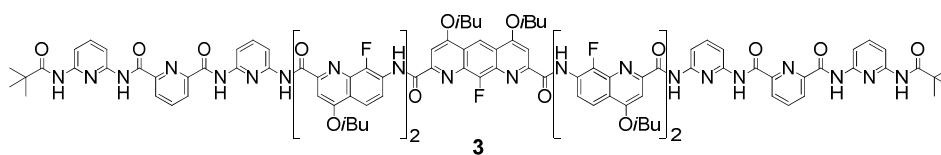
All reactions were carried out under a dry nitrogen atmosphere. Commercial reagents were purchased from Sigma-Aldrich or Alfa-Aesar and were used without further purification unless otherwise specified. Tetrahydrofuran (THF) and dichloromethane (DCM) were dried over alumina columns; chloroform, triethylamine (Et₃N) and diisopropylethylamine (DIEA) were distilled over calcium hydride (CaH₂) prior to use. Reactions were monitored by thin layer chromatography (TLC) on Merck silica gel 60-F254 plates and observed under UV light. Column chromatography purifications were carried out on Merck GEDURAN Si60 (40-63 μm). Melting points were measured on a Büchi B-540. ESI and MALDI mass spectra were obtained on a Waters LCT Premier and a Bruker Reflex III spectrometers respectively, from the Mass Spectrometry Laboratory at the European Institute of Chemistry and Biology (UMS 3033 - IECB), Pessac, France.

5.4.1 Synthesis of helix **2**



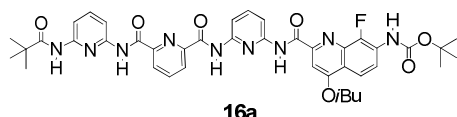
15mer 2. Diacid¹¹ **11** (38.7 mg, 0.085 mmol) was suspended in anhydrous CHCl₃ (10 mL). 1-chloro-*N,N*,2-trimethylpropenylamine (0.08 mL, 0.6 mmol) was added and the reaction was allowed to stir at room temperature for 3 h. The reaction mixture remains a suspension, but the reaction does work under these conditions. The solvent and excess reagents were removed under vacuum and the residue was dried under vacuum for at least 2 h to yield acid chloride **12** as a yellow-orange solid. To a solution of heptamer amine¹⁹ **16c** (180 mg, 0.12 mmol) and distilled diisopropylethylamine (DIEA) (0.17 mL, 0.96 mmol) in anhydrous CHCl₃ (10 mL) was added dropwise a solution of the freshly prepared diacid chloride **12** in anhydrous CHCl₃ (10 mL) via a syringe at 0°C. The reaction was allowed to proceed at room temperature for 12 h. The solution was evaporated and the residue was purified by flash chromatography (SiO₂) eluting with EtOAc/CH₂Cl₂ (5:95 to 20:80, vol/vol) to obtain **2** as a yellowish solid (130 mg, 68% yield). ¹H NMR (CDCl₃, 300 MHz): δ 10.10-9.72 (m, 10H), 9.36 (br, 2H), 9.19 (br, 2H), 8.45-8.40 (m, 2H), 8.32 (br, 1H), 8.05-8.00 (m, 2H), 7.74-7.47 (m, 11H), 7.20-6.07 (m, 29H), 4.21-4.08 (m, 8H), 3.88-3.66 (m, 8H), 3.48-3.46 (m, 2H), 3.28-3.23 (m, 2H), 2.43-2.33 (m, 5H), 2.31-2.22 (m, 5H), 1.32-1.00 (m, 60H), 0.25 (s, 18H). MS (MALDI-TOF): *m/z* calcd for C₁₇₈H₁₇₀F₉N₃₂O₂₆ [M+H]⁺ 3342.28 found 3342.02, calcd for C₁₇₈H₁₆₉F₉N₃₂NaO₂₆ [M+Na]⁺ 3364.26 found 3364.05.

5.4.2 Synthesis of helix 3

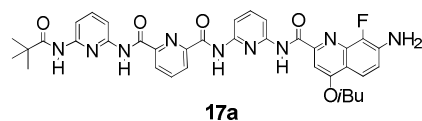


11mer 3. Diacid¹¹ **11** (32 mg, 0.07 mmol) was suspended in anhydrous CHCl_3 (10 mL). 1-chloro-*N,N*,2-trimethylpropenylamine (0.07 mL, 0.56 mmol) was added and the reaction was allowed to stir at room temperature for 3 h. The reaction mixture remains a suspension, but the reaction does work under these conditions. The solvent and excess reagents were removed under vacuum and the residue was dried under vacuum for at least 2 h to yield acid chloride **12** as a yellow-orange solid. To a solution of pentamer amine¹⁹ **16b** (115 mg, 0.12 mmol) and distilled DIEA (0.17 mL, 0.96 mmol) in anhydrous CHCl_3 (10 mL) was added dropwise a solution of the freshly prepared diacid chloride **12** in anhydrous CHCl_3 (10 mL) via a syringe at 0°C . The reaction was allowed to proceed at room temperature for 12 h. The solution was evaporated and the residue was purified by flash chromatography (SiO_2) eluting with $\text{EtOAc}/\text{CH}_2\text{Cl}_2$ (2:98 to 15:85, vol/vol) to obtain **3** as a yellowish solid (70 mg, 51% yield). ^1H NMR (CDCl_3 , 300 MHz): δ 10.45 (br, 2H), 10.11 (br, 2H), 9.92 (br, 6H), 8.58 (br, 1H), 8.45 (m, 2H), 8.04 (m, 2H), 7.64-7.58 (m, 6H), 7.46 (d, $J(\text{H}, \text{H}) = 9.0$, 2H), 7.08-6.25 (m, 20H), 4.35-3.57 (m, 12H), 2.57-2.48 (m, 2H), 2.38-2.29 (m, 2H), 2.25-2.17 (m, 2H), 1.40-1.14 (m, 36H), 0.38 (s, 18H). MS (MALDI-TOF): m/z calcd for $\text{C}_{122}\text{H}_{118}\text{F}_5\text{N}_{24}\text{O}_{18}$ $[\text{M}+\text{H}]^+$ 2301.90 found 2301.93, $\text{C}_{122}\text{H}_{117}\text{F}_5\text{N}_{24}\text{NaO}_{18}$ $[\text{M}+\text{Na}]^+$ 2323.88 found 2323.92.

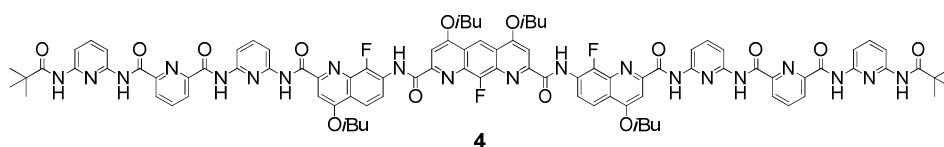
5.4.3 Synthesis of helix 4



Tetramer 16a. To a solution of trimer amine¹¹ **14** (0.11 g, 0.25 mmol) and distilled DIEA (0.27 mL, 1.54 mmol) in dry dichloromethane (10 mL) was added dropwise a solution of the freshly prepared acid chloride¹⁷ **15** (0.12 g, 0.29 mmol) in dichloromethane (10 mL) via a syringe at 0°C . The reaction mixture was allowed to proceed at room temperature for 12 h. The solution was evaporated and the residue was purified by flash chromatography (SiO_2) eluting with cyclohexane/ EtOAc (60:40, vol/vol) to obtain product **16a** as a light yellow solid (0.13 g, 63% yield). ^1H NMR (CDCl_3 , 300 MHz): δ 10.71 (s, 1H), 10.49 (s, 1H), 10.38 (s, 1H), 8.53 (s, 1H), 8.50 (s, 1H), 8.44 (t, $J(\text{H}, \text{H}) = 9.1$, 1H), 8.21-7.97 (m, 7H), 7.91 (t, $J(\text{H}, \text{H}) = 8.0$, 1H), 7.83 (t, $J(\text{H}, \text{H}) = 8.0$, 1H), 7.66 (s, 1H), 7.07 (d, $J(\text{H}, \text{H}) = 2.6$, 1H), 4.10 (d, $J(\text{H}, \text{H}) = 6.6$, 2H), 2.35-2.26 (m, 1H), 1.60 (s, 9H), 1.15 (d, $J(\text{H}, \text{H}) = 6.6$, 6H), 0.98 (s, 9H). ^{13}C NMR (CDCl_3 , 75 MHz): δ 177.5, 163.4, 163.3, 162.4, 161.7, 161.6, 152.4, 151.0, 150.3, 149.6, 149.4, 149.2, 148.6, 148.5, 147.2, 143.9, 141.0, 140.7, 139.4, 137.5, 137.4, 127.8, 127.7, 125.9, 125.8, 120.8, 118.8, 117.7, 117.6, 110.7, 110.4, 110.2, 110.1, 98.0, 81.6, 75.5, 39.6, 28.4, 28.2, 27.0, 19.3. HRMS (ES^+): m/z calcd for $\text{C}_{41}\text{H}_{45}\text{FN}_9\text{O}_7$ $[\text{M}+\text{H}]^+$ 794.3426 found 794.3439.



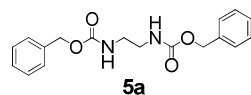
Tetramer amine 17a. Tetramer **16a** (0.12 g, 0.15 mmol) was dissolved in dichloromethane (4 mL), and excess trifluoroacetic acid (TFA) (1 mL) was added dropwise. The mixture was allowed to stir at room temperature for 3 h. The solvent was evaporated and the residue was dissolved in CH₂Cl₂ (20 mL), washed with saturated NaHCO₃, dried over Na₂SO₄, filtered and then concentrated to give amine **17a** (0.10 g, 95% yield) as a yellow solid which was used without further purification. ¹H NMR (CDCl₃, 300 MHz): δ 10.71 (s, 1H), 10.13 (s, 1H), 10.04 (s, 1H), 8.56 (s, 1H), 8.53 (s, 1H), 8.22-7.81 (m, 9H), 7.57 (s, 1H), 7.08-7.03 (m, 1H), 4.20 (br, 2H), 4.08 (d, *J*(H, H) = 6.6, 6H), 2.32-2.23 (m, 1H), 1.14 (d, *J*(H, H) = 6.6, 6H), 1.07 (s, 9H). ¹³C NMR (CDCl₃, 75 MHz): δ 177.6, 163.3, 163.3, 162.9, 161.8, 161.7, 150.7, 150.3, 149.6, 149.3, 149.1, 148.9, 145.3, 142.1, 141.0, 140.7, 139.7, 138.7, 138.6, 135.3, 135.1, 126.2, 119.3, 118.0, 116.0, 110.4, 110.2, 96.7, 75.3, 39.8, 29.8, 28.3, 27.2, 19.4. HRMS (ES⁺): *m/z* calcd for C₃₆H₃₇FN₉O₅ [M+H]⁺ 694.2902 found 694.2925.



9 mer 4. To a solution of amine **17a** (0.10 g, 0.15 mmol) and distilled DIEA (0.21 mL, 1.22 mmol) in anhydrous CHCl₃ (10 mL) was added dropwise a solution of the freshly prepared diacid chloride **12** (45 mg, 0.09 mmol) in anhydrous CHCl₃ (10 mL) via a syringe at 0°C. The reaction mixture was allowed to proceed at room temperature for 12 h. The solution was evaporated and the residue was purified by flash chromatography (SiO₂) eluting with EtOAc/CH₂Cl₂ (2:98 to 15:85, vol/vol) to obtain compound **4** as a yellowish solid (60 mg, 45% yield). ¹H NMR (CDCl₃, 300 MHz): δ 10.41 (br, 2H), 10.09 (br, 2H), 9.87 (br, 2H), 9.76 (br, 2H), 8.81 (br, 1H), 8.45 (br, 2H), 7.73-7.08 (m, 24H), 4.29 (br, 4H), 4.14-3.99 (m, 4H), 2.57-2.46 (m, 2H), 2.43-2.35 (m, 2H), 1.39 (d, *J*(H, H) = 6.3, 12H), 1.30-1.26 (m, 12H), 0.54 (s, 18H). HRMS (ES⁺): *m/z* calcd for C₉₄H₉₂F₃N₂₀O₁₄ [M+H]⁺ 1781.7054 found 1781.6201.

5.4.4 Synthesis of guests

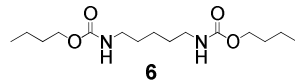
Synthesis of guests terminated by benzylcarbamate group:



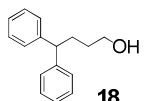
Benzylethane-1,2-dicarbamate 5a. To 1,2-diaminoethane (0.13 mL, 2.0 mmol) and DIEA (2.0 mL, 12.0 mol) in CH₂Cl₂ (10 mL) at 0°C was added dropwise benzyl chloroformate (0.62 mL, 4.4 mmol). Then the reaction mixture was allowed to reach room temperature and stirred for 12 h. The solution was evaporated and the residue was purified by flash chromatography (SiO₂) eluting with CH₂Cl₂/EtOAc (15:85, vol/vol) to obtain product **5a** as a white solid (0.58 g, 88% yield). ¹H NMR (CDCl₃, 300 MHz): δ 7.36-7.34 (m, 10H), 5.09 (br, 6H), 3.34 (s, 4H). ¹³C NMR (CDCl₃, 75 MHz): δ 156.9, 136.5, 128.7, 128.3, 128.3, 67.0, 41.4. HRMS (ES⁺): *m/z* calcd for C₁₈H₂₁N₂O₄ [M+H]⁺ 329.1501 found 329.1501. m.p.: 168.1-168.5°C.

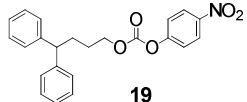
Other guests terminated by benzylcarbamate group **5b-5g** were synthesized using the similar method as guests **5a**.

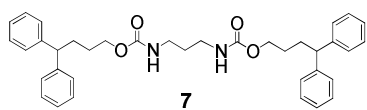
Synthesis of guest terminated by *n*-butyl group:

 ***n*-butylpentane-1,5-dicarbamate 6**. To a solution of 4-nitrophenyl chloroformate (1.19 g, 5.91 mmol) in dry CH₂Cl₂ (10 mL) was added dropwise a mixture of 1-butanol (0.49 mL, 5.37 mmol) and distilled triethylamine (Et₃N) (1.80 mL, 10.74 mmol) in CH₂Cl₂ (10 mL) via a syringe at 0°C. After 5 min stirring, a solution of 1,5-diaminopentane (0.315 mL, 2.68 mmol) and Et₃N (1.80 mL, 10.74 mmol) in CH₂Cl₂ (10 mL) was added via a syringe. Then the reaction mixture was allowed to proceed at room temperature for 12 h. The solution was evaporated and the residue was purified by flash chromatography (SiO₂) eluting with EtOAc/CH₂Cl₂ (10:90 to 30:70, vol/vol) to obtain product **6** as a white solid (0.63 g, 78% yield). ¹H NMR (CDCl₃, 300 MHz): δ 4.83 (br, 2H), 4.02 (t, *J*(H, H) = 6.6, 4H), 3.14 (q, *J*(H, H) = 6.3, *J*(H, H) = 6.6, 4H), 1.58-1.42 (m, 8H), 1.38-1.26 (m, 6H), 0.90 (t, *J*(H, H) = 6.6, 6H). ¹³C NMR (CDCl₃, 75 MHz): δ 157.0, 64.6, 40.7, 31.2, 29.7, 23.8, 19.1, 13.8. HRMS (ES⁺): *m/z* calcd for C₁₅H₃₁N₂O₄ [M+H]⁺ 303.2284 found 303.2286. m.p.: 63.3-63.6°C.

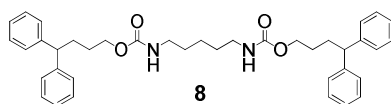
Synthesis of rods terminated by 4,4-diphenyl groups:

 **4,4-diphenylbutan-1-ol 18**.³⁶ To a stirred suspension of lithium aluminium hydride (LiAlH₄) (3.3 g, 87 mmol) in dry THF (20 mL) was added a solution of 4,4-diphenylbutanoic acid³⁷ (4.2 g, 18 mmol) in THF (20 mL) at 0°C, then the resulting mixture was stirred at room temperature for 6 h. The reaction mixture was quenched by 1 N NaOH with ice-cooling bath. The THF layer was separated and dried over Na₂SO₄. After concentration, the residue was purified by flash chromatography (SiO₂) eluting with EtOAc/CH₂Cl₂ (5:95, vol/vol) to obtain product **18** as colourless oil (3.6 g, 91% yield). ¹H NMR (CDCl₃, 300 MHz): δ 7.31-7.14 (m, 10H), 3.94 (t, *J*(H, H) = 8.7, 1H), 3.69 (q, *J*(H, H) = 6.3, *J*(H, H) = 6.0, 2H), 2.17-2.09 (m, 2H), 1.59-1.50 (m, 2H), 1.18 (t, *J*(H, H) = 5.4, 1H). ¹³C NMR (CDCl₃, 75 MHz): δ 145.1, 128.6, 128.0, 126.3, 63.0, 51.3, 32.0, 31.5.

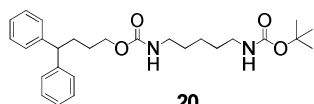
 **4,4-diphenylbutyl-(4-nitrophenyl)carbonate 19**. To a solution of 4-nitrophenyl chloroformate (1.76 g, 8.7 mmol) in dry CH₂Cl₂ (20 mL) was added dropwise a mixture of 4,4-diphenylbutan-1-ol **18** (1.88 g, 8.3 mmol) and Et₃N (3.46 mL, 25.0 mmol) in CH₂Cl₂ (10 mL) via a syringe at 0°C. Then the reaction mixture was allowed to proceed at room temperature for 12 h. The solution was evaporated and the residual oil was purified by flash chromatography (SiO₂) eluting with Hexane/CH₂Cl₂ (20:80, vol/vol) to obtain product **19** as colourless oil (2.5 g, 77% yield). ¹H NMR (CDCl₃, 300 MHz): δ 8.29 (d, *J*(H, H) = 6.9, 2H), 7.37 (d, *J*(H, H) = 6.9, 2H), 7.32-7.17 (m, 10H), 4.32 (t, *J*(H, H) = 6.6, 2H), 3.97 (t, *J*(H, H) = 7.8, 1H), 2.24-2.16 (m, 2H), 1.79-1.69 (m, 2H). ¹³C NMR (CDCl₃, 75 MHz): δ 155.7, 152.6, 145.5, 144.5, 128.7, 128.6, 127.9, 126.5, 126.4, 125.4, 121.9, 69.5, 51.1, 31.8, 27.3.

**7**

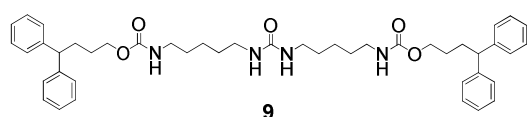
(4,4-diphenylbutyl)propane-1,3-dicarbamate 7. To a solution of 4,4-diphenylbutyl-(4-nitrophenyl)carbonate **19** (0.18 g, 0.46 mmol) in dry CH_2Cl_2 (10 mL) was added dropwise a mixture of 1,3-diaminopropane (0.02 mL, 0.23 mmol) and DIEA (0.50 mL, 2.8 mmol) in CH_2Cl_2 (10 mL) by a syringe at 0°C . Then the reaction mixture was allowed to proceed at room temperature for 12 h. The solution was evaporated and the residue was purified by flash chromatography (SiO_2) eluting with EtOAc/ CH_2Cl_2 (30:70, vol/vol) to obtain product **7** as a white solid (0.11 g, 79% yield). ^1H NMR (CDCl_3 , 300 MHz): δ 7.31-7.16 (m, 20H), 5.06 (br, 2H), 4.09 (t, $J(\text{H}, \text{H}) = 6.0$, 4H), 3.94 (t, $J(\text{H}, \text{H}) = 7.8$, 2H), 3.22 (q, $J(\text{H}, \text{H}) = 6.0$, $J(\text{H}, \text{H}) = 6.0$, 4H), 2.15 (q, $J(\text{H}, \text{H}) = 7.8$, $J(\text{H}, \text{H}) = 7.8$, 4H), 1.64-1.56 (m, 6H). ^{13}C NMR (CDCl_3 , 75 MHz): δ 157.2, 144.8, 128.6, 127.9, 126.3, 66.8, 51.1, 37.5, 32.0, 30.6, 27.7. HRMS (ES^+): m/z calcd for $\text{C}_{37}\text{H}_{43}\text{N}_2\text{O}_4$ [$\text{M}+\text{H}$] $^+$ 579.3223 found 579.3235. m.p.: 57.9 - 59.3°C .

**8**

(4,4-diphenylbutyl)pentane-1,5-dicarbamate 8. To a solution of 4,4-diphenylbutyl-(4-nitrophenyl)carbonate **19** (0.18 g, 0.46 mmol) in dry CH_2Cl_2 (10 mL) was added dropwise a mixture of cadaverine (0.03 mL, 0.23 mmol) and DIEA (0.50 mL, 2.8 mmol) in CH_2Cl_2 (10 mL) by a syringe at 0°C . Then the reaction mixture was allowed to proceed at room temperature for 12 h. The solution was evaporated and the residue was purified by flash chromatography (SiO_2) eluting with EtOAc/ CH_2Cl_2 (30:70, vol/vol) to obtain product **8** as a white solid (0.11 g, 79% yield). ^1H NMR (CDCl_3 , 300 MHz): δ 7.31-7.15 (m, 20H), 4.64 (br, 2H), 4.08 (t, $J(\text{H}, \text{H}) = 6.3$, 4H), 3.93 (t, $J(\text{H}, \text{H}) = 7.8$, 2H), 3.15 (m, 4H), 2.15 (q, $J(\text{H}, \text{H}) = 7.8$, $J(\text{H}, \text{H}) = 7.8$, 4H), 1.60-1.51 (m, 4H), 1.49-1.44 (m, 4H), 1.36-1.27 (m, 2H). ^{13}C NMR (CDCl_3 , 75 MHz): δ 156.9, 144.9, 128.6, 127.9, 126.3, 66.7, 51.1, 40.8, 32.0, 29.7, 27.8, 23.9. HRMS (ES^+): m/z calcd for $\text{C}_{39}\text{H}_{47}\text{N}_2\text{O}_4$ [$\text{M}+\text{H}$] $^+$ 607.3536 found 607.3552. m.p.: 83.5 - 84.1°C .

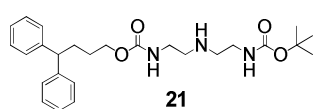
**20**

(4,4-diphenylbutyl)-*N*-tert-butoxycarbonylaminopentyl-carbamate 20. To 4,4-diphenylbutyl-(4-nitrophenyl)carbonate **19** (0.55 g, 1.40 mmol) in dry CH_2Cl_2 (10 mL) was added dropwise a mixture of *tert*-butyl-*N*-(5-aminopentyl)carbamate (0.32 mL, 1.50 mmol) and Et_3N (0.78 mL, 5.60 mmol) in CH_2Cl_2 (10 mL) via a syringe at 0°C . Then the reaction mixture was allowed to proceed at room temperature for 12 h. The solution was evaporated and the residual oil was purified by flash chromatography (SiO_2) eluting with EtOAc/ CH_2Cl_2 (15:85, vol/vol) to obtain product **20** as colourless oil (0.58 g, 91% yield). ^1H NMR (CDCl_3 , 300 MHz): δ 7.30-7.14 (m, 10H), 4.65 (br, 1H), 4.50 (br, 1H), 4.08 (t, $J(\text{H}, \text{H}) = 6.3$, 2H), 3.93 (t, $J(\text{H}, \text{H}) = 7.8$, 1H), 3.14-3.07 (m, 4H), 2.14-2.07 (m, 2H), 1.62-1.55 (m, 2H), 1.52-1.47 (m, 4H) 1.44 (s, 9H) 1.37-1.29 (m, 2H). ^{13}C NMR (CDCl_3 , 75 MHz): δ 156.9, 156.2, 144.9, 128.6, 127.9, 126.3, 79.3, 64.8, 51.1, 40.9, 40.4, 32.0, 29.9, 29.7, 28.6, 27.8, 23.9. HRMS (ES^+): m/z calcd for $\text{C}_{27}\text{H}_{38}\text{N}_2\text{NaO}_4$ [$\text{M}+\text{Na}$] $^+$ 477.2729 found 477.2747.

**9**

Bis-(4,4-diphenylbutyl)-1,1'-pentylcarbamate-5,5'-urea 9. (4,4-diphenylbutyl)-*N*-tert-butoxycarbonylaminopentyl-carbamate **20** (0.45 g 1.0 mmol) was dissolved in

CH₂Cl₂ (6 mL), and excess trifluoroacetic acid (1.5 mL) was added. The reaction mixture was stirred at room temperature for 3 h. The solvent was evaporated and the residue was dissolved in CH₂Cl₂ (20 mL), washed with saturated NaHCO₃, dried over Na₂SO₄ and then concentrated to give amine as colourless oil. To a solution of this amine and Et₃N (0.55 mL, 4.00 mmol) in dry CH₂Cl₂ (10 mL) was added dropwise a solution of 4-nitrophenyl chloroformate (0.10 g, 0.50 mmol) in CH₂Cl₂ (10 mL) via a syringe at 0°C. The reaction mixture was allowed to proceed at room temperature for 12 h. The solution was washed with 1N NaOH and brine several times, then dried over Na₂SO₄. After filtration and concentration, the residual oil was purified by flash chromatography (SiO₂) eluting with EtOAc/CH₂Cl₂ (10:90 to 90:10, vol/vol) to obtain product **9** as a white solid (0.19 g, 52% yield). ¹H NMR (CDCl₃, 300 MHz): δ 7.31-7.15 (m, 20H), 4.80 (br, 2H), 4.64 (br, 2H), 4.07 (t, *J*(H, H) = 6.3, 4H), 3.93 (t, *J*(H, H) = 7.8, 2H), 3.17 (m, 8H), 2.15 (q, *J*(H, H) = 7.8, *J*(H, H) = 7.8, 4H), 1.63-1.51 (m, 4H), 1.49-1.44 (m, 8H), 1.36-1.27 (m, 4H). ¹³C NMR (CDCl₃, 75 MHz): δ 158.6, 157.0, 144.8, 128.6, 127.9, 126.4, 66.8, 51.1, 40.8, 40.2, 32.0, 29.9, 29.7, 27.8, 23.9. HRMS (ES⁺): *m/z* calcd for C₄₅H₅₉N₄O₅ [M+H]⁺ 735.4485 found 735.4512. m.p.: 107.1-108.3°C.

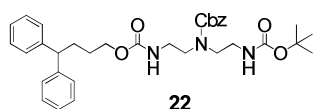


4,4-diphenylbutyl

5-(2-(tert-butoxycarbonylamino)ethylamino)

pentylcarbamate 21. To a solution of 4,4-diphenylbutyl-(4-nitrophenyl) carbonate

19 (0.46 g, 1.22 mmol) in dry CH₂Cl₂ (10 mL) was added dropwise a mixture of *tert*-butyl-2-(2-aminoethylamino)ethylcarbamate³⁸ (0.26 g, 1.28 mmol) and Et₃N (0.70 mL, 5.00 mmol) in CH₂Cl₂ (10 mL) via a syringe at 0°C. Then the reaction mixture was allowed to proceed at room temperature for 12 h. The solution was washed with 1N NaOH and brine several times, then dried over Na₂SO₄. After filtration and concentration, the residual oil was purified by flash chromatography (SiO₂) eluting with MeOH/CH₂Cl₂ (5:95 to 15:85, vol/vol) to obtain product **21** as yellowish oil (0.26 g, 47% yield). ¹H NMR (CDCl₃, 300 MHz): δ 7.30-7.14 (m, 10H), 5.07 (br, 1H), 4.88 (br, 1H), 4.08 (t, *J*(H, H) = 6.6, 2H), 3.93 (t, *J*(H, H) = 7.8, 1H), 3.26-3.17 (m, 4H), 2.75 (q, *J*(H, H) = 5.7, *J*(H, H) = 5.7, 4H), 2.15-2.07 (m, 2H), 1.61-1.54 (m, 2H), 1.44 (s, 9H). ¹³C NMR (CDCl₃, 75 MHz): δ 157.0, 156.3, 144.8, 128.6, 127.9, 126.3, 79.4, 64.8, 51.1, 48.9, 48.8, 40.7, 40.4, 32.0, 28.5, 27.7. HRMS (ES⁺): *m/z* calcd for C₂₆H₃₈N₃O₄ [M+H]⁺ 456.2862 found 456.2867.

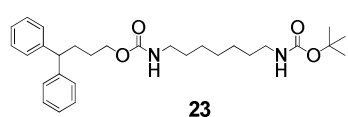


4,4-diphenylbutyl-5-(2-(tert-butoxycarbonylamino)ethylbenzyloxycarbonylamino)pentylcarbamate

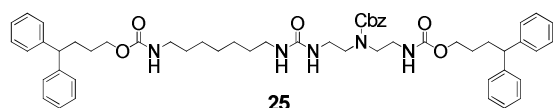
22.

To

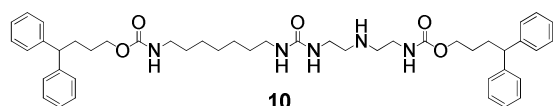
4,4-diphenylbutyl-5-(2-(tert-butoxycarbonylamino)ethylamino)pentylcarbamate **21** (0.40 g, 0.88 mmol) and Et₃N (0.49 mL, 3.5 mmol) in dry CH₂Cl₂ (10 mL) was added dropwise a solution of benzyl chloroformate (0.15 mL, 1.00 mmol) at 0°C. Then the reaction mixture was allowed to proceed at room temperature for 12 h. The solution was evaporated and the residual oil was purified by flash chromatography (SiO₂) eluting with EtOAc/CH₂Cl₂ (5:95 to 30:70 vol/vol) to obtain product **22** as colourless oil (0.51 g, 92% yield). ¹H NMR (CDCl₃, 300 MHz): δ 7.33-7.14 (m, 15H), 5.32 (br, 1H), 5.10 (s, 2H), 4.97 (br, 1H), 4.04 (br, 2H), 3.92 (t, *J*(H, H) = 7.8, 1H), 3.39-3.30 (m, 8H), 2.09-2.08 (m, 2H), 1.59 (br, 2H), 1.42 (s, 9H). ¹³C NMR (CDCl₃, 75 MHz): δ 157.0, 156.4, 156.1, 144.8, 136.4, 128.7, 128.6, 128.3, 128.1, 127.9, 126.3, 79.6, 67.7, 64.9, 51.1, 48.0, 40.1, 39.6, 32.0, 28.5, 27.7. HRMS (ES⁺): *m/z* calcd for C₃₄H₄₃N₃NaO₆ [M+Na]⁺ 612.3050 found 612.3064.

**23**

(4,4-diphenylbutyl)-*N*-tert-butoxycarbonylaminoheptyl-carbamate 23. To 4,4-diphenylbutyl-(4-nitrophenyl)carbonate **19** (0.48 g, 1.20 mmol) in dry CH₂Cl₂ (10 mL) was added dropwise a mixture of *tert*-butyl-*N*-(7-aminoheptyl)carbamate (0.34 g, 1.50 mmol) and Et₃N (0.68 mL, 4.9 mmol) in CH₂Cl₂ (10 mL) via a syringe at 0°C. Then the reaction mixture was allowed to proceed at room temperature for 12 h. The solution was evaporated and the residue was purified by flash chromatography (SiO₂) eluting with EtOAc/CH₂Cl₂ (15:85, vol/vol) to obtain product **23** as a white solid (0.52 g, 88% yield). ¹H NMR (CDCl₃, 300 MHz): δ 7.30-7.14 (m, 10H), 4.60 (br, 1H), 4.49 (br, 1H), 4.08 (t, *J*(H, H) = 6.3, 2H), 3.93 (t, *J*(H, H) = 7.8, 1H), 3.17-3.06 (m, 4H), 2.14 (q, *J*(H, H) = 7.8, *J*(H, H) = 7.8, 2H), 1.65-1.55 (m, 2H), 1.44 (br, 13H) 1.29 (br, 6H). ¹³C NMR (CDCl₃, 75 MHz): δ 156.8, 156.1, 144.9, 128.6, 128.0, 126.3, 79.2, 64.7, 51.1, 41.0, 40.7, 32.0, 30.1, 29.0, 28.6, 27.8, 26.8. HRMS (ES⁺): *m/z* calcd for C₂₉H₄₂N₂NaO₄ [M+Na]⁺ 505.3042 found 505.3054. m.p.: 64.3-64.9°C.

**25**

Guest 25. Compound **22** (1.46 g, 2.3 mmol) and **23** (1.11 g, 2.3 mmol) were respectively dissolved in CH₂Cl₂ (6 mL), and excess trifluoroacetic acid (3 mL) was added separately. The two reactions were stirred at room temperature for 3 h. The solvent was evaporated and the residue was dissolved in CH₂Cl₂ (20 mL), washed with saturated NaHCO₃, dried over Na₂SO₄ respectively and then concentrated to give the corresponding amines as oils. To a solution of amine **24** corresponding to **23** and Et₃N (0.64 mL, 4.6 mmol) in dry CH₂Cl₂ (10 mL) was added dropwise a solution of 4-nitrophenyl chloroformate (0.46 g, 2.3 mmol) in CH₂Cl₂ (10 mL) via a syringe at 0°C. The reaction mixture was stirred for 5 min before adding the other amine corresponding to **22** and Et₃N (0.64 mL, 4.6 mmol) in dry CH₂Cl₂ (10 mL). The resulting reaction mixture was then allowed to proceed at room temperature for 12 h. The solution was washed several times with 1N NaOH and brine, then dried over Na₂SO₄. After filtration and concentration, the residual oil was purified by flash chromatography (SiO₂) eluting with MeOH/CH₂Cl₂ (5:95 to 25:85, vol/vol) to obtain product **25** as colourless oil (0.58 g, 28% yield). ¹H NMR (CDCl₃, 300 MHz): δ 7.30-7.14 (m, 20H), 5.39 (br, 1H), 5.33 (br, 1H), 5.09 (s, 2H), 4.74 (br, 2H), 4.07-4.01 (m, 4H), 3.93-3.86 (m, 2H), 3.36 (br, 8H), 3.14-3.09 (m, 4H), 2.15-2.05 (m, 4H), 1.57 (br, 4H), 1.44 (br, 4H) 1.27 (br, 6H). ¹³C NMR (CDCl₃, 75 MHz): δ 158.7, 158.4, 157.5, 157.1, 156.8, 144.8, 144.7, 136.4, 128.7, 128.6, 128.2, 127.9, 126.3, 126.3, 67.5, 65.0, 64.7, 51.0, 49.3, 48.8, 48.4, 40.9, 40.4, 39.5, 32.0, 31.9, 30.1, 29.9, 28.9, 27.7, 27.7, 26.7, 26.6. HRMS (ES⁺): *m/z* calcd for C₅₄H₆₇N₅NaO₇ [M+Na]⁺ 920.4938 found 920.4952.

**10**

Guest 10. Compound **25** (0.4 g, 0.45 mmol) was dissolved in EtOAc (40 mL), and 10% Pd/C (40 mg) was added. The reaction mixture was stirred for 48 h under hydrogen at atmospheric pressure. After filtration through celite and concentration, the residual oil was purified by flash chromatography (SiO₂) eluting with MeOH/CH₂Cl₂ (5:95 to 40:60, vol/vol) to obtain product **10** as colourless oil (0.20 g, 59% yield). ¹H NMR (CDCl₃, 300 MHz): δ 7.30-7.14 (m, 20H), 5.10 (br, 1H), 4.98 (br, 1H), 4.68 (br, 2H),

4.05 (br, 4H), 3.92-3.87 (m, 2H), 3.24-3.21 (m, 4H), 3.14-3.12 (m, 4H), 2.73-2.70 (m, 4H), 2.14-2.06 (m, 4H), 1.57 (br, 4H), 1.45 (br, 4H) 1.29 (br, 6H). ^{13}C NMR (CDCl_3 , 75 MHz): δ 159.2, 157.2, 156.9, 144.8, 144.8, 128.6, 128.0, 127.9, 126.3, 126.3, 64.9, 64.7, 51.0, 49.4, 48.9, 40.9, 40.3, 39.9, 32.0, 32.0, 30.2, 29.9, 28.8, 27.7, 26.7, 26.6. HRMS (ES^+): m/z calcd for $\text{C}_{46}\text{H}_{62}\text{N}_5\text{O}_5$ $[\text{M}+\text{H}]^+$ 764.4751 found 764.4780.

6. References

- 1 R. D. Vale, The molecular motor toolbox for intracellular transport. *Cell*, **2003**, *112*, 467–480.
- 2 J. D. Badjic, V. Balzani, A. Credi, S. Silvi, J. F. Stoddart, A molecular elevator. *Science*, **2004**, *303*, 1845–1849.
- 3 V. Serreli, C.-F. Lee, E. R. Kay, D. A. Leigh, A molecular information ratchet. *Nature*, **2007**, *445*, 523–527.
- 4 M. R. Panman, P. Bodis, D. J. Shaw, B. H. Bakker, A. C. Newton, E. R. Kay, A. M. Brouwer, W. J. Buma, D. A. Leigh, S. Woutersen, Operation mechanism of a molecular machine revealed using time-resolved vibrational spectroscopy. *Science*, **2010**, *328*, 1255–1258.
- 5 S. P. Fletcher, F. Dumur, M. M. Pollard, B. L. Feringa, A reversible, unidirectional molecular rotary motor driven by chemical energy. *Science*, **2005**, *310*, 80–82.
- 6 N. Ruangsupapichat, M. M. Pollard, S. R. Harutyunyan, B. L. Feringa, Reversing the direction in a light-driven rotary molecular motor, *Nature Chem.*, **2011**, *3*, 53–60.
- 7 T. Muraoka, K. Kinbara, T. Aida, Mechanical twisting of a guest by a photoresponsive host. *Nature*, **2006**, *440*, 512–515.
- 8 P. Mobian, J.-M. Kern, J.-P. Sauvage, Light-driven machine prototypes based on dissociative excited states: photoinduced decoordination and thermal recoordination of a ring in a ruthenium(II)-containing [2]Catenane. *Angew. Chem. Int. Ed.*, **2004**, *43*, 2392–2395.
- 9 W. Saenger, Principles of Nucleic Acid Structure, Springer-Verlag, New York, **1984**.
- 10 A. Tanatani, T. S. Hughes, J. S. Moore, Foldamers as dynamic receptors: probing the mechanism of molecular association between helical oligomers and rodlike ligands. *Angew. Chem. Int. Ed.*, **2002**, *41*, 325–328.
- 11 C. Bao, B. Kauffmann, Q. Gan, K. Srinivas, H. Jiang, I. Huc, Converting sequences of aromatic amino acid monomers into functional three-dimensional structures: second-generation helical capsules. *Angew. Chem. Int. Ed.* **2008**, *47*, 4153–4156.
- 12 I. Huc, Aromatic oligoamide foldamers, *Eur. J. Org. Chem.*, **2004**, *1*, 17–29.
- 13 V. Berl, R. G. Khoury, I. Huc, M. J. Krische, J.-M. Lehn, Interconversion of single and double helices formed from synthetic molecular strands. *Nature*, **2000**, *407*, 720–723.
- 14 V. Berl, I. Huc, R. Khoury, J.-M. Lehn, Helical molecular programming. folding of oligopyridine-dicarboxamides into molecular single helices. *Chem. Eur. J.*, **2001**, *7*, 2798–2809.
- 15 V. Berl, I. Huc, R. Khoury, J.-M. Lehn, Helical Molecular programming. Supramolecular double helices by dimerization of helical oligopyridine-dicarboxamide strands. *Chem. Eur. J.*, **2001**, *7*, 2810–2820.
- 16 B. Baptiste, J. Zhu, D. Haldar, B. Kauffmann, J.-M. Léger, I. Huc, Hybridization of long pyridine-dicarboxamide oligomers into multi-turn double helices: slow strand association and dissociation, solvent dependence, and solid state structures. *Chem. Asian J.*, **2010**, *5*, 1364–1375.
- 17 Q. Gan, C. Bao, B. Kauffmann, A. Grélard, J. Xiang, S. Liu, I. Huc, H. Jiang, Quadruple and double helices of 8-fluoroquinoline oligoamides. *Angew. Chem. Int. Ed.*, **2008**, *47*, 1715–1718.
- 18 E. Berni, J. Garric, C. Lamit, B. Kauffmann, J.-M. Léger, I. Huc, Interpenetrating single helical capsules. *Chem. Comm.*, **2008**, *17*, 1968–1970.
- 19 C. Bao, Q. Gan, B. Kauffmann, H. Jiang, I. Huc, A self-assembled foldamer capsule: combining single and double helical segments in one aromatic amide sequence, *Chem. Eur. J.*, **2009**, *15*, 11530–11536.
- 20 N. Delsuc, T. Kawanami, J. Lefeuvre, A. Shundo, H. Ihara, M. Takafuji, I. Huc, Kinetics of helix handedness inversion: folding and unfolding in aromatic amide oligomers. *ChemPhysChem*, **2008**, *9*, 1882–1890.
- 21 B. Baptiste, Jiang Zhu, D. Haldar, B. Kauffmann, J.-M. Léger, I. Huc, Hybridization of long pyridine-dicarboxamide oligomers into multi-turn double helices: slow strand association and dissociation, solvent dependence, and solid state structures. *Chem. Asian J.*, **2010**, *5*, 1364–1375.

- 22 Y. Cohen, L. Avram, L. Frish, Diffusion NMR spectroscopy in supramolecular and combinatorial chemistry: an old parameter-new insights. *Angew. Chem. Int. Ed.*, **2005**, *44*, 520–554.
- 23 T. Nishinaga, A. Tanatani, K. Oh, J. S. Moore, The size-selective synthesis of folded oligomers by dynamic templation. *J. Am. Chem. Soc.*, **2002**, *124*, 5934–5935.
- 24 A. Petitjean, L. A. Cuccia, M. Schmutz, J.-M. Lehn, Naphthyridine-based helical foldamers and macrocycles: synthesis, cation binding, and supramolecular assemblies. *J. Org. Chem.*, **2008**, *73*, 2481–2495.
- 25 C. A. Hunter, C. M. R. Low, M. J. Packer, S. E. Spey, J. G. Vinter, M. O. Vysotsky, C. Zonta, Noncovalent assembly of [2]rotaxane architectures. *Angew. Chem. Int. Ed.*, **2001**, *40*, 2678–2682.
- 26 S.-Y. Chang, H.-Y. Jang, K.-S. Jeong, Quantitative comparison of kinetic stabilities of metallomacrocycle-based rotaxane. *Chem. Eur. J.*, **2003**, *9*, 1535–1541.
- 27 P. T. Glink, A. I. Oliva, J. F. Stoddart, A. J. P. White, D. J. Williams, Template-directed synthesis of a [2]Rotaxane by the clipping under thermodynamic control of a crown ether like macrocycle around a dialkylammonium ion. *Angew. Chem. Int. Ed.*, **2001**, *40*, 1870–1875.
- 28 M. Horn, J. Ihringer, P. T. Glink, J. F. Stoddart, Kinetic versus thermodynamic control during the formation of [2]rotaxanes by a dynamic template-directed clipping process. *Chem. Eur. J.*, **2003**, *9*, 4046–4054.
- 29 C. L. Perrin, T. J. Dwyer, Application of two-dimensional NMR to kinetics of chemical exchange. *Chem. Rev.* **1990**, *90*, 935–967.
- 30 Proteum II suite Bruker AXS version **2005**.
- 31 W. J. Kabsch, Automatic processing of rotation diffraction data from crystals of initially unknown symmetry and cell constants. *J. Appl. Crystallogr.*, **1993**, *26*, 795–800
- 32 G. M. Sheldrick, A short history of SHELX. *Acta Cryst.*, **2008**, *A64*, 112–122.
- 33 L. Palatinus, G. Chapuis, SUPERFLIP—a computer program for the solution of crystal structures by charge flipping in arbitrary dimensions. *Appl. Crystallogr.*, **2007**, *40*, 786–790.
- 34 P. van der Sluis, A. L. Spek, BYPASS: an effective method for the refinement of crystal structures containing disordered solvent regions. *Acta Cryst.*, **1990**, *A46*, 194–201.
- 35 L. J. Farrugia, WinGX suite for single crystal small molecule crystallography. *J. Appl. Cryst.*, **1999**, *32*, 837–838.
- 36 V. N'Goka, G. Schlewer, J.-M. Linget, J.-P. Chambon, C.-G. Wermuth, GABA-uptake inhibitors: construction of a general pharmacophore model and successful prediction of a new representative. *J. Med. Chem.*, **1991**, *34*, 2547–2557.
- 37 S. Miyano, T. Tatsuoka, K. Suzuki, K. Imao, F. Satoh, T. Ishihara, I. Hirotsu, T. Kihara, M. Hatta, Y. Horikawa, K. Sumoto, The synthesis and antilipidperoxidation activity of 4,4-diarylbutylamines and 4,4-diarylbutylanamides. *Chem. Pharm. Bull.*, **1990**, *38*, 1570–1574.
- 38 S. Fixon-Owoo, F. Levasseur, K. Williams, T. N. Sabado, M. Lowe, M. Klose, A. J. Mercier, P. Fields, J. Atkinson, Preparation and biological assessment of hydroxycinnamic acid amides of polyamines. *Phytochemistry*, **2003**, *63*, 315–334.

Chapter 3

Double-helical foldaxanes: template induced screw motions

1. Introduction

Important steps have been made to control motions at the molecular scale in synthetic systems. Examples of elementary molecular motions such as rotations^{1,2} and translations^{3,4} have been reported, as well as combined motions such as coupled rotations,⁵⁻⁷ coupled translations^{8,9} and spring-like extensions.¹⁰⁻¹² In addition, the direction of molecular movements can sometimes be controlled in translations (shuttling)¹³⁻¹⁵ and in rotations.¹⁶⁻²⁰

Folding is the process nature has selected to control the conformation of its molecular machinery. Thus, foldamers, defined as artificial folded molecular architectures, have been constructed to mimic the structures and functions of “biomachinery”. Already, some examples of functional foldamers capable of processing motion have been designed. For example, some helical molecules can unfold into a linear strand and refold to a helical conformation by pH control.²¹⁻²³ In an other example, a double helical system, sliding of the two single helices along one another has been demonstrated by our group.¹² Recently, Yashima and Furusho have revealed that a spiroborate-based double helix in which the central sodium cation was coordinated to the spiroborate moieties can do extension–contraction motion by the sequential addition of cryptands and NaPF₆ in an alternating manner.¹⁰ In this case, sodium cation binding and release processes are keys to trigger the spring-like motion.

In the previous chapter, we described the ability of some multi-turn single helical aromatic amide foldamers to wind around rod like guests and form stable complexes in which the guest resides through the helix cavity.²⁴ By analogy with rotaxanes, these complexes can be termed foldaxanes. When the rods have bulky residues at the termini, foldaxanes do not form by the threading of the rod into the helix cavity but by an unfolding-refolding mechanism of the helix. This creates a high kinetic barrier, due to the high energy cost to unfold a helical aromatic oligoamides as shown, for example, in quinolinecarboxamide oligomers.²⁵ The unusual kinetic stability of foldaxanes has allowed us to induce and observe shuttling of the helix between distinct stations along a dumbbell rod at timescales that are much shorter than the timescale of foldaxane dissociation. Foldaxane formation is thermodynamically favored owing to intermolecular hydrogen bonds between binding sites, which are located at each extremity of the helix (namely 2,6-pyridinedicarboxamide hydrogen-bond donors) and anchor points on the rods (carbonyl hydrogen-bond acceptors). It follows that a strict match between helix and rod lengths is required to ensure foldaxane stability; the tolerance is typically one CH₂ unit of the rod.

Following this, we devised that foldaxanes might form not only with aromatic oligoamide sequences folded as single helices, but also when they hybridize into double helices.^{12,26,27} For example, sequences related to **1** (Figure 1) have been shown to hybridize into stable double helical antiparallel duplexes.²⁸ Because (**1**)₂ possesses two 2,6-pyridinedicarboxamide hydrogen bond donors, that is one on each strand, we predicted that it might also bind to rod-like guests having carbonyl hydrogen-bond donors. Furthermore, in the presence of guests of different lengths, the two strands of the duplex could undergo a relative screw motion to adjust the distance between hydrogen bond donors located at the end of one of their extremities so that the length of the duplexes matches with the length of the guest (Figure 1).

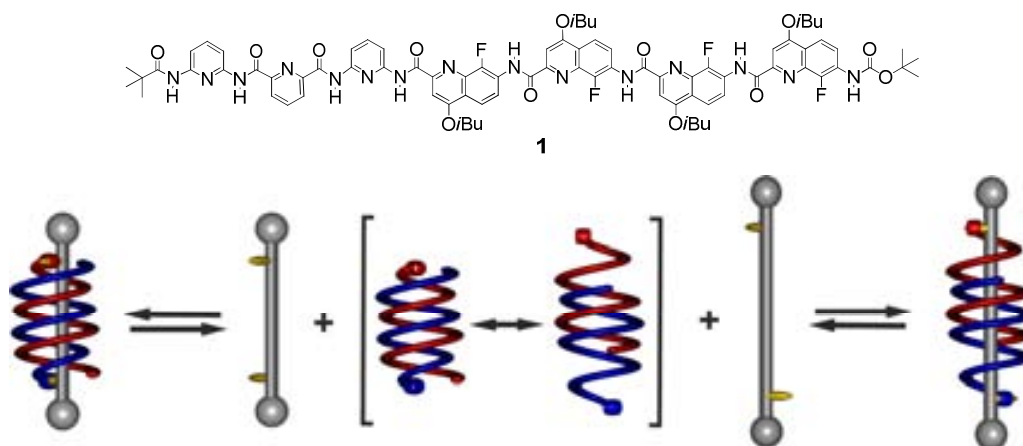


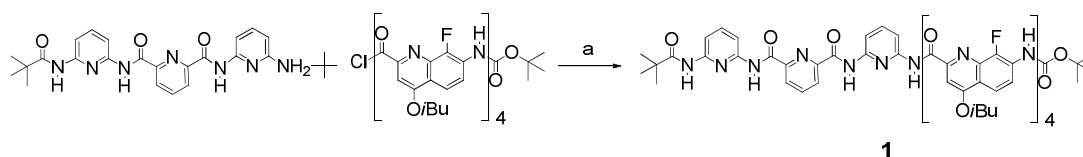
Figure 1. a) The structure of sequence **1**. b) Cartoon representation of the screw motion of the two strands of a molecular duplex and of the trapping of screwed (left) and unscrewed (right) double helices upon binding to short and long rod-like guests, respectively. Hydrogen-bond acceptors (the golden sticks protruding from the rods) on the guests match with hydrogen-bond donors (small rings) at the ends of a double helix.

2. Synthesis

2.1 Synthesis of helices

Aromatic oligoamides **1** comprises at one extremity of a trimer of 2,6-diaminopyridine and 2,6-pyridinedicarboxylic acid (P), that can form a cleft that bind to hydroxyl or amino groups that may thus constitute hot spots to anchor guests within the helix cavity.^{24,28,29} A tetrameric amide segment of 7-amino-8-fluoro-2-quinolinecarboxylic acid (Q^f) was also included in **1**, and this segment was known to hybridize into duplex or quadruplex architecture.^{27,28} Thus, **1** was envisaged to form an antiparallel double helix with two hydrogen bond donors at the termini.

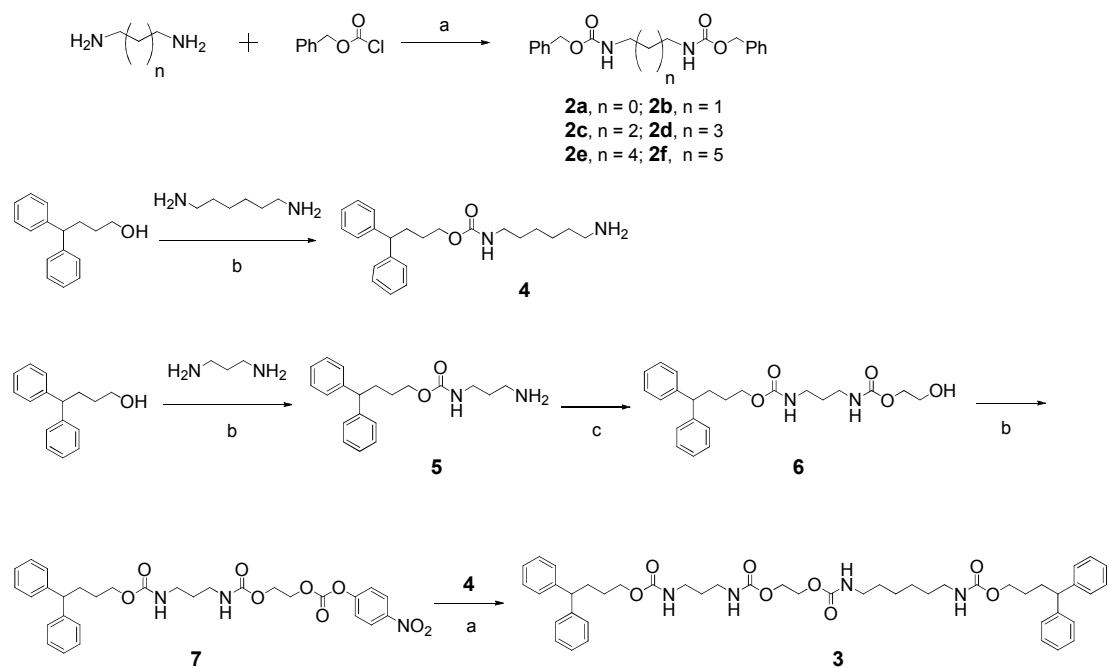
The synthetic procedures of **1** via a convergent approach have been described in early studies,²⁸ and are depicted in Scheme 1. The oligoamides **1** was successfully achieved from coupling monoamine mono-pivaloyl-protected trimer P₃ with acid chloride of Q^f₄ in the moderate yield.



Scheme 1. The synthesis of **1**: a) DIEA, DCM, r.t.

2.2 Synthesis of guests

The dumbbell-shaped guests **2a-2f** were synthesized through the reaction of benzyl chloroformate with corresponding diamine as shown in chapter 1. The guest **3** with two stations was obtained from diphenylbutanol. The hydroxyl group of diphenylbutanol was first activated with 4-nitrophenyl chloroformate, then coupled to an excess of 1,6-diaminohexane to yield **4**. Compound **5** can be prepared by the same procedure. The activation of **5** with 4-nitrophenyl chloroformate, subsequent reaction with an excess of ethylene glycol afforded **6**, which activated again and coupled with **4** to generate guest **3**. The detailed synthesis is shown in Scheme 2.



Scheme 2. The synthesis of guests **2** and **3**: a) DIEA, DCM, r.t.; b) 4-nitrophenyl chloroformate, TEA, DCM, r.t.; c) 4-nitrophenyl chloroformate, TEA, DCM, r.t., then ethylene glycol, reflux.

3. Results and discussion

3.1 The double-helical foldaxane formation

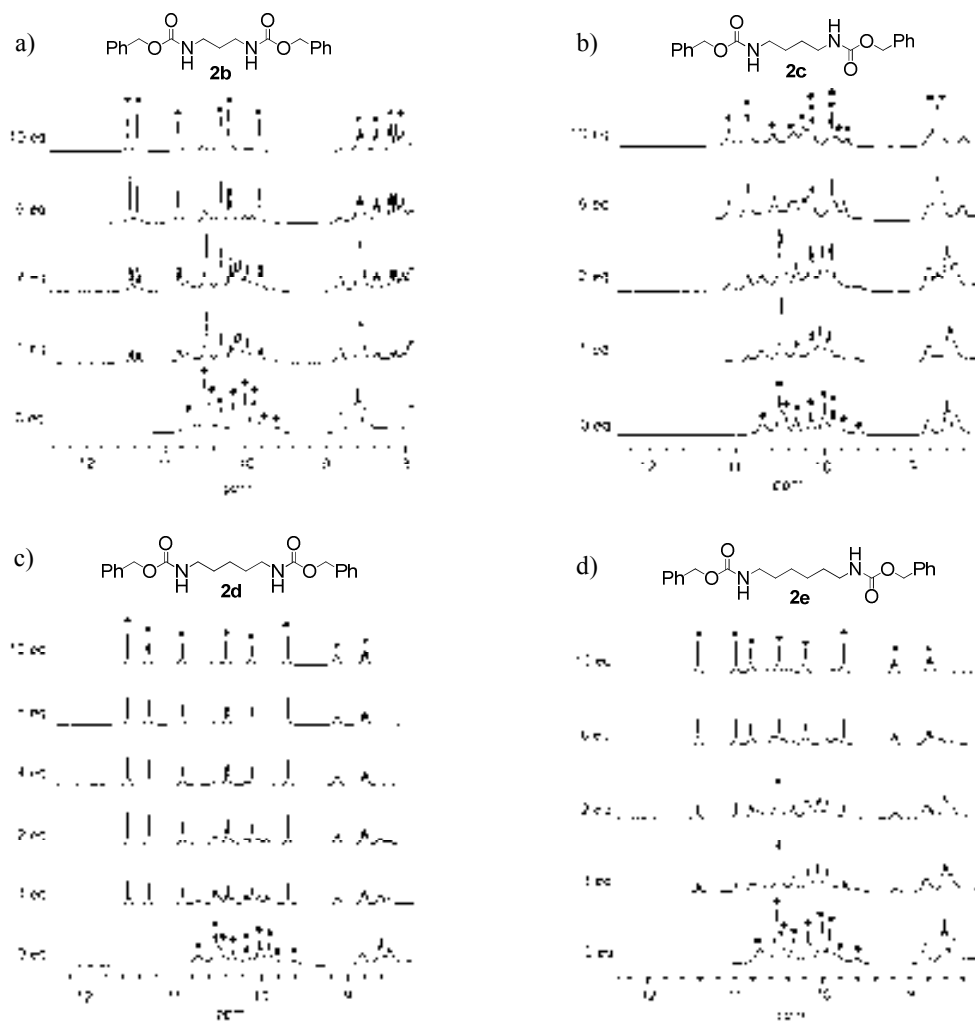


Figure 2. Representative 300 MHz NMR spectra of **1** (8 mM) in CDCl₃ at 298K titrated with guests a) **2b**; b) **2c**; c) **2d**; d) **2e**. Amide signals of the double helix and foldaxane are marked with black diamond and black circles, respectively. Aromatic proton resonances are marked with stars.

Titration between double helix (**1**)₂ and guests **2a-2f** in CDCl₃ were monitored by ¹H NMR spectroscopy and, in some cases, revealed the formation of a new species in slow exchange with (**1**)₂ on the NMR timescale (Figure 2). Specifically, the longest (**2f**) and shortest (**2a**) rods do not form inclusion complexes, whereas rods of intermediate sizes **2b-2e** do. The binding constants, listed in table 1, based on integration signals of free double helix and complex (Figure 3), were

calculated to be 55, 20, 140 and 35 L.mol⁻¹ for (1)₂⊃2b, (1)₂⊃2c, (1)₂⊃2d and (1)₂⊃2e, respectively. These complexes all formed at rates too fast to monitor by NMR; equilibrium is reached before the first NMR spectrum can be measured, which takes approximately 2 minutes. This process is faster than that previously observed for single-helical foldaxanes that are derived from longer aromatic amide sequences. Thus, to bind a rod of given length, two short strands appear to unwind and rewind faster than a long one.

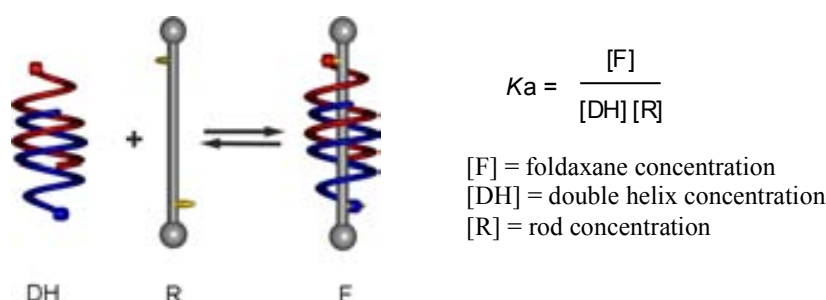


Figure 3. Scheme of calculation of the association constant K_a .

Table 1. Titration of oligomer **1** by different dumbbell molecules monitored by NMR (300 MHz) in CDCl₃ at 298K. Dashes reflect no affinity of the oligomers for the rods. All experimental errors < 5%. K_a in L.mol⁻¹.

	2a	2b	2c	2d	2e	2f
(1) ₂	-	55	20	140	35	-

The crystal structures of (1)₂⊃2b, (1)₂⊃2d, and (1)₂⊃2e were obtained from the slow diffusion of hexane into a chloroform solution of **1** mixed with guests **2b**, **2d** and **2e**, respectively (Figure 4). They confirmed the stoichiometry, symmetry and structure of the double helical foldaxanes, in agreement with NMR titration data. In particular the crystal structures revealed: (i) the expected hydrogen bonds between the 2,6-pyridinedicarboxamide units and carbonyl groups on the rod as observed for single helical foldaxanes;²⁴ (ii) the antiparallel nature of the double helices; (iii) the C₂ symmetrical structure of the complexes; (iv) that the double helix cavity accommodates the alkyl and carbamate moieties of the guest but that the terminal benzyl groups are too large to be threaded through the helix, thus suggesting a helix unfolding-refolding mechanism of formation for the double-helical foldaxanes as demonstrated for single-helical foldaxanes.²⁴

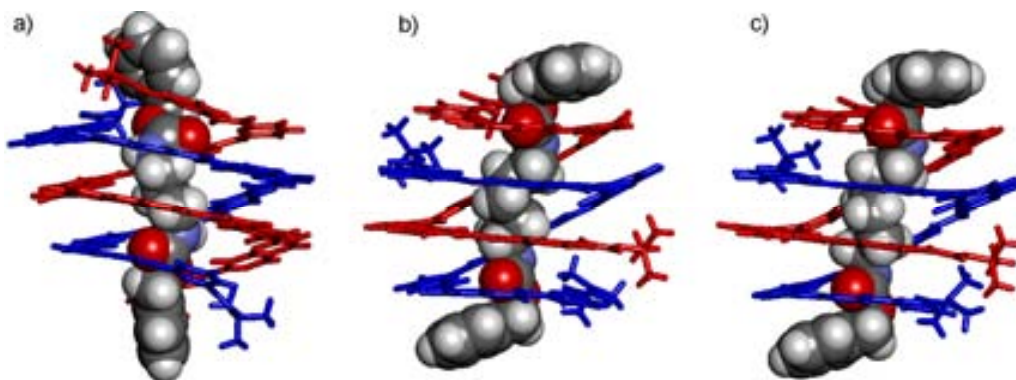


Figure 4. Solid state structures of a) $(\mathbf{1})_2 \supset \mathbf{2b}$; b) $(\mathbf{1})_2 \supset \mathbf{2d}$; and c) $(\mathbf{1})_2 \supset \mathbf{2e}$. The antiparallel strands of $(\mathbf{1})_2$ are shown in red and blue (tube representation). Rod-like guests are shown in CPK (C grey, H white, O red, N light blue). Isobutyl side chains and solvent molecules have been omitted for clarity.

3.2 The screw motion of the double-helical foldaxane

Unlike single-helical foldaxanes, double helical-foldaxanes feature a high tolerance with respect to guest length: $\mathbf{2e}$ is three CH_2 units longer than $\mathbf{2b}$ yet they have comparable affinities for $(\mathbf{1})_2$. In addition, the binding constants as a function of guest length do not follow a trend. A close-up look at the crystal structures shows that, to accommodate $\mathbf{2b}$ or $\mathbf{2d}$, the two strands of $(\mathbf{1})_2$ undergo a relative screw motion of over a third of a turn to adjust the distance along the helix axis between the two 2,6-dicarboxamide units and their angular orientation perpendicular to the helix axis (Figure 5). The structure of $(\mathbf{1})_2 \supset \mathbf{2e}$ is almost superimposable on that of $(\mathbf{1})_2 \supset \mathbf{2d}$, except that the alkyl segment of the guest is compacted in the case of $\mathbf{2e}$ so as to accommodate its extra CH_2 unit, an effect which has been observed in other systems.^{30,31} In agreement with the solid-state structures, ^1H NMR analysis of the solutions showed that signals belonging to terminal functionalities of the strands, for example, the pivaloyl protons and some pyridine protons (Figure 6), consistently shift upfield when the guest is shortened (from $\mathbf{2e}$ to $\mathbf{2b}$), thus suggesting an increase of ring-current effects as would be expected when the two strands screw into one another.

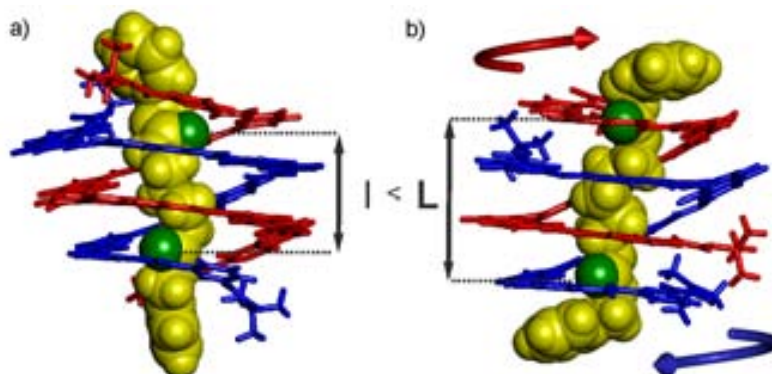


Figure 5. Solid state structures of a) $(1)_2 \supset 2b$; b) $(1)_2 \supset 2d$ illustrating the screw motion. Rods are in yellow CPK representations. The carbonyl oxygen atoms of the carbamate groups are shown in green. l and L represent the distance between the two pyridine clefs in each complex $(1)_2 \supset 2b$ and $(1)_2 \supset 2d$ and are equal to 6.8 Å and 9.0 Å, respectively. The red and blue arrows illustrate the screw motion mechanism between complex $(1)_2 \supset 2b$ and $(1)_2 \supset 2d$. Isobutyl side chains and solvent molecules have been omitted for clarity.

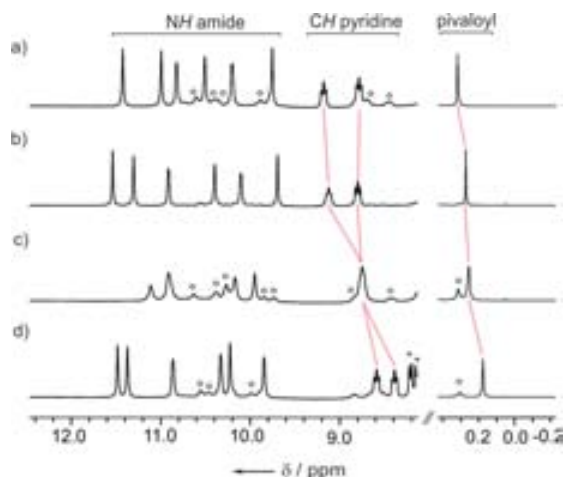


Figure 6. 300 MHz NMR spectra of **1** (8 mM) in $CDCl_3$ at 25°C titrated with a) **2b** (10 equiv.); b) **2c** (20 equiv.); c) **2d** (10 equiv.); d) **2e** (10 equiv.). Unlabeled signals are those of the foldaxanes. Circles denote residual signals of $(1)_2$. The resonances of pivaloyl protons and of pyridine protons in position 4 shift to higher fields when the guest is shortened, consistent with the screwing of the two strands into one another, resulting in an increased ring current effect. In contrast, NH amide protons which converge towards the helix cavity do not shift.

Screwing is also the mechanism by which these double helices are presumed to form from single-stranded precursors in the absence of rod-like guest.³² Here, it is the length of the guest that templates the extent of relative screwing of the two strands within each duplex. The binding constants as a function of guest length do not follow a trend; this result is probably due to the fact that an adjustment in the distance between the 2,6-pyridinedicarboxamide units of the duplex is accompanied by a concomitant change in their angular orientation, therefore not allowing a perfect match for all guests.

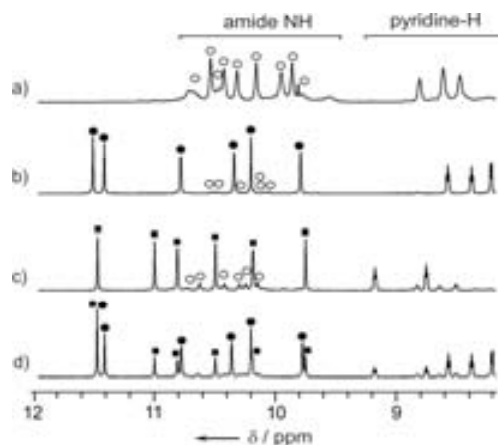


Figure 7. Part of the ^1H NMR spectra (700 MHz) showing the amide and some pyridine proton resonances of $(\mathbf{1})_2$ (8 mM) in CDCl_3 : a) at 25°C in the absence of guest; b) at 0°C in the presence of $\mathbf{2b}$ (10 equiv.); c) at 0°C in the presence of $\mathbf{2e}$ (10 equiv.); d) at 0°C in the presence of $\mathbf{2b}$ and $\mathbf{2e}$ (10 equiv. each). The signals of the starting double helix $(\mathbf{1})_2$ are marked with empty circles (\circ), the signals of $(\mathbf{1})_2 \rightarrow \mathbf{2b}$ with black circles (\bullet) and the signals of $(\mathbf{1})_2 \rightarrow \mathbf{2e}$ with black squares (\blacksquare). Sharper NMR spectra could be recorded at 0°C and are shown in this figure.

A titration of $(\mathbf{1})_2$ with an equimolar mixture of $\mathbf{2b}$ and $\mathbf{2e}$ was then carried out, producing a mixture of $(\mathbf{1})_2 \rightarrow \mathbf{2b}$ and $(\mathbf{1})_2 \rightarrow \mathbf{2e}$ in a 2:1 ratio (Figure 7d). Rotating-frame nuclear Overhauser effect 2D spectroscopy (ROESY) measurements (Figure 8) were recorded on this mixture and showed intense exchange peaks between corresponding protons of the two complexes. Correlations were also observed between each foldaxane and the uncomplexed (free) double helix $(\mathbf{1})_2$. This experiment demonstrates that the double helices may dissociate from one rod and then reassociate with another rod having a different length. The net outcome of this exchange process is a screw or unscrew motion within the duplex, yet it does not proceed through correlated translations and rotations of the strands, but through an unwinding/rewinding mechanism.

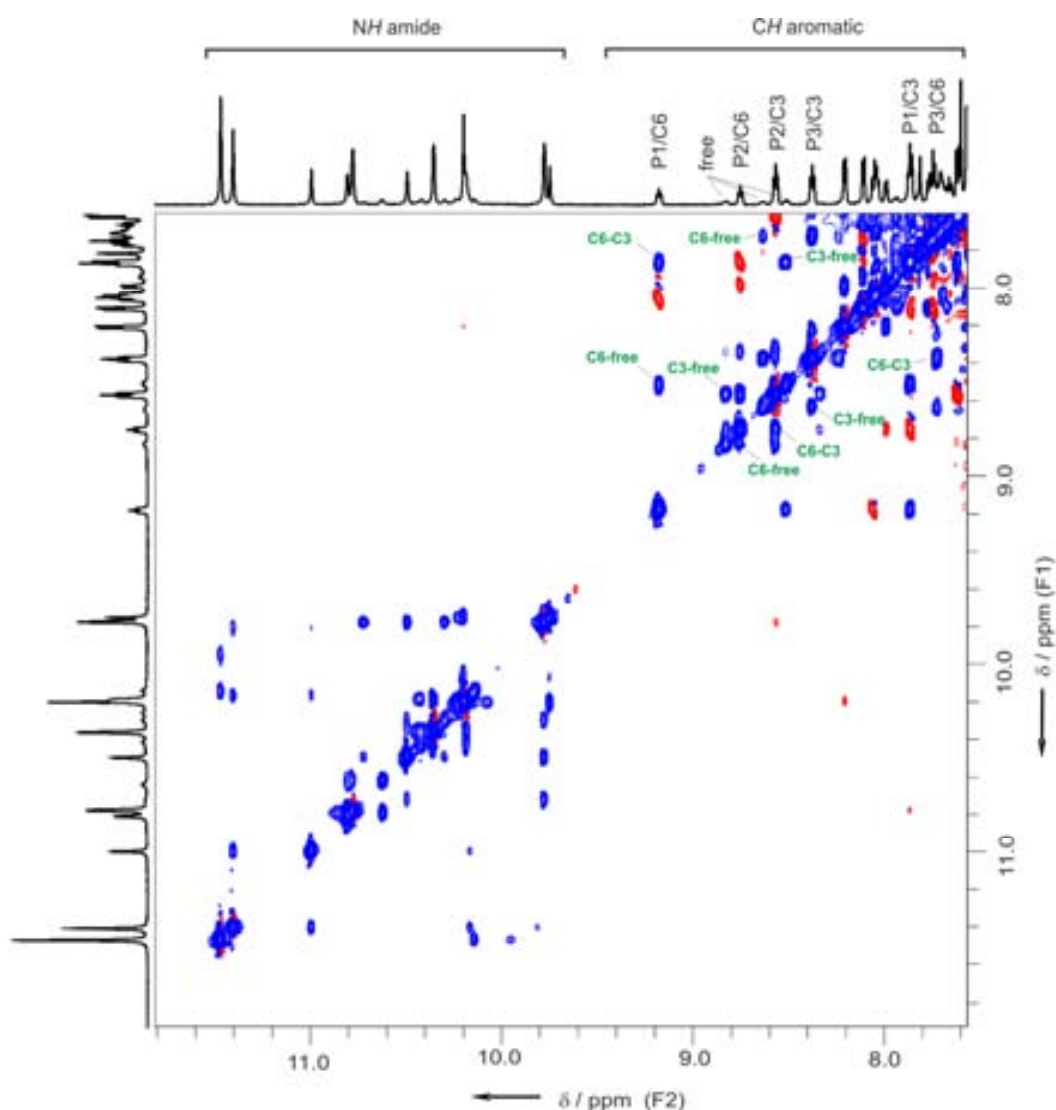


Figure 8. Expansion of the ^1H - ^1H ROESY spectrum (700 MHz) at 4°C of $(\mathbf{1})_2$ (8 mM) in the presence of $\mathbf{2b}$ and $\mathbf{2e}$ (10 equiv. each) recorded with 300 ms mixing time. Intense cross peaks show that protons of the free double helix $(\mathbf{1})_2$, $(\mathbf{1})_2 \rightarrow \mathbf{2b}$ and $(\mathbf{1})_2 \rightarrow \mathbf{2e}$ complex exchange in a slow exchange regime on the NMR time scale. NOEs cross peaks are observed in red whereas exchange peaks are seen in blue. Some exchanges cross peaks have been labelled in green. P1, P2, P3 denote protons belong to independent pyridine spin systems but have not been assigned to each pyridine rings in the sequence. C3 or C6 denotes the number (3 or 6) of CH_2 units of the alkyl chain of the guest on which the double helix resides.

3.3 The screw motion through the shuttling

A step further consisted in placing two helix binding stations of different lengths on a single rod. For this purpose, guest $\mathbf{3}$ was equipped with two binding stations equivalent to those of $\mathbf{2b}$ and $\mathbf{2e}$ (Scheme 2). Upon titrating $(\mathbf{1})_2$ with a large excess of $\mathbf{3}$, a complex $(\mathbf{1})_2 \rightarrow \mathbf{3}$ forms in which a single duplex binds to $\mathbf{3}$. No measurable amount of the higher aggregate, in which two double

helices bound to **3**, was observed. As expected, the ^1H NMR spectrum of $(\mathbf{1})_2 \supset \mathbf{3}$ revealed two sets of signals that corresponded to two isomers of position of $(\mathbf{1})_2$ either on the long station or on the short station of **3** (Figure 9). Neither of these two isomers has a symmetrical structure: the two strands of the duplex are inequivalent in each isomer (Figure 10a). Consequently, the ^1H NMR spectrum of $(\mathbf{1})_2 \supset \mathbf{3}$ features four times as many signals as that of, for example $(\mathbf{1})_2 \supset \mathbf{2b}$ (Figure 9b, 9d).

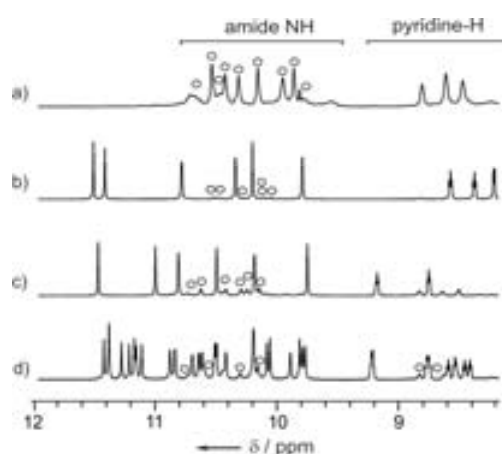


Figure 9. Part of the ^1H NMR spectra (700 MHz) showing the amide and some pyridine proton resonances of $(\mathbf{1})_2$ (8 mM) in CDCl_3 : a) at 25°C in the absence of guest; b) at 0°C in the presence of **2b** (10 equiv.); c) at 0°C in the presence of **2e** (10 equiv.); d) at 0°C in the presence of **3** (10 equiv.). The signals of the starting double helix $(\mathbf{1})_2$ are marked with empty circles (O). Sharper NMR spectra could be recorded at 0°C and are shown in this figure.

ROESY experiments on $(\mathbf{1})_2 \supset \mathbf{3}$ in CDCl_3 solutions revealed that intense exchange takes place between the isomer in which $(\mathbf{1})_2$ is positioned on the long station of **3** and the one in which $(\mathbf{1})_2$ is positioned on the short station, while cross-peaks with traces of the free $(\mathbf{1})_2$ were very weak. As above, the net outcome of this exchange is a screw or an unscrew motion within $(\mathbf{1})_2$. Remarkably, ROESY data demonstrate that exchange and consequently the screw/unscrew motion, proceeds through the shuttling of the duplex along the guest and not via a dissociation-association mechanism. If the latter would occur, each of the four signals of any given proton of the duplex would correlate with the three others (Figure 10c) because the positions of the strands would be randomized in the dissociation process. However, correlations show that any given proton of one isomer of $(\mathbf{1})_2 \supset \mathbf{3}$ exchanges with a single proton of the other isomer (Figure 10b, d), consistent with the shuttling of the duplex along the rod, and the concomitant screw motion. Shuttling requires the disruption of hydrogen bonds between the rod and the duplex and the screw motion of the two strands into one another, but these processes occur faster than foldaxane dissociation.

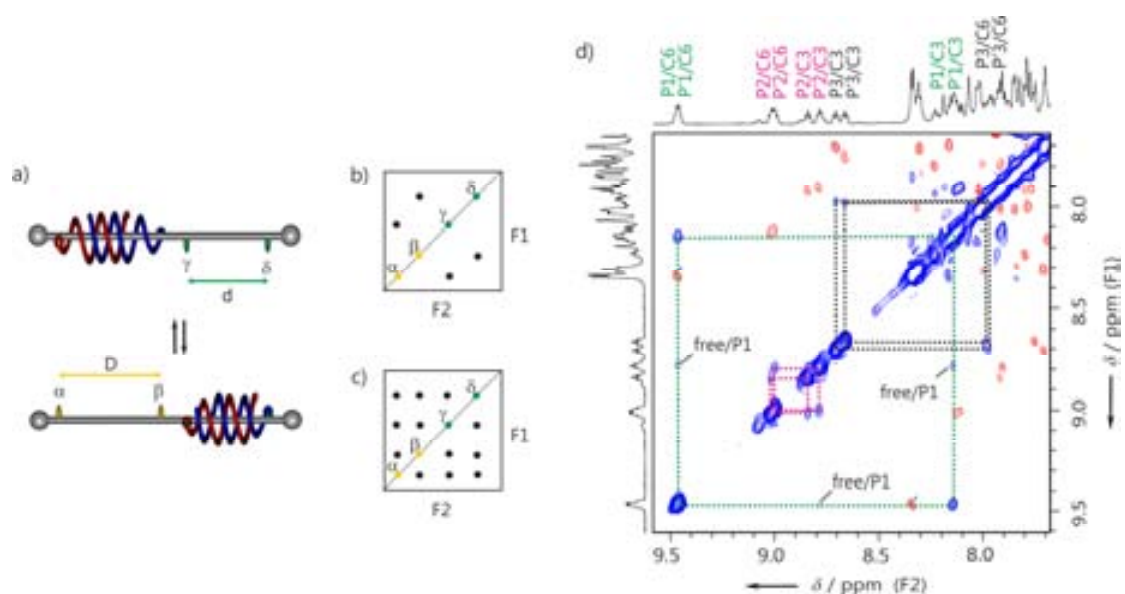


Figure 10. a) A schematic representation of the controlled screw/unscREW of a molecular duplex by its shuttling between two inequivalent stations of a rodlike guest. b) A schematic representation of the number of cross-peaks upon exchange of the duplex between the two inequivalent stations when exchange takes place by shuttling or c) by a dissociation/association mechanism. d) Expansion of the ^1H - ^1H ROESY spectrum (700 MHz) at 4°C of $(\mathbf{1})_2>\mathbf{3}$ (8 mm) recorded with 300 ms mixing time, thus showing that any given proton of one isomer of $(\mathbf{1})_2>\mathbf{3}$ exchanges with a single proton of the other isomer. NOEs cross peaks are observed in red whereas exchange peaks are seen in blue. P1, P2, P3 denote protons that belong to independent pyridine spin systems but have not been assigned to each pyridine rings in the sequence. C3 or C6 denotes the number (3 or 6) of CH_2 units of the alkyl chain of the guest on which the double helix resides.

4. Conclusion

This work showed that an anti-parallel double helical aromatic oligoamide foldamer binds to a series of rod-like guests of various lengths upon winding of the duplex around the guests. The two strands of the duplex undergo a relative screw motion to match with the length of the guests.

The next step could be a regulatory screw motion by triggering it through an external stimulus. Or control the absolute sense of rotation in right- or left-handed helices. One may also be expected to bind this system with a useful function to a surface and achieve relative action. All of these would set the stage for the construction of a truly molecular machinery.

5. Experimental part

5.1 Methods for NMR

NMR spectra were recorded on 2 different NMR spectrometers: (1) an Avance II NMR spectrometer (Bruker Biospin) with a vertical 7,05T narrow-bore/ultrashield magnet operating at 300 MHz for ^1H observation and 75 MHz for ^{13}C observation by means of a 5-mm direct BBO H/X probe with Z gradient capabilities; (2) an Avance III NMR spectrometer (Bruker Biospin) with a vertical 16,45T narrow-bore/ultrashield magnet operating at 700 MHz for ^1H observation by means of a 5-mm TXI $^1\text{H}/^{13}\text{C}/^{15}\text{N}$ probe with Z gradient capabilities. Chemical shifts are reported in parts per million (ppm, δ) relative to the ^1H residual signal of the deuterated solvent used. ^1H NMR splitting patterns with observed first-order coupling are designated as singlet (s), doublet (d), triplet (t), or quartet (q). Coupling constants (J) are reported in hertz. Samples were not degassed. Data processing was performed with Topspin 2.0 software.

ROESY. Rotating-frame Overhauser spectroscopy (ROESY) experiments were recorded at 700 MHz and were used to distinguish dipolar interactions and exchange between free and bound double helices with the following acquisition parameters: the acquisition was performed with 2048(t_2) x 512(t_1) data points, in States-TPPI mode with Z gradients selection and with CW-spinlock for mixing, relaxation delay of 2 s, and 64 scans per increment; sweep width of 14000 Hz in both dimensions; mixing time of 300 ms. Processing was done after a sine-bell multiplication in both dimensions and Fourier transformation in 1K x 1K real points.

5.2 Methods for X-ray crystallography

The data for crystal structures of compounds $(\mathbf{1})_2 \supset \mathbf{2b}$, $(\mathbf{1})_2 \supset \mathbf{2d}$ and $(\mathbf{1})_2 \supset \mathbf{2e}$, have been collected at the European Institute for Chemistry and Biology X-ray facility (UMS 3033) on a Bruker X8 proteum rotating anode at the $\text{CuK}\alpha$ radiation wavelength. The system features the microstar microfocus x-ray source with the PLATINUM135 CCD detector combined with the 4-circle KAPPA goniometer and the Helios multilayer graded optics. The system is driven by the PROTEUM2 software.³³ The unit cell determinations have been performed using a combination of Fast Fourier and Difference Vector techniques, the data were integrated using SAINT and scaled and corrected for absorption with SADABS. All the structures have been solved by direct methods with SHELXD and refined by full-matrix least-squares methods using SHELXL.³⁴ The WinGX-software was used for modelling.³⁵ It has to be noticed that all the crystals described

below contain a large percentage of disordered solvent molecules and very few of them could be modelled in the Fourier difference density maps. High flux X-ray Beams on small crystals with high solvent contents can explain the modest quality of the refinement statistics reported in this study.

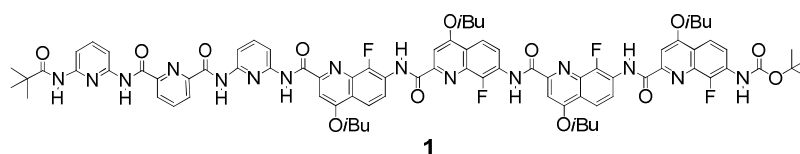
5.3 Summary of X-Ray crystallographic data

Name	Foldaxane (1) ₂ →2b	Foldaxane (1) ₂ →2d	Foldaxane (1) ₂ →2e
Formula	C ₉₇ H ₉₆ Cl ₉ F ₄ N ₁₆ O _{17.5}	C ₁₉₆ H ₂₀₆ Cl _{17.91} F ₈ N ₃₁ O _{34.5}	C ₁₉₅ H ₂₀₁ Cl ₂₁ F ₈ N ₃₂ O _{46.75}
M	2160.95	3980.4	4637.34
Crystal system	Triclinic	Triclinic	Triclinic
Space group	P-1	P-1	P-1
a/Å	19.909(4)	17.764(4)	17.995(4)
b/Å	21.829(4)	21.407(4)	23.036(5)
c/Å	25.945(4)	30.835(4)	31.217(6)
α/o	78.12(3)	101.31(3)	74.79(3)
β/o	84.31(3)	100.24(3)	81.13(3)
γ/o	78.30(4)	112.31(3)	78.79(3)
U/Å ³	10785	10219	12152
T /K	213	213	213
Z	4	2	2
ρ/g cm ⁻¹	1.331	1.294	1.267
size (mm)	0.1 x 0.05 x 0.05	0.05 x 0.02 x 0.02	0.1 x 0.05 x 0.05
λ / Å	1.54178	1.54178	1.54178
μ/mm ⁻¹	2.782	1.702	2.838
Absorption correction	none	none	none
unique data	21169	15775	19696
parameters/restraints	2586/12	2426/44	2646/22
R1, wR2	0.1126, 0.3815	0.1869, 0.4340	0.1796, 0.4477
goodness of fit	1.824	1.135	1.914
CCDC#	816152	816315	816316

5.4 Methods for chemical synthesis

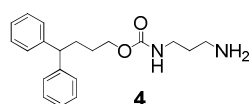
All reactions were carried out under a dry nitrogen atmosphere. Commercial reagents were purchased from Sigma-Aldrich or Alfa-Aesar and were used without further purification unless otherwise specified. Tetrahydrofuran (THF) and dichloromethane (DCM) were dried over alumina column; triethylamine (Et_3N) was distilled from calcium hydride (CaH_2) prior to use. Reactions were monitored by thin layer chromatography (TLC) on Merck silica gel 60-F254 plates and observed under UV light. Column chromatographies were carried out on Merck GEDURAN Si60 (40-63 μm). Melting points were measured on a Büchi B-540. ESI mass spectra were obtained on a Waters LCT Premier from the Mass Spectrometry Laboratory at the European Institute of Chemistry and Biology (UMS 3033 - IECB), Pessac, France.

5.4.1 Synthesis of helix 1



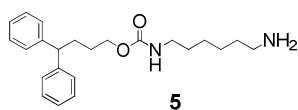
Heptamer 1. Trimer²⁸ P_3 (68 mg, 0.16 mmol) and DIEA (0.1 mL, 1.27 mmol) were dissolved in dry CH_2Cl_2 (10 mL), the freshly prepared tetramer acid chloride²⁷ (200 mg, 0.17 mmol) in CH_2Cl_2 (5 mL) was added dropwise at r.t. After stirring overnight, solvents were evaporated and the product was purified by flash chromatography (SiO_2) eluting with cyclohexane/EtOAc (70:30, vol/vol) to obtain heptamer **1** as a white solid (0.17 g, 68%). ^1H NMR (d_6 -DMSO, 300 MHz): δ 11.47 (s, 1H), 11.28 (s, 1H), 11.02 (s, 1H), 10.42 (s, 1H), 10.08 (s, 1H), 9.94 (s, 1H), 9.20 (s, 1H), 8.48 (t, $J(\text{H,H}) = 8.1$, 1H), 8.06 (d, $J(\text{H,H}) = 6.6$, 1H), 7.94 (t, $J(\text{H,H}) = 8.1$, 2H), 7.86-7.82 (m, 3H), 7.70 (d, $J(\text{H,H}) = 7.5$, 2H), 7.63-7.56 (m, 4H), 7.23 (d, $J(\text{H,H}) = 9.0$, 1H), 7.16-7.14 (m, 2H), 6.96-6.94 (m, 3H), 6.83 (t, $J(\text{H,H}) = 8.1$, 1H), 6.67 (d, $J(\text{H,H}) = 8.4$, 1H), 6.52 (s, 1H), 4.34-4.17 (m, 6H), 4.08-4.00 (m, 2H), 2.42-2.27 (m, 4H), 1.35-1.20 (m, 33H), 0.67 (s, 9H). MS (ESI) : m/z : 1574.54 [$2\text{M}+2\text{H}$]²⁺, 1586.54 [$2\text{M}+\text{Na}+\text{H}$]²⁺, 1596.51 [$2\text{M}+2\text{Na}$]²⁺

5.4.2 Synthesis of guests

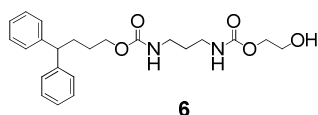


4,4-diphenylbutyl 3-aminopropylcarbamate 4. To a solution of 4-nitrophenyl chloroformate (1.1 g, 5.5 mmol) in dry CH_2Cl_2 (20 mL) was added dropwise a solution of 4,4-diphenylbutan-1-ol³⁶ (1.1 g, 5.0 mmol) and Et_3N (2.8 mL, 20.0 mmol) in CH_2Cl_2 (10 mL) via a syringe at 0°C . After 30 min stirring at room temperature, the reaction mixture was added dropwise over a 1 h period to a solution of 1,3-diaminopropane (4.2 mL, 50.0 mmol) in dry CH_2Cl_2 (100 mL) at 0°C . Then the

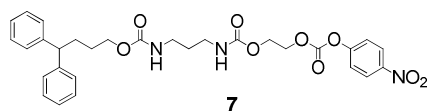
reaction mixture was allowed to proceed at room temperature for 12 h. The solution was washed with 1N NaOH and brine several times, dried over Na₂SO₄. After filtration and concentration, the residual oil was purified by flash chromatography (SiO₂) eluting with MeOH/CH₂Cl₂/Et₃N (10:90:1 to 30:70:1, vol/vol) to obtain product **4** as yellow oil (1.32 g, 83% yield). ¹H NMR (CDCl₃, 300 MHz): δ 7.29-7.14 (m, 10H), 5.12 (br, 1H), 4.08 (t, *J*(H, H) = 6.6, 2H), 3.93 (t, *J*(H, H) = 7.8, 1H), 3.29 (q, *J*(H, H) = 6.0, *J*(H, H) = 6.6, 2H), 2.80 (t, *J*(H, H) = 6.6, 2H), 2.14 (q, *J*(H, H) = 7.8, *J*(H, H) = 7.8, 2H), 1.70 (br, 2H), 1.65-1.53 (m, 4H). ¹³C NMR (CDCl₃, 75 MHz): δ 157.0, 144.7, 128.5, 127.8, 126.2, 64.6, 50.9, 39.1, 38.6, 32.1, 31.9, 27.6. HRMS (ES⁺): *m/z* calcd for C₂₀H₂₆N₂O₂ [M+H]⁺ 327.2073 found 327.2067.



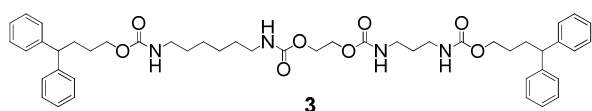
4,4-diphenylbutyl 6-aminohexylcarbamate 5. To a solution of 4-nitrophenyl chloroformate (0.35 g, 1.7 mmol) in dry CH₂Cl₂ (20 mL) was added dropwise a solution of 4,4-diphenylbutan-1-ol³³ (0.36 g, 1.6 mmol) and Et₃N (0.89 mL, 6.4 mmol) in CH₂Cl₂ (10 mL) via a syringe at 0°C. After 30 min stirring at room temperature, the reaction mixture was added dropwise over a 1 h period to a solution of 1,6-diaminohexane (0.93 g, 8.0 mmol) in dry CH₂Cl₂ (100 mL) at 0°C. Then the reaction mixture was allowed to proceed at room temperature for 12 h. The solution was washed with 1N NaOH and brine several times, dried over Na₂SO₄. After filtration and concentration, the residual oil was purified by flash chromatography (SiO₂) eluting with MeOH/CH₂Cl₂/Et₃N (10:90:1 to 30:70:1, vol/vol) to obtain product **5** as yellow oil (0.47 g, 80% yield). ¹H NMR (CDCl₃, 300 MHz): δ 7.30-7.14 (m, 10H), 4.62 (br, 1H), 4.08 (t, *J*(H, H) = 6.3, 2H), 3.93 (t, *J*(H, H) = 7.8, 1H), 3.17 (q, *J*(H, H) = 6.6, *J*(H, H) = 6.6, 2H), 2.68 (br, 2H), 2.14 (q, *J*(H, H) = 7.8, *J*(H, H) = 7.8, 2H), 1.60-1.32 (m, 12H). ¹³C NMR (CDCl₃, 75 MHz): δ 156.8, 144.8, 128.6, 127.9, 126.3, 64.7, 51.1, 42.1, 41.0, 32.0, 30.1, 27.7, 26.6, 26.6. HRMS (ES⁺): *m/z* calcd for C₂₃H₃₂N₂O₂ [M+H]⁺ 369.2542 found 369.2529.



Compound 6. To a solution of 4-nitrophenyl chloroformate (0.734 g, 3.6 mmol) in dry CH₂Cl₂ (20 mL) was added dropwise a solution of 4,4-diphenylbutyl 6-aminohexylcarbamate (1.08 g, 3.3 mmol) and Et₃N (1.83 mL, 13.2 mmol) in CH₂Cl₂ (10 mL) via a syringe at 0°C. After 30 min stirring at room temperature, the above reaction mixture was added dropwise over a 1 h period to a solution of ethylene glycol (9.2 mL, 0.16 mol) in dry THF (100 mL) at 0°C. Then the reaction mixture was allowed to proceed at room temperature for 12 h. The solution was washed with 1N NaOH and brine several times, dried over Na₂SO₄. After filtration and concentration, the residual oil was purified by flash chromatography (SiO₂) eluting with EtOAc/CH₂Cl₂ (20:80 to 60:40, vol/vol) to obtain product **6** as colourless oil (0.58 g, 42% yield). ¹H NMR (CDCl₃, 300 MHz): δ 7.30-7.15 (m, 10H), 5.39 (br, 1H), 5.04 (br, 1H), 4.20 (t, *J*(H, H) = 4.2, 2H), 4.08 (t, *J*(H, H) = 6.6, 2H), 3.93 (t, *J*(H, H) = 7.8, 1H), 3.80 (t, *J*(H, H) = 4.2, 2H), 3.24-3.18 (m, 4H), 2.52 (br, 1H), 2.14 (q, *J*(H, H) = 7.8, *J*(H, H) = 7.8, 2H), 1.67-1.55 (m, 4H). ¹³C NMR (CDCl₃, 75 MHz): δ 157.5, 157.3, 144.8, 128.6, 127.9, 126.3, 66.9, 65.0, 61.9, 51.1, 37.7, 37.6, 32.0, 30.5, 27.7. HRMS (ES⁺): *m/z* calcd for C₂₃H₃₀N₂NaO₅ [M+Na]⁺ 437.2052 found 437.2045.



Compound 7. To a solution of 4-nitrophenyl chloroformate (0.21 g, 1.06 mmol) in dry CH_2Cl_2 (20 mL) was added dropwise a solution of **6** (0.4 g, 0.97 mmol) and Et_3N (0.54 mL, 3.86 mmol) in CH_2Cl_2 (10 mL) via a syringe at 0°C . Then the reaction mixture was allowed to proceed at room temperature for 2 h. The solution was evaporated and the residual oil was purified by flash chromatography (SiO_2) eluting with $\text{EtOAc}/\text{CH}_2\text{Cl}_2$ (10:90 to 30:70, vol/vol) to obtain product **7** as colourless oil (0.50 g, 88% yield). ^1H NMR (CDCl_3 , 300 MHz): δ 8.30-8.25 (m, 2H), 7.41-7.38 (m, 2H), 7.30-7.14 (m, 10H), 5.32 (br, 1H), 4.93 (br, 1H), 4.48-4.45 (m, 2H), 4.38-4.36 (m, 2H), 4.08 (t, $J(\text{H}, \text{H}) = 6.6$, 2H), 3.93 (t, $J(\text{H}, \text{H}) = 7.8$, 1H), 3.26-3.20 (m, 4H), 2.14 (q, $J(\text{H}, \text{H}) = 7.8$, $J(\text{H}, \text{H}) = 7.8$, 2H), 1.68-1.53 (m, 4H). ^{13}C NMR (CDCl_3 , 75 MHz): δ 157.2, 156.3, 155.3, 152.3, 145.3, 144.6, 128.4, 127.7, 126.1, 125.2, 121.7, 67.4, 64.7, 61.9, 50.8, 37.5, 37.3, 31.8, 30.2, 27.5. HRMS (ES^+): m/z calcd for $\text{C}_{30}\text{H}_{33}\text{N}_3\text{NaO}_9$ [$\text{M}+\text{Na}$] $^+$ 602.2114 found 602.2063.



Rod 3. To compound **7** (0.33 g, 0.58 mmol) in dry CH_2Cl_2 (10 mL) was added dropwise a solution of 4,4-diphenylbutyl 6-aminohexylcarbamate (0.21 g, 0.58 mmol) and Et_3N (0.32 mL, 2.3 mmol) in CH_2Cl_2 (10 mL) via a syringe at 0°C . Then the reaction mixture was allowed to proceed at room temperature for 12h. The solution was washed with 1 N NaOH and brine several times, dried over Na_2SO_4 . After filtration and concentration, the residual oil was purified by flash chromatography (SiO_2) eluting with $\text{EtOAc}/\text{CH}_2\text{Cl}_2$ (20:80 to 50:50, vol/vol) to obtain product **3** as a white solid (0.39 g, 84% yield). ^1H NMR (CDCl_3 , 300 MHz): δ 7.30-7.14 (m, 20H), 5.18 (br, 1H), 5.04 (br, 1H), 4.81 (br, 1H), 4.67 (br, 1H), 4.23 (br, 4H), 4.08 (t, $J(\text{H}, \text{H}) = 6.6$, 4H), 3.93 (t, $J(\text{H}, \text{H}) = 7.8$, 2H), 3.23-3.12 (m, 8H), 2.14 (q, $J(\text{H}, \text{H}) = 7.8$, $J(\text{H}, \text{H}) = 7.8$, 4H), 1.66-1.53 (m, 6H), 1.47-1.45 (m, 4H), 1.31 (br, 4H). ^{13}C NMR (CDCl_3 , 75 MHz): δ 157.2, 156.8, 156.7, 156.3, 144.8, 144.7, 128.5, 127.8, 126.3, 64.8, 64.6, 63.2, 63.1, 51.0, 40.9, 40.8, 37.6, 37.5, 31.9, 30.4, 29.9, 29.8, 27.7, 26.3. HRMS (ES^+): m/z calcd for $\text{C}_{47}\text{H}_{60}\text{N}_4\text{NaO}_8$ [$\text{M}+\text{H}$] $^+$ 831.4309 found 831.4313. m.p.: 101.5 - 102.3°C .

6. References

- 1 D. B. Amabilino, C. O. Dietrich-Buchecker, A. Livoreil, L. Pérez-García, J.-P. Sauvage, J. F. Stoddart, A switchable hybrid [2]-catenane based on transition metal complexation and π -electron donor-acceptor interactions. *J. Am. Chem. Soc.*, **1996**, *118*, 3905–3913.
- 2 T. C. Bedard, J. S. Moore, Design and synthesis of a “mMolecular tumstile”. *J. Am. Chem. Soc.*, **1995**, *117*, 10662–10671.
- 3 C.-F. Lee, D. A. Leigh, R. G. Pritchard, D. Schultz, S. J. Teat, G. A. Timco, R. E. P. Winpenny, Hybrid organic–inorganic rotaxanes and molecular shuttles. *Nature*, **2009**, *458*, 314–318.
- 4 P. L. Anelli, N. Spencer, J. F. Stoddart, A Molecular Shuttle. *J. Am. Chem. Soc.*, **1991**, *113*, 5131–5133.
- 5 S. Hiraoka, E. Okuno, T. Tanaka, M. Shiro, M. Shionoya, Ranging correlated motion (1.5 nm) of two coaxially arranged rotors mediated by helix inversion of a supramolecular transmitter. *J. Am. Chem. Soc.*, **2008**, *130*, 9089–9098.
- 6 T. Muraoka, K. Kinbara, T. Aida, Mechanical twisting of a guest by a photoresponsive host. *Nature*, **2006**, *440*, 512–515.
- 7 J. Clayden, J. H. Pink, Concerted rotation in a tertiary aromatic amide: towards a simple molecular gear. *Angew. Chem. Int. Ed.*, **1998**, *37*, 1937–1939.
- 8 J. D. Badjic, V. Balzani, A. Credi, S. Silvi, J. F. Stoddart, A molecular elevator. *Science*, **2004**, *303*, 1845–1849.
- 9 M. C. Jiménez, C. Dietrich-Buchecker, J.-P. Sauvage, Towards synthetic molecular muscles: contraction and stretching of a linear rotaxane dimer. *Angew. Chem. Int. Ed.*, **2000**, *39*, 3284–3287.
- 10 K. Miwa, Y. Furusho, E. Yashima, Ion-triggered spring-like motion of a double helicate accompanied by anisotropic twisting. *Nature chemistry*, **2010**, *2*, 444–449.
- 11 V. Percec, J. G. Rudick, M. Peterca, P. A. Heiney, Nanomechanical function from self-organizable dendronized helical polyphenylacetylenes. *J. Am. Chem. Soc.*, **2008**, *130*, 7503–7508.
- 12 V. Berl, R. G. Khoury, I. Huc, M. J. Krische, J.-M. Lehn, Interconversion of single and double helices formed from synthetic molecular strands. *Nature*, **2000**, *407*, 720–723.
- 13 M. R. Panman, P. Bodis, D. J. Shaw, B. H. Bakker, A. C. Newton, E. R. Kay, A. M. Brouwer, W. J. Buma, D. A. Leigh, S. Woutersen, Operation mechanism of a molecular machine revealed using time-resolved vibrational spectroscopy. *Science*, **2010**, *328*, 1255–1258.
- 14 V. Serreli, C.-F. Lee, E. R. Kay, D. A. Leigh, A molecular information ratchet. *Nature*, **2007**, *445*, 523–527.
- 15 J. E. Green, J. W. Choi, A. Boukai, Y. Bunimovich, E. Johnston-Halperin, E. DeIonno, Y. Luo, B. A. Sheriff, K. Xu, Y.S. Shin, H.-R. Tseng, J. F. Stoddart, J. R. Heath, A 160-kilobit molecular electronic memory patterned at 10^{11} bits per square centimeter. *Nature*, **2007**, *445*, 414–417.
- 16 N. Ruangsupapichat, M. M. Pollard, S. R. Harutyunyan, B. L. Feringa, Reversing the direction in a light-driven rotary molecular motor. *Nature Chem.*, **2011**, *3*, 53–60.
- 17 D. A. Leigh, J. K. Y. Wong, F. Dehez, F. Zerbetto, Unidirectional rotation in a mechanically interlocked molecular rotor. *Nature*, **2003**, *424*, 174–179.
- 18 T. R. Kelly, H. De Silva, R. A. Silva, Unidirectional rotary motion in a molecular system. *Nature*, **1999**, *401*, 150–152.
- 19 N. Koumura, R. W. J. Zijlstra, R. A. van Delden, N. Harada, B. L. Feringa, Light-driven monodirectional molecular rotor. *Nature*, **1999**, *401*, 152–155.
- 20 S. P. Fletcher, F. Dumur, M. M. Pollard, B. L. Feringa, A reversible, unidirectional molecular rotary motor driven by chemical energy. *Science*, **2005**, *310*, 80–82.
- 21 C. Dolain, V. Maurizot, I. Huc, Protonation-induced transition between two distinct helical conformations of a

- synthetic oligomer via a linear intermediate. *Angew. Chem. Int. Ed.*, **2003**, *42*, 2738–2740.
- 22 E. Kolomiets, V. Berl, I. Odriozola, A. M. Stadler, N. Kyritsakas, J.-M. Lehn, Contraction/extension molecular motion by protonation/deprotonation induced structural switching of pyridine derived oligoamides. *Chem. Commun.*, **2003**, 2868–2869.
 - 23 D. Kanamori, T.-a. Okamura, H. Yamamoto, N. Ueyama, Linear-to-turn conformational switching induced by deprotonation of unsymmetrically linked phenolic oligoamides. *Angew. Chem. Int. Ed.*, **2005**, *44*, 969–972.
 - 24 Q. Gan, Y. Ferrand, C. Bao, B. Kauffmann, A. Grélard, H. Jiang, I. Huc, Helix-rod host-guest complexes with shuttling rates much faster than disassembly. *Science*, **2011**, *331*, 1172–1175.
 - 25 N. Delsuc, T. Kawanami, J. Lefeuvre, A. Shundo, H. Ihara, M. Takafuji, Ivan Huc, Kinetics of helix handedness inversion: folding and unfolding in aromatic amide oligomers. *ChemPhysChem*, **2008**, *9*, 1882–1890
 - 26 E. Berni, B. Kauffmann, C. Bao, J. Lefeuvre, D. M. Bassani, I. Huc, Assessing the mechanical properties of a molecular spring. *Chem. Eur. J.*, **2007**, *13*, 8463–8469.
 - 27 Q. Gan, C. Bao, B. Kauffmann, A. Grélard, J. Xiang, S. Liu, I. Huc, H. Jiang, Quadruple and double helices of 8-fluoroquinoline oligoamides. *Angew. Chem. Int. Ed.*, **2008**, *47*, 1715–1718.
 - 28 C. Bao, Q. Gan, B. Kauffmann, H. Jiang, I. Huc, A self-assembled foldamer capsule: combining single and double helical segments in one aromatic amide sequence. *Chem. Eur. J.*, **2009**, *15*, 11530–11536.
 - 29 C. Bao, B. Kauffmann, Q. Gan, K. Srinivas, H. Jiang, I. Huc, Converting sequences of aromatic amino acid monomers into functional three-dimensional structures: second-generation helical capsules. *Angew. Chem. Int. Ed.*, **2008**, *47*, 4153–4156.
 - 30 D. Ajami, J. Rebek, Jr., Compressed alkanes in reversible encapsulation complexes. *Nature Chem.*, **2009**, *1*, 87–90.
 - 31 L. Trembleau, J. Rebek Jr., Helical conformation of alkanes in a hydrophobic cavitand. *Science*, **2003**, *301*, 1219–1220.
 - 32 A. Acocella, A. Venturini, F. Zerbetto, Pyridinedicarboxamide strands form double helices via an activated slippage mechanism. *J. Am. Chem. Soc.*, **2004**, *126*, 2362–2367.
 - 33 Proteum II suite Bruker AXS version **2005**.
 - 34 G. M. Sheldrick, A short history of SHELX. *Acta Cryst.*, **2008**, *A64*, 112–122.
 - 35 L. J. Farrugia, WinGX suite for single crystal small molecule crystallography. *J. Appl. Cryst.*, **1999**, *32*, 837–838.
 - 36 V. N'Goka, G. Schlewer, J.-M. Linget, J.-P. Chambon, C.-G. Wermuth, GABA-uptake inhibitors: construction of a general pharmacophore model and successful prediction of a new representative. *J. Med. Chem.*, **1991**, *34*, 2547–2557.

Chapter 4

Identification of a foldaxane kinetic by-product during guest-induced single to double helix conversion

1. Introduction

Self-assembly has been widely applied in biological system, chemistry, material science and nanotechnology.¹⁻⁴ Following Whitesides and Grzybowski,⁴ self-assembly can be defined as a process by which pre-existing discrete components organize into patterns or structures without human intervention. This process is generally assumed to involve the cooperative procedures of misassembly, dissociation, correction, and reassembly, leading from initial kinetic intermediates to final thermodynamic product.^{6,7}

Indeed, some investigations have found that these kinetically controlled reaction steps in self-assembly events is crucial to construct out-of-equilibrium artificial ordered aggregates,⁸⁻¹⁰ complex self assemblies¹¹⁻¹³ or sophisticated molecular machines^{14,15} that would resemble their biological counterparts. However, the detailed understanding of kinetic steps is still a challenge, since the kinetic compounds that form prior to the final thermodynamic product normally can not be easily observed or characterized due to their short life time and multi-component equilibrium processes. A successful way to get the kinetically controlled products have been achieved by using a robust metal coordination method in which the structures of intermediates could be stabilized and the whole self-assembly process slow down.^{11,16}

Here, we noticed that our foldaxane systems could be used for the same purpose: An aromatic helix as a trapper could catch a dumbbell-shaped guest to form a 1:1 host-guest complex. This complex was found to be a long-lived kinetic supramolecular by-product as it slowly transformed into a thermodynamically more favorable 2:2 architecture. The details of design are as follows.

Recently, we introduced helical aromatic oligoamide foldamer molecular capsule **1** which can bind tartaric acid diastereoselectively (Figure 1a).^{17,18} Its design is based on amino-acid units coding for a large helix cavity in the center of the sequence and a narrow helix diameter at the ends, thus creating a binding site completely surrounded by the helix backbone. In previous chapters, we showed that multi-turn single or double helical oligoamide foldamers possessing open cavities can wind around urethane dumbbell guests to form thermodynamically stable complexes in which the two bulky stoppers of the guest protrude from each side of the helix cavity in a pseudo-rotaxane-like geometry.^{19,20} These complexes were termed foldaxanes. We devised that a combination of these two concepts may allow assembly of foldaxanes using dumbbell guests **3**, derived from tartaric acid and oligomer **2** based on the shortened version of **1**.

On one hand, the helix of **2** without the terminal quinoline units is expected to possess an open cavity and could bind to the guests **3** to form a 1:1 foldaxane via hydrogen bonds between carboxylic acid groups of the guest and the naphthyridine units of the helix. On the other hand, the helix **2** could also hybridize itself to duplex $(2)_2$, and the symmetrical pyridine units at the termini of $(2)_2$ may thus provide hydrogen bonding sites suitable for the guest, and as a result of form a 2:2 host-guest complex in which two guest molecules are located at the extremities of a double helix. Compared to the 1:1 foldaxane, the 2:2 complex is more thermodynamic stable. Therefore, when mixed, the helical host **2** and the guest **3** initially form the foldaxane (kinetic product) and then slowly transform into the 2:2 host-guest complex (Figure 1).

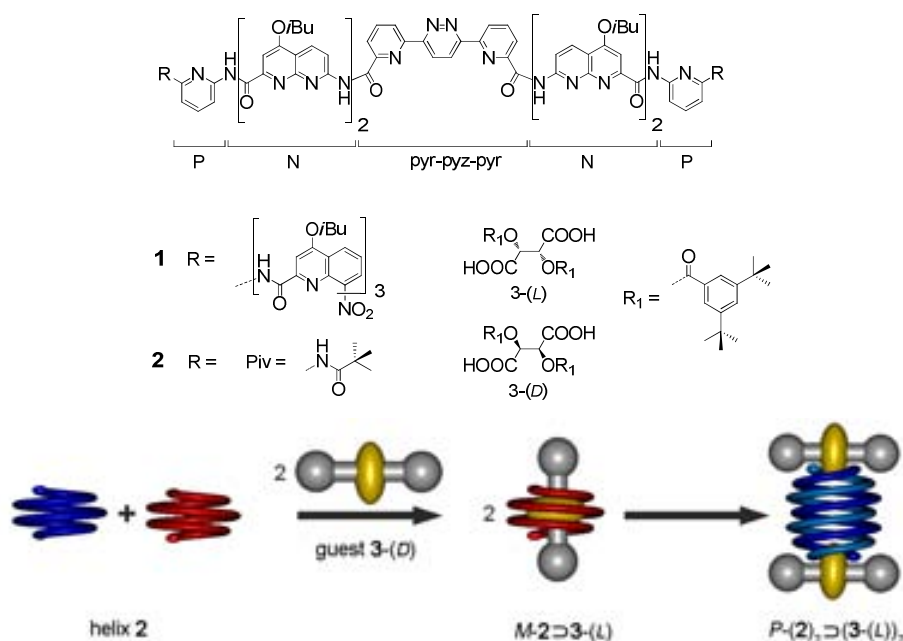


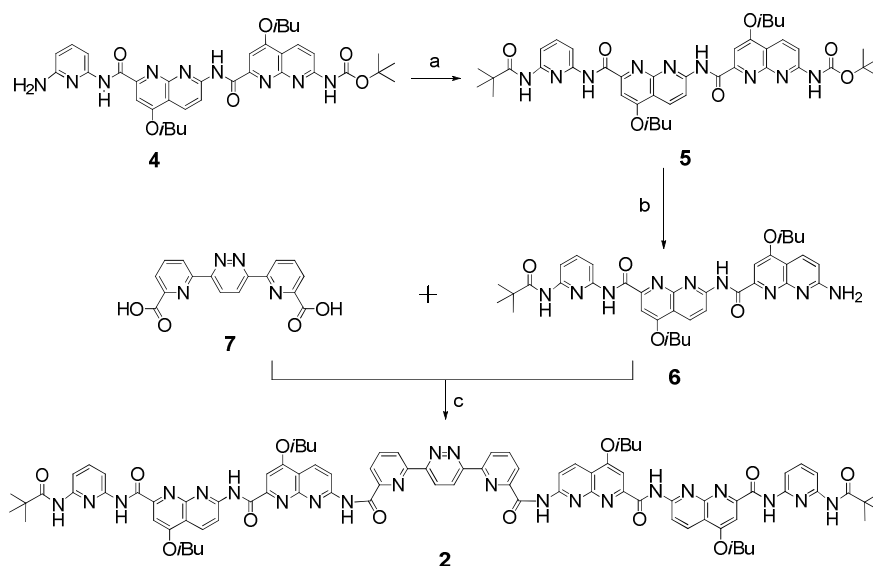
Figure 1. a) Structures of oligomers **1** and **2** and of dumbbell guest **3**. A letter code is used for the abbreviations of the oligomer subunits. b) Cartoon representation of self-assembly process from single helix **2** to 1:1 kinetic by-product $M-2 \supset 3-(L)$, then to 2:2 thermodynamic complex $P-(2)_2 \supset (3-(L))_2$.

During the transformation process, it was found that the chiroptical signals which reflect the handedness of helix also reversed by circular dichroism (CD) detection, that is, the same guest is thus able to induce *P* or *M* helicity depending on whether it interacts with a single or a double helix.

2. Synthesis

2.1 Synthesis of helix

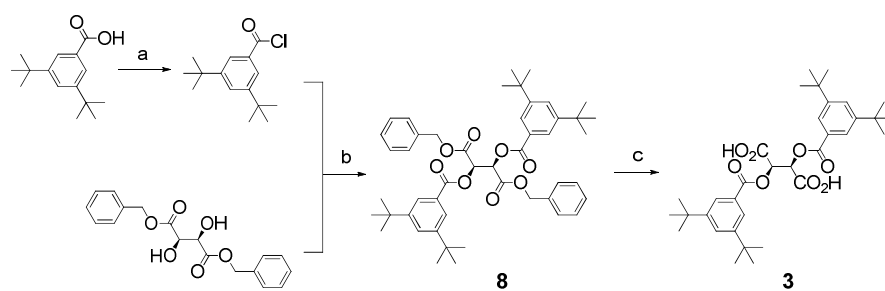
The structure of the aromatic oligoamides **2** and its synthetic procedures were listed in Scheme 1. The synthesis of **2** involves the piv-PN₂-Boc building block which, after Boc cleavage, was coupled twice to the acids of the central pyridine-pyridazine-pyridine unit (pyr-pyz-pyr).



Scheme 1. The synthesis of foldamer **2**: a) pivaloyl chloride, Et₃N, DCM, rt, 12 h (83%); b) TFA, DCM, rt, 6 h (95%); c) PyBOP, Et₃N, CHCl₃, 45 °C, 12 h (88%).

2.2 Synthesis of guests

The two optically pure enantiomers **3-(D)** and **3-(L)** were prepared upon coupling 3,5-di-*tert*-butylbenzoyl chloride to either *D* or *L*-dibenzyl tartrate, respectively, followed by the Pd/C catalyzed hydrogenolysis of the benzyl groups (Scheme 2).



Scheme 2. Synthesis of guest **3** (*R,R*)-Tartaric acid di-3,5-di-*tert*-butylbenzoate. a) oxalyl chloride, DCM, rt, 3 h (78%); b) Et₃N, DMAP, DCM, rt, 24 h; c) H₂, Pd/C, EtOAc, rt, 12 h (quant.).

3. Results and discussion

3.1 Hybridization behavior of foldamer **2**

A preliminary investigation of the behavior of **2** in solution revealed that, like many other aromatic amide sequences,²¹⁻²³ its single helical conformation is at equilibrium with a double helical species. This is reflected by *e.g.* two sets of signals on ¹H NMR spectra assigned to the monomer and the dimer, the proportion of which vary with concentration (Figure 2).

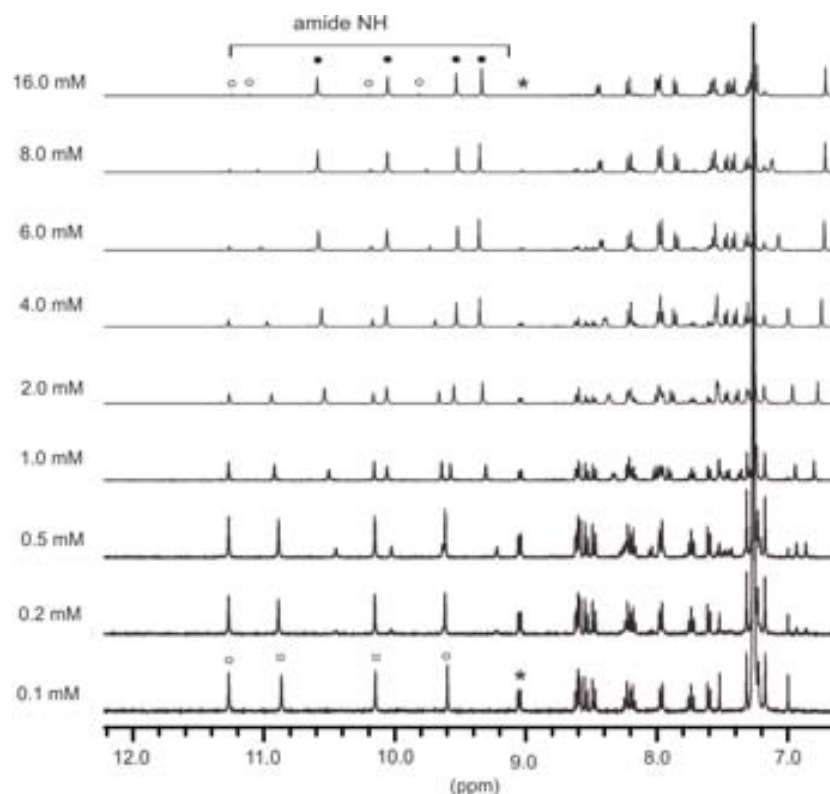


Figure 2. Part of 400MHz ¹H NMR of **2** at various concentrations in CDCl₃ at 293K. Empty circles indicate a single helix configuration, black circles indicate a double helix configuration whereas stars denote an aromatic resonance. Each measurement has been performed 10 minutes after the preparation of the sample.

A ¹H DOSY measurement on a 2 mM solution of **2** at 293 K (Figure 3) showed two distinct diffusion coefficients for **2** and its double helix (**2**)₂ which were calculated to be 7.38×10^{-10} and $6.44 \times 10^{-10} \text{ m}^2 \text{ s}^{-1}$, respectively.

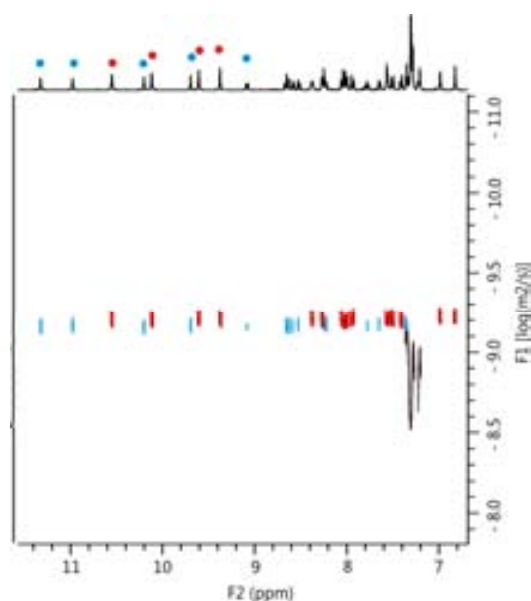


Figure 3. Part of ^1H DOSY (diffusion ordered spectroscopy) NMR spectrum (400 MHz) of a mixture of **2** (blue circles) and **(2)₂** (red circles) at 2 mM in CDCl_3 (293K) showing the NH amide and CH aromatic region of both single and double helix of **2**.

However, unlike for other aromatic amide double helices,²¹⁻²³ we found that the NMR signals of the double helix also varied with concentration ($\Delta\delta$ up to 0.2 ppm) (Figure 2), indicating another aggregation phenomenon that takes place rapidly on the NMR time scale. Self-aggregation of the double helices themselves due to the aromatic and hydrogen bonding groups present at their termini could explain these chemical shift variations. This resulted in a bias of the single helix \rightleftharpoons double helix equilibrium, which shifted in favor of the double helix at high concentration. For example, the apparent dimerization constants were measured to be 420 M^{-1} at 0.5 mM and 4900 M^{-1} at 8 mM, based on the integration of the single helix vs the double helix amide resonances (Table 1).

Table 1. Dimerization constants (K_{dim}) of **2** calculated using dilution experiments at 293K

Concentration (mM)	0.2	0.5	1	2	4	6	8	16
$K_{\text{dim}} (\text{L}\cdot\text{mol}^{-1})$	367	422	829	1243	1860	3034	4861	8940

Exchange Spectroscopy (EXSY) NMR experiments at 293 K allowed to calculate the rate constants of double helix formation and dissociation to be $107 \text{ s}^{-1}\text{M}^{-1}$ and 0.061 s^{-1} , respectively (Figure 4). The double helical dimer was also characterized in the solid state by x-ray

crystallography (Figure 5). These results further expand to the central pyr-pyz-pyr segment the already wide range of aromatic amino acids that are compatible with double helix formation. Double helices do not form in the case of the capsule sequence **1** from which **2** is derived.^{17,18} This is explained by the poor ability of the terminal quinoline units to undergo the spring-like extension required for double helix formation.²⁴ Suppressing (or reducing the number of) quinoline units that code for a narrow helix diameter has been observed to promote double helix formation in other systems.²⁵

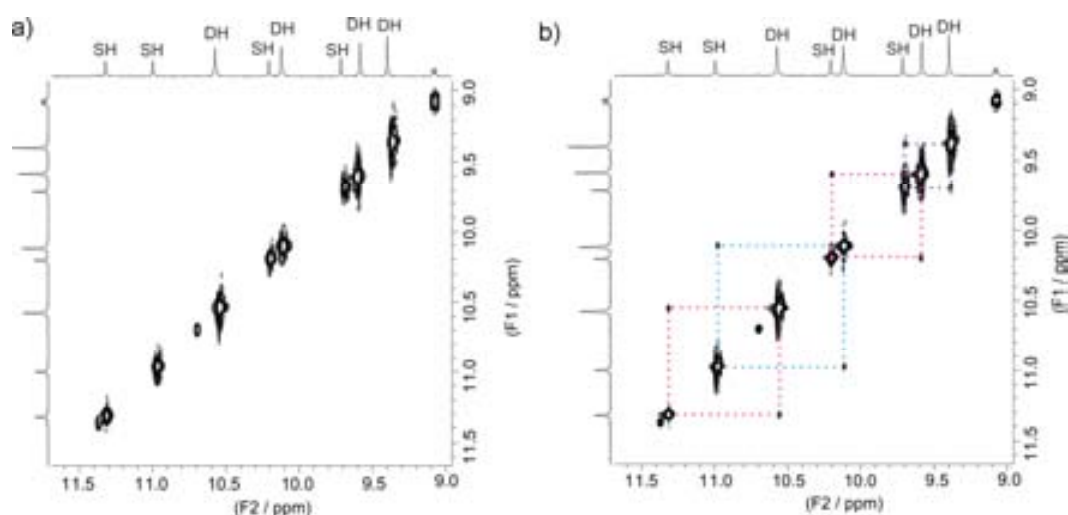


Figure 4. Part of 2D-EXSY spectrum at 400 MHz of **2** (2.4 mM CDCl₃, 293K) at: a) $\tau_m = 0$ ms; b) $\tau_m = 150$ ms. SH donates amide peaks of the single helix and DH donates amide peaks of the double helix.

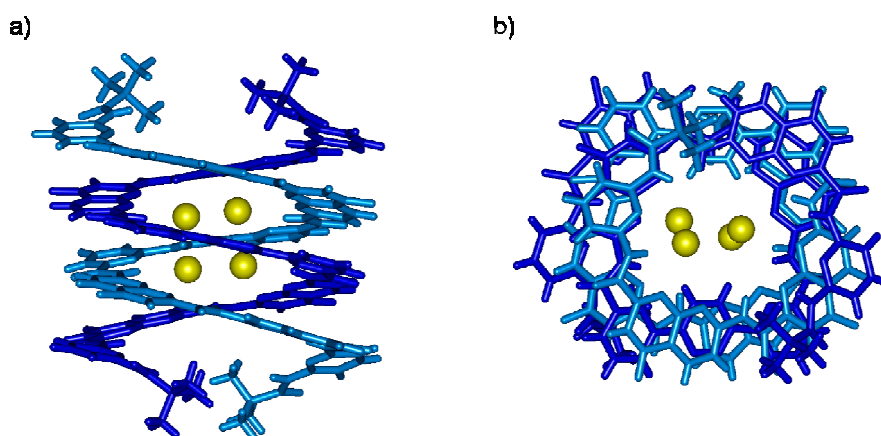


Figure 5. a) Side view of the crystal structure of (**2**)₂; b) Top view of the crystal structure of (**2**)₂ in tube representation. Encapsulated water molecules are highlighted in yellow. Isobutyl side chains and included solvent molecules (other than encapsulated water molecules) have been removed for clarity.

3.2 The kinetic formation of 1:1 foldaxane

Host-guest interactions were then investigated both by ^1H NMR and circular dichroism (CD) to estimate the ability of **2** to fold around tartaric acid derivative **3**. Upon adding **3** to a solution of **2** in CDCl_3 (0.1 mM), a concentration at which the single helical conformation of **2** predominates (>99%), (Figure 6, empty circles), the NMR signals of the latter disappeared and a new species emerged that corresponds to a complex in which **3** is bound within the cavity of **2** (Figure 6, empty squares). The binding constant was measured accurately by titration experiments (Figure 7) through the integral ratios of the free and bound receptor amide resonances to be $K_a = 2.7 \times 10^4 \text{ L mol}^{-1}$ at 298 K in CDCl_3 . Based on previous investigations of the binding of tartaric acid to **1**,¹⁷ the sharp signal at 15.7 ppm in the spectrum of **2**⋮**3** was assigned to the acid protons of the guest which are hydrogen-bonded to the central naphthyridine units of **2**, suggesting similar modes of binding of tartaric acid by **1** and **2**. This similarity is further expressed in CD titrations for which strong responses of opposite signs appeared upon the addition of either **3**-(*D*) or **3**-(*L*).

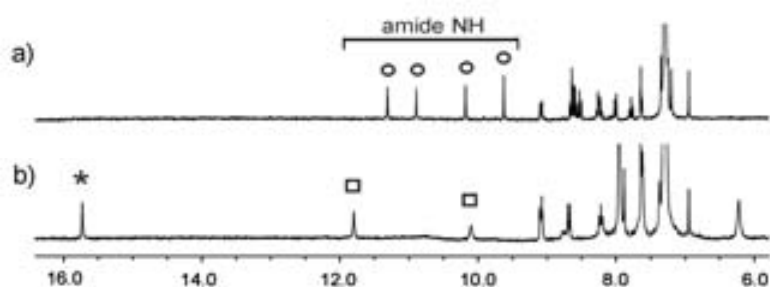


Figure 6. a) Part of ^1H NMR spectra at 298 K (300 MHz) of single helix of **2** (0.1 mM); b) ^1H NMR spectra at 298K of single helix of **2** (0.1 mM) after the addition of guest **3** (0.6 mM) in 10 min.

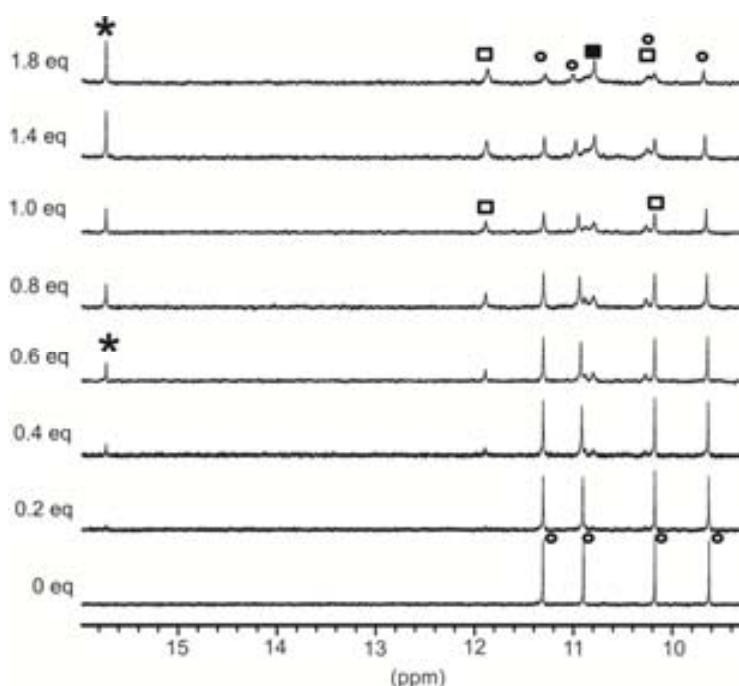


Figure 7. Part of the 700 MHz NMR spectra recorded for the binding study of **2** as a single helix vs. guest **3** in CDCl_3 at 298K. $[\mathbf{2}]_{\text{initial}} = 50 \mu\text{M}$, $[\mathbf{3}]_{\text{titrant}} = 2 \text{ mM}$. Empty black circles correspond to the empty receptor as a single helix. The star (*) denotes the hydrogen bonded acid protons of the guest in single helix \rightarrow guest **3**. NH amides of the single helix \rightarrow guest **3** are marked with empty squares whereas those of the complex with double helix are marked with a black square. Measurements have been performed 5 minutes after each addition of guest.

The host-guest interaction is fully diastereoselective and results in an induced handedness in **2**. A strong negative Cotton effect at 360 nm for **2** \rightarrow **3**-(*L*) suggests that the same handedness preference occurs in **2** \rightarrow **3** as in **1** \rightarrow tartaric acid: the *L* enantiomer favors *M* helicity. CD was also employed as an additional technique to support NMR titrations. The progressive addition of **3**-(*D*) into a solution of **2** (10 μM) resulted into the appearance a positive signal which gave an excellent fit to a 1:1 binding model (Figure 8). The binding constant measured by CD at 273 K ($4.4 \times 10^4 \text{ L mol}^{-1}$) was reasonably close to that obtained by NMR at 298 K.

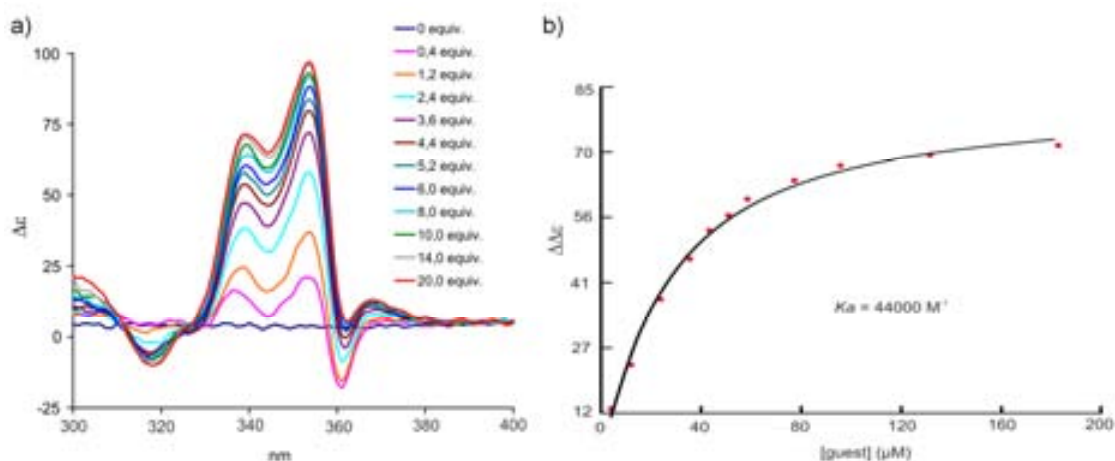


Figure 8. a) CD spectra recorded for the binding study of **2** as a single helix vs. guest **3** in CDCl_3 at 273K. $[\mathbf{2}]_{\text{initial}} = 10 \mu\text{M}$, $[\mathbf{3}]_{\text{titrant}} = 2 \text{mM}$. Measurements have been performed 5 minutes after each addition of guest. b) Experimental (red circles) and calculated (black line) values for the CD binding study. Association constant K_a measured at 340 nm: 44000M^{-1} .

These results, along with the detailed structural data available for the complex of **1**⊃tartaric acid¹⁷ allow to propose an energy minimized model of the structure of *M*-**2**⊃**3**-(*L*) having the expected foldaxane architecture with the helix wrapped around the dumbbell guest (Figure 9) and carboxylic acid groups of the guest hydrogen bonded to naphthyridines of the host.

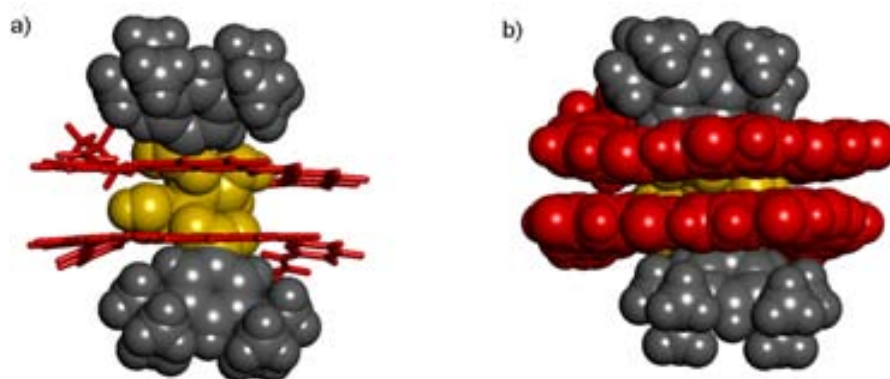


Figure 9. a) CPK (guest) and tube (host), and b) CPK (host and guest) representations of the foldaxane *M*-**2**⊃**3**-(*L*) as obtained by molecular modeling (MMFF's force field) using Maestro v.6.5.

3.3 The formation of 2:2 thermodynamic complex

The kinetics of the quantitative formation of **2**⊃**3** from the single helix of **2** and the kinetics of guest-induced single helix handedness inversion are fast: a steady state is reached within seconds (before CD or NMR measurements can be carried out). When stored at -18°C , a sample remains

unchanged for weeks. However, upon standing at 25°C, the complex $2 \rightarrow 3$ slowly disappears over the course of days and is quantitatively replaced by another species, showing that $2 \rightarrow 3$ is not a thermodynamic product. This conversion can be monitored both by NMR where all initial signals, including the guest resonance at 15.7 ppm, disappear (Figure 10a), and by CD where a remarkable inversion of sign at 360 nm is observed. This modification reflects an inversion of the handedness¹³ of **2** mediated by the guest which, in the case of **3-(D)**, changes the helicity from *P* to *M*, and from *M* to *P* for **3-(L)** (Figure 10b, c).

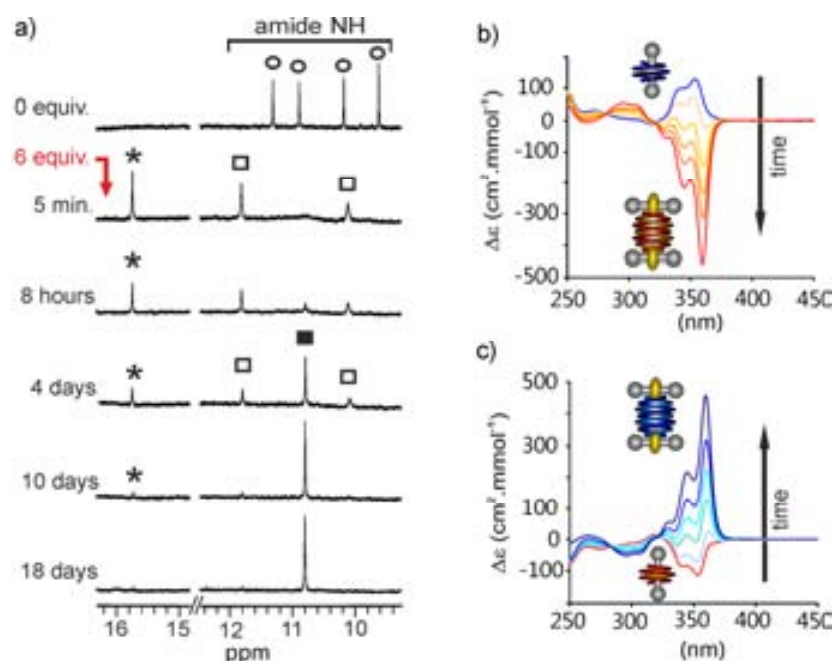


Figure 10. a) Part of the 300 MHz ¹H NMR spectra of **2** (0.1 mM) in CDCl₃ at 298K before the addition of guest (top), and 5 min., 8 hours, 4 days, 10 days and 18 days after the addition of **3** (6 equiv.). Empty black circles correspond to the empty capsule. The star (*) denotes the hydrogen bonded acid protons of the guest in single helix-guest **3**. NH amides of the single helical host-guest complex are marked with empty squares whereas those of the double helical host-guest complex are marked with a black square. b) CD spectra of **2** (0.1 mM) in CDCl₃ at 298K 10 min. after the addition of 6 equiv. of **3-(D)** (blue spectrum) then after 5 hours, 15 hours, 30 hours, 70 hours and 18 days (increasing red intensity). c) CD spectra of **2** (0.1 mM) in CDCl₃ 10 min. after the addition of 6 equiv. of **3-(L)** (red spectrum) then after 5 hours, 15 hours, 30 hours, 70 hours and 18 days (increasing blue intensity).

X-ray quality single crystals were obtained from the slow diffusion of hexane into a chloroform solution of **2** mixed with racemic **3** at thermodynamic equilibrium. The structure in the solid state was solved (Figure 11). It revealed an original architecture, completely different from that of the foldaxane $2 \rightarrow 3$, composed of a 2:2 complex consisting of (**2**)₂ as a double helix with two bound molecules of **3** capping the helix cavity at each extremity. The structure of (**2**)₂ complexed with **3** much resembles its structure without bound **3**. As a slight difference, the duplex diameter is

slightly decreased in the complex with **3**, as reflected by a helix span longer by about half a pyridine ring (Figure 12). In the crystal structure, **3**-(*L*) is bound to *P*-(**2**)₂ and **3**-(*D*) is bound to *M*-(**2**)₂, consistent with the inversion of preferred handedness observed over time when titrating **2** with either **3**-(*L*) or **3**-(*D*) (Figure 10). Each tartaric acid derivative adopts a typical conformation with *trans* acid groups and *gauche* hydroxy groups. Carboxylic acid groups are oriented perpendicular to the edge of the helical strand and doubly hydrogen bonded to the distal pyridines ($d_{\text{OH}\cdots\text{N}} = 2.63 \text{ \AA}$, $d_{\text{NH}\cdots\text{OC}} = 2.99 \text{ \AA}$) giving a total of eight intermolecular hydrogen bonds. Interactions between **3** and (**2**)₂ differ from those between **3** and single helical **2** in that hydrogen bonds occur with naphthyridine units of **2** and pyridine units of (**2**)₂. Also, van der Waals contacts between the 3,5-di-*tert*-butyl-phenyl rings of **3** and **2** appear to be more extensive in the crystal structure of (**2**)₂⊃(**3**)₂ than in the calculated structure of **2**⊃**3**. However, it is unclear why these differences result in a much higher stability of (**2**)₂⊃(**3**)₂.

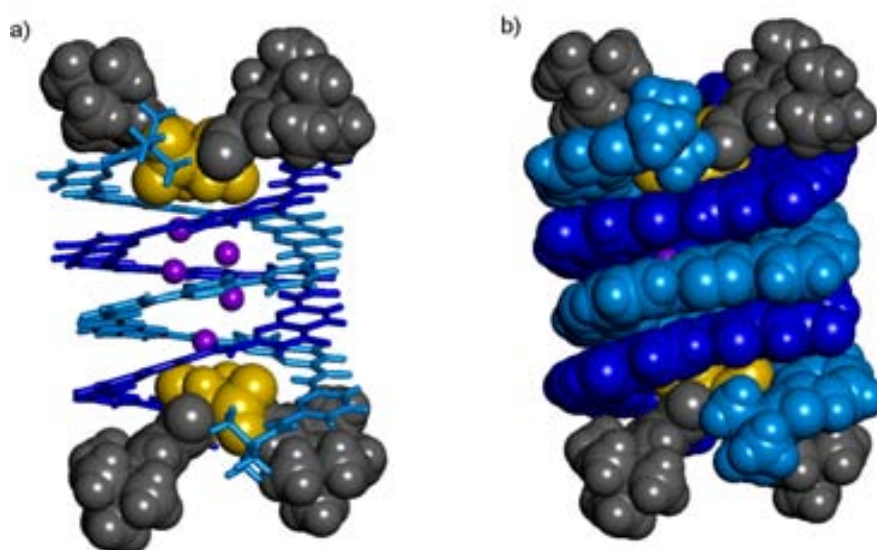


Figure 11. a) CPK (guest) and tube (host), and b) CPK (host and guest) representations of the solid-state structures of *P*-(**2**)₂⊃(**3**-(*L*))₂. Isobutoxy side chains and solvent molecules have been omitted for clarity, except the water cluster included in the cavity of the double helix (purple balls).

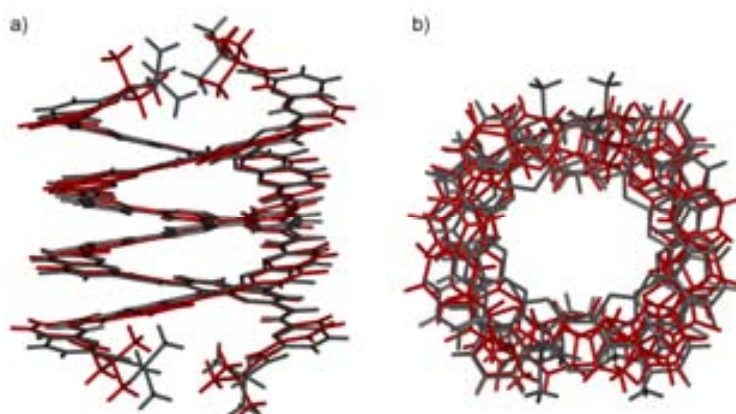


Figure 12. a) Side view; b) Top view of the overlay of the solid state structures in tube representation of the double helix (2)₂ (red) and the double helical complex (2)₂⊃(3)₂ (grey). Guest molecules 3, isobutyl side chains and included solvent molecules have been removed for clarity.

Consistent with the solid state structure, evidence was found of the double helical nature of the host in solution. In particular, ¹H signals of **2** in (2)₂⊃(3)₂ are strongly upfield shifted from those of **2** in 2⊃3 due to enhanced ring current effects in the double helical dimer.²¹⁻²³ A ¹H DOSY experiment confirmed the larger size of the species whose signals are assigned to (2)₂⊃(3)₂ than 2⊃3 (Figure 13).

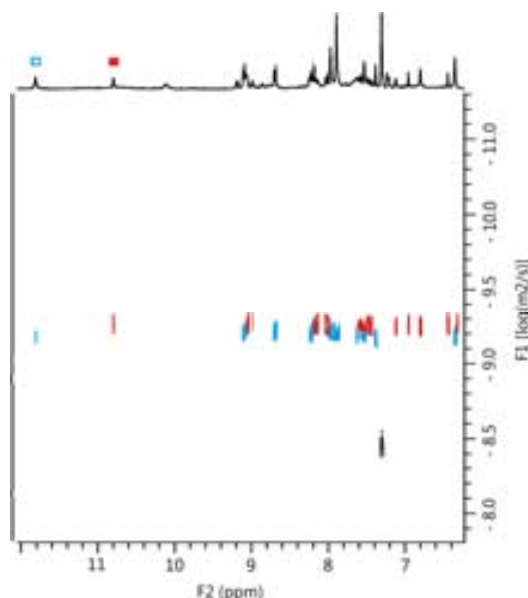


Figure 13. Part of ¹H DOSY (diffusion ordered spectroscopy) NMR spectrum (400 MHz) of a mixture of 2⊃3-(L) (blue empty square) and (2)₂⊃(3-(L))₂ (red square) at 2 mM in CDCl₃ (293K) showing the NH amide and CH aromatic region of both single and double helix of **2**. The diffusion coefficients were calculated to be 7.21x10⁻¹⁰ and 5.26x10⁻¹⁰ m²s⁻¹, for 2⊃3-(L) and (2)₂⊃(3-(L))₂, respectively.

Adding racemic **3** to a racemic (*P/M*) solution of (**2**)₂ (at 30 mM the double helix prevails) readily caused shifts of both aromatic and amide signals reflecting that *P/M*-(**2**)₂ and its complexes with **3**-(*L*) and **3**-(*D*) exchange fast on the NMR timescale (Figure 14). The association constant between (**2**)₂ and **3** was too high to be accurately calculated from a curve fitting of the titration data (Figure 15). Indeed, this binding is expected to be significantly higher than the binding of **3** to single helical **2** (i.e., higher than $2.7 \times 10^4 \text{ L mol}^{-1}$) as the apparent dimerization of **2** into (**2**)₂ is strongly enhanced in the presence of **3** (Figure 10). Also, this titration experiment did not allow to characterize any cooperativity between the binding of the first and second guests.

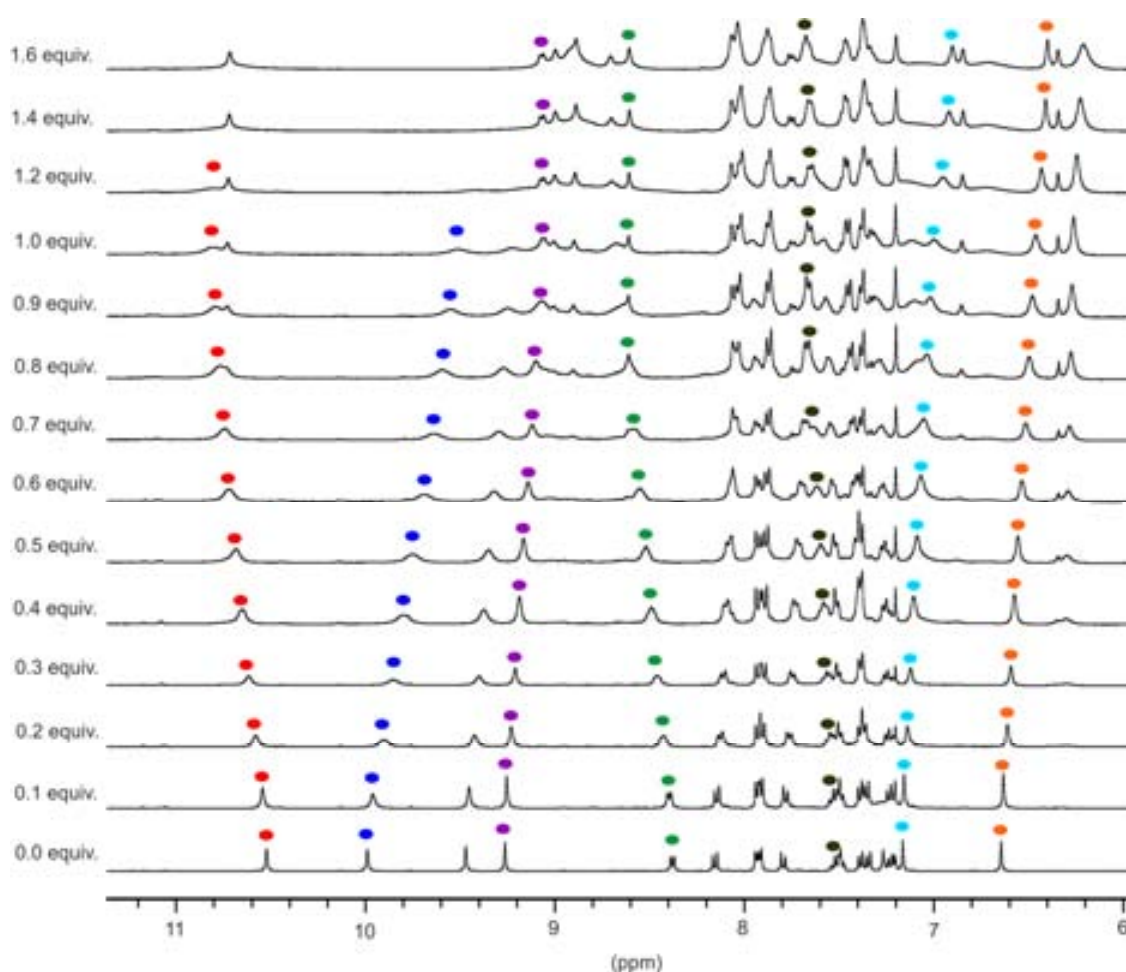


Figure 14. Part of the 400 MHz NMR spectra recorded for the binding study of (**2**)₂ vs. guest **3** (racemic) in CDCl₃ at 293K. [**2**]_{initial} = 30 mM, [**3**]_{titrant} = 90 mM. A 3 mm NMR tube was used for this titration. The number of guest equivalent on the left are compared to the double helix of **2**. Measurements have been performed 5 minutes after each addition of guest.

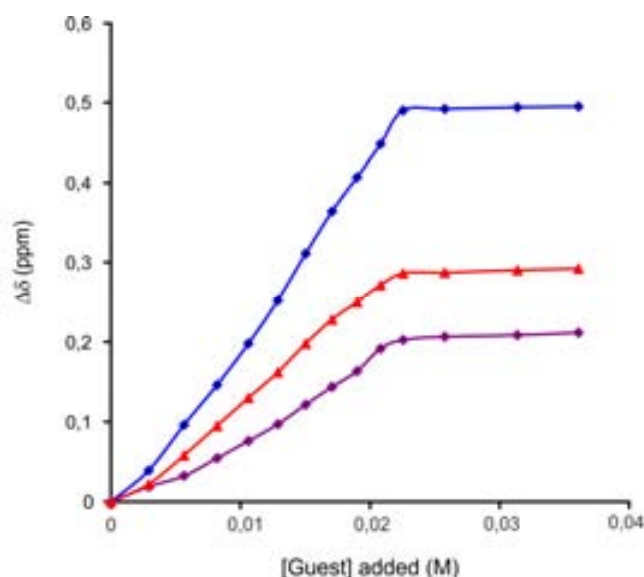


Figure 15. Experimental values for the NMR binding study of double helix $(\mathbf{2})_2$ vs. guest $\mathbf{3}$ (racemic) in CDCl_3 at 293K, analyzing three different signals starting at $\delta = 10.52$, 10.0 and 9.26 ppm. $[\mathbf{2}]_{\text{initial}} = 30$ mM, $[\mathbf{3}]_{\text{titrant}} = 90$ mM. Saturation of the host is observed at two equivalent (referring to the double helical host) indicating a very high binding constant. A host concentration (DH) of 15 mM was chosen in order to favor the double helix, however at this high concentration it is not possible to give a precise quantification of the strength of the complexation.

In another titration, a single enantiomer of $\mathbf{3}$ was added to a racemic (*P/M*) solution of $(\mathbf{2})_2$ (Figure 16). This resulted in the induction of CD bands and in the splitting of ^1H NMR signals into two sets, one having chemical shift values identical to those observed in the titration with racemic $\mathbf{3}$ and one having chemical shift values almost identical to those of free $(\mathbf{2})_2$. This reflects that the pure enantiomer of $\mathbf{3}$ forms a stable complex with the $(\mathbf{2})_2$ duplex that has a matching stereochemistry, and a weak or no complex at all with the $(\mathbf{2})_2$ duplex that has a mismatching stereochemistry, suggesting that the interaction between $(\mathbf{2})_2$ and $\mathbf{3}$ is also strongly diastereoselective. Since the equilibrium between *P*- $(\mathbf{2})_2$ and *M*- $(\mathbf{2})_2$ is slow on the NMR timescale, $\mathbf{3}$ acts as a sort of chiral shift reagent that resolves them into distinct signals before their interconversion occurs.

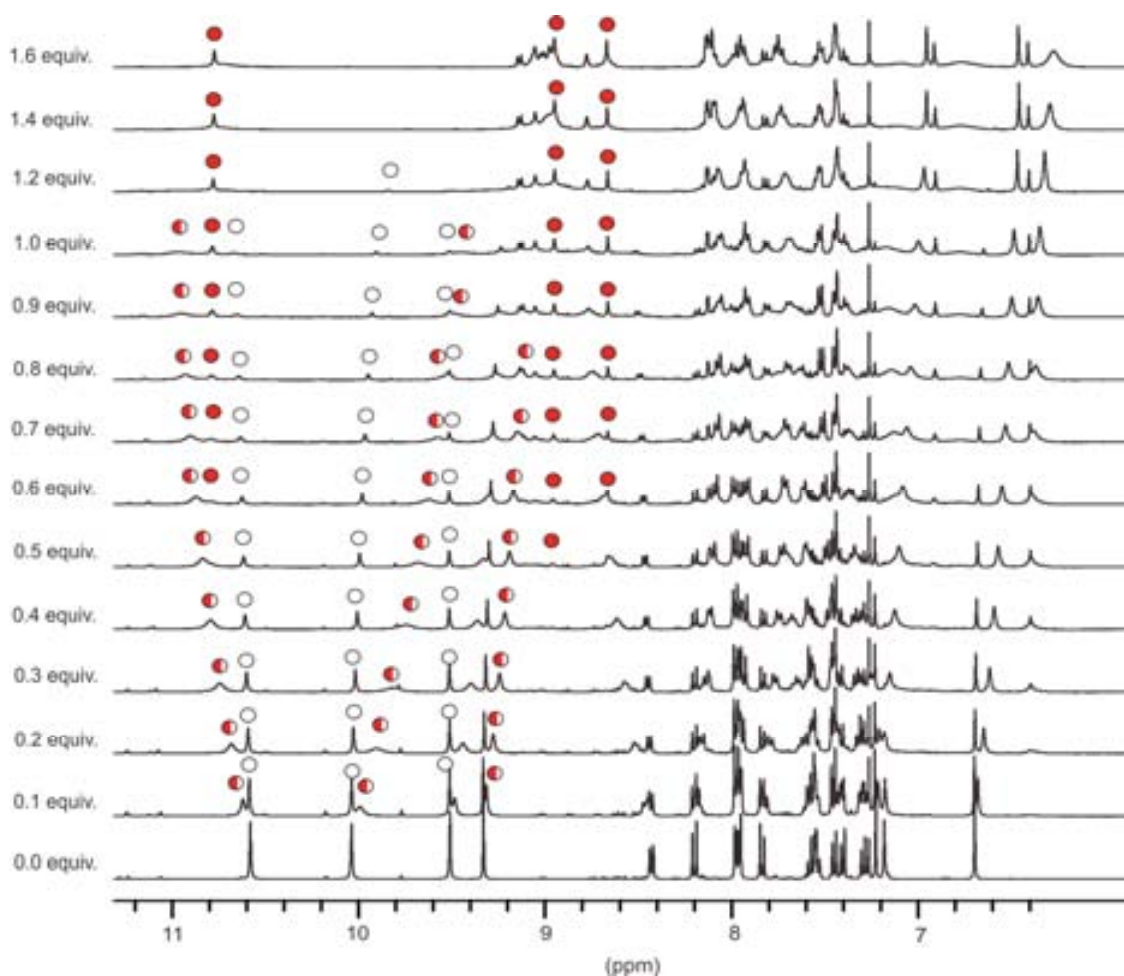


Figure 16. Part of the 400 MHz NMR spectra recorded for the binding study of (2)₂ vs. guest 3-(L) in CDCl₃ at 293K. [2]_{initial} = 30 mM, [3]_{titrant} = 90 mM. A 3 mm NMR tube was used for this titration. Empty circles denote the free double helix (2)₂ or weakly hydrogen bonded mismatching complex M-(2)₂⊃3-(L). Half-filled red circles denote 2:1 matching complex P-(2)₂⊃3-(L). Red circles denote the 2:2 matching complex P-(2)₂⊃(3-(L))₂. The number of guest equivalent on the left are compared to the double helix of 2. Measurements have been performed 5 minutes after each addition of guest.

Interestingly, the induced CD spectrum of 2 resulting from a handedness bias by 3 was found to be about five time more intense in (2)₂⊃(3)₂ than in 2⊃3 (Figure 10b, c) despite the fact that handedness induction is (close to) quantitative in both cases. Δε values appear to be higher for double helical (2)₂ than for single helical 2 whose helix pitch is half as small.

4. Conclusion

In summary, guest **3** enhances the thermodynamic stability of double helical duplex (**2**)₂ but it simultaneously reduces the kinetics of formation of (**2**)₂ upon forming a foldaxane with monomeric **2** which can be long-lived at low temperature. While each individual equilibrium appears to be relatively fast when assessed in the mM range, the formation of **2**⊃**3** at 0.1 mM results in a very low concentration of remaining free single helix **2** which slows down the formation of (**2**)₂. Similarly, the formation of (**2**)₂⊃(**3**)₂ is slower when the concentrations of both (**2**)₂ and free **3** are low. The sequence of steps to convert **2**⊃**3** into (**2**)₂⊃(**3**)₂ is shown in Figure 17: (i) dissociation into **2** and **3**; (ii) helix handedness inversion of **2**;²⁶ (iii) association of **2** into (**2**)₂; (iv) binding of **3** to (**2**)₂. The timescales involved in the equilibria at each step, allow to isolate both kinetic and thermodynamic supramolecular products and to monitor the inversion of chiroptical properties with time as the system first evolves towards a product with one handedness and then reverts into another product having an opposite handedness.

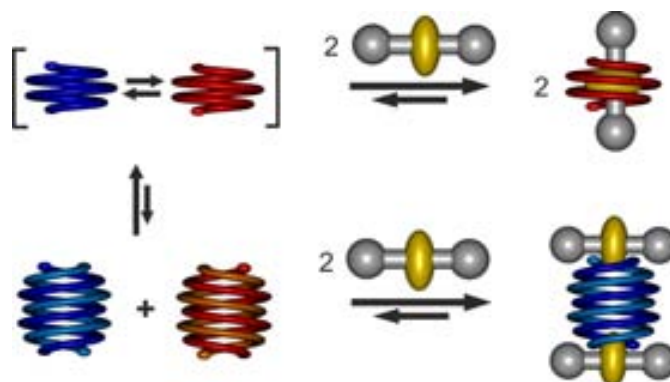


Figure 17. (Left) Equilibrium between oligomer **2** as *P* (blue) and *M* (red) single helices and *P* and *M* double helices; (Top) Equilibrium between oligomer **2** as *P* and *M* single helices and *M*-**2**⊃**3**-(*L*); (Bottom) Equilibrium between oligomer **2** as *P* and *M* double helices and a 2:2 complex between *P*-(**2**)₂ as a double helix and two **3**-(*L*) molecules. Note that the *P* and *M* single helices are at equilibrium whereas the *P* and *M* double helices are not unless they first dissociate into single helices.

These results represent a striking illustration of the multiple processes that compete and take place at different time scales in supramolecular reaction sequences. The combined features of supramolecular systems – constitution, dynamics, and information – are leading toward a supramolecular science of complex, informed, evolutive matter, as mentioned by Lehn.⁶ A next step could be coupled systems with multiple chiral and achiral distinct stations, transferring the

chiral information from a passage to others. The incorporation of time irreversibility implies the passages may change their information from one to another.

5. Experimental part

5.1 Methods for NMR

NMR spectra were recorded on 3 different NMR spectrometers: (1) an Avance II NMR spectrometer (Bruker Biospin) with a vertical 7,05T narrow-bore/ultrashield magnet operating at 300 MHz for ^1H observation and 75 MHz for ^{13}C observation by means of a 5-mm direct BBO H/X probe with Z gradient capabilities; (2) an Avance 400 NMR spectrometer (Bruker Biospin) with a vertical 9.4T narrow-bore/ultrashield magnet operating at 400 MHz for ^1H observation by means of a 5-mm direct QNP $^1\text{H}/^{13}\text{C}/^{31}\text{P}/^{19}\text{F}$ probe with gradient capabilities; (3) an Avance III NMR spectrometer (Bruker Biospin) with a vertical 16.45T narrow-bore/ultrashield magnet operating at 700 MHz for ^1H observation by means of a 5-mm TXI $^1\text{H}/^{13}\text{C}/^{15}\text{N}$ probe with Z gradient capabilities. Chemical shifts are reported in parts per million (ppm, δ) relative to the ^1H residual signal of the deuterated solvent used. ^1H NMR splitting patterns with observed first-order coupling are designated as singlet (s), doublet (d), triplet (t), or quartet (q). Coupling constants (J) are reported in hertz. Data processing was performed with Topspin 2.0 software. Samples were not degassed. CDCl_3 from Eurisotop was used after filtration through an alumina pad followed by a distillation over calcium hydride.

DOSY. Diffusion Ordered spectroscopy (DOSY) experiments were recorded at 400 MHz and were used to study diffusion coefficients of the single and double helices with the following parameters: longitudinal eddy current delay (LED) using sine-shaped gradient of 2 ms (δ), Δ of 100 ms, a relaxation delay of 2 s and 32 scans for each gradient intensity (2 to 95%, 10A gradient unit).

EXSY. Exchange spectroscopy (EXSY) experiments and were recorded at 400 MHz with use of a standard phase-sensitive NOESY pulse program (noesyph) with the following parameters: the acquisition was performed with 2048(t_2) x 512(t_1) data points, in States-TPPI mode with Z gradients selection, relaxation delay of 2 s, and 80 scans per increment; sweep width of 14000 Hz in both dimensions at 318K. Processing was done after a Sine Square multiplication in F1, Gaussian multiplication in F2 and Fourier transformation in 1K x 1K real points. Magnetization exchange rates were obtained from cross and diagonal peak integration using Topspin 2.0 at different mixing times. EXSYCalc software was used to extract the magnetization exchange rate constants k_{ass}^* and k_{diss}^* from the integrations of single and double helix exchange diagonal- and

cross-peaks.

5.2 Methods for Circular Dichroism

Circular dichroism studies were carried out in distilled chloroform using 2 or 10 mm pathlength cell on a JASCO J-815 Circular Dichroism spectrometer.

5.3 Methods for X-ray crystallography

Needle shaped crystals of the double helix **(2)**₂ were obtained from slow diffusion of n-hexane into chloroform. The data were collected at a synchrotron beamline (PROXIMA1 SOLEIL). The data were integrated and scaled using the XDS package.²⁷ Plate shaped crystals of the complex **(2)**₂⊃**(3)**₂ grew from slow diffusion of n-hexane into chloroform. Data were collected on a home source Bruker X8 proteum rotating anode at the CuK α wavelength. SAINT²⁸ was used for integrating and scaling the diffraction intensities. Both structures were solved using the charge flipping algorithm implemented in Superflip²⁹ and were refined using SHELXL.³⁰ The positions of the H atoms were deduced from coordinates of the non-H atoms. The non-H atoms were refined with anisotropic temperature parameters. H atoms were included for structure factor calculations but not refined.

The crystals of the complex **(2)**₂⊃**(3)**₂ are composed of more than 10% of disordered solvent molecules. In order to get convergence of the refinement process, the structure factors were squeezed using the procedure implemented in PLATON.³¹

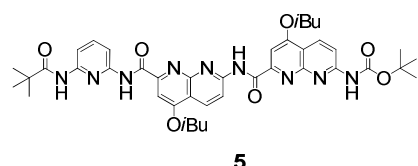
5.4 Summary of X-Ray crystallographic data

Name	Double helix (2) ₂	complex (2) ₂ ⊃3 ₂
Formula	C ₁₇₉ H ₁₇₉ Cl ₉ N ₄₄ O ₂₈	C ₁₂₆ H ₁₃₄ Cl ₁₂ N ₂₂ O ₂₅
M	3713.72	2781.96
Crystal system	Monoclinic	Monoclinic
Space group	P2(1)/n	P2(1)/c
<i>a</i> /Å	23.453(5)	23.097(4)
<i>b</i> /Å	37.806(8)	31.196(5)
<i>c</i> /Å	25.788(5)	40.446(6)
α/o	90.00	90.00
β/o	115.10(3)	100.388(7)
γ/o	90.00	90.00
U/Å ³	20707(7)	28666(8)
T /K	100	180
Z	4	8
ρ/g cm ⁻¹	1.220	1.289
size (mm)	0.1 x 0.05 x 0.05	0.1 x 0.1 x 0.01
λ Å	0.82650	1.54178
μ/mm ⁻¹	0.287	2.727
Absorption correction	20647	29514
unique data	100361	165090
parameters/restraints	2342/23	3312/10
R1, wR2	0.1554, 0.3787	0.1429, 0.3437
goodness of fit	1.455	1.807

5.5 Methods for chemical synthesis

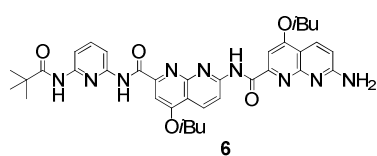
All reactions were carried out under a dry nitrogen atmosphere. Commercial reagents were purchased from Sigma-Aldrich or TCI and were used without further purification unless otherwise specified. Dichloromethane (DCM) was dried over alumina column; chloroform (CHCl₃) and triethylamine (Et₃N) were distilled from calcium hydride (CaH₂) prior to use. Reactions were monitored by thin layer chromatography (TLC) on Merck silica gel 60-F254 plates and observed under UV light. Column chromatographies were carried out on Merck GEDURAN Si60 (40-63 μm). Melting points were measured on a Büchi B-540. ESI mass spectra were obtained on a Waters LCT from the IMAGIF CNRS Laboratory at the Gif/Yvette, France.

5.5.1 Synthesis of helix 2



Piv-PN₂-Boc 5. To a solution of the amine NH₂-PN₂-Boc¹⁷ **4**ⁱ (1.2 g, 1.7 mmol) and Et₃N (2.4 mL, 17 mmol) in dry CH₂Cl₂ (20 mL) was added pivaloyl chloride (0.4 mL, 3.4 mmol) dropwise via a syringe at 0 °C.

Then the reaction mixture was allowed to proceed at room temperature for 12 h. The solution was evaporated, and the residue was purified by flash chromatography (SiO₂) eluting with EtOAc/CH₂Cl₂ (5:95 to 30:70) to obtain product **5** as white solid (1.12 g, 83% yield). ¹H NMR (CDCl₃, 300 MHz): δ 11.27 (s, 1H), 10.61 (s, 1H), 8.12 (d, *J*(H, H) = 9.0, 1H), 8.74 (d, *J*(H, H) = 9.0, 1H), 8.60 (d, *J*(H, H) = 9.3, 1H), 8.39 (d, *J*(H, H) = 9.3, 1H), 8.12 (d, *J*(H, H) = 8.1, 1H), 8.03 (d, *J*(H, H) = 8.1, 1H), 7.96 (br, 1H), 7.89 (br, 1H), 7.82 (t, *J*(H, H) = 8.1, 1H), 7.80 (s, 1H), 7.75 (s, 1H), 4.15-4.11 (m, 4H), 2.36-2.27 (m, 2H), 1.38 (s, 9H), 1.28 (s, 9H), 1.17 (d, *J*(H, H) = 6.9, 6H), 1.16 (d, *J*(H, H) = 6.9, 6H). ¹³C NMR (CDCl₃, 75 MHz): δ 183.6, 177.2, 164.2, 164.1, 163.6, 162.5, 155.5, 154.9, 154.6, 154.4, 153.7, 152.8, 152.3, 150.2, 149.3, 140.8, 134.5, 134.2, 115.2, 115.1, 114.3, 114.1, 109.7, 109.6, 99.0, 98.7, 82.2, 75.9, 39.9, 38.7, 28.4, 28.2, 27.7, 27.4, 19.3. HRMS (TOF-ES⁺): *m/z* calcd for C₄₁H₄₈N₉O₇ [M-H]⁺ 778.3677; found 778.3664.

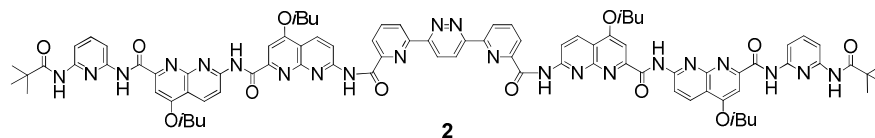


Piv-PN₂-NH₂ 6. Piv-PN₂-Boc **5** (0.47 g, 0.6 mmol) was dissolved in CH₂Cl₂ (5 mL), and excess trifluoroacetic acid (TFA) (2 mL) was added dropwise. Then the reaction mixture was allowed to proceed at room temperature for 6 h. The solution was evaporated, and the residue was dissolved in CH₂Cl₂

(20 mL), washed with saturated NaHCO₃, dried over Na₂SO₄, filtered and then concentrated to give amine of Piv-PN₂ **6** (0.39 g, 95% yield) as a white solid which was used without further purification. ¹H NMR (CDCl₃, 300 MHz): δ 11.34 (s, 1H), 10.66 (s, 1H), 8.79 (d, *J*(H, H) = 9.0, 1H), 8.72 (d, *J*(H, H) = 9.0, 1H), 8.34 (d, *J*(H, H) = 8.7,

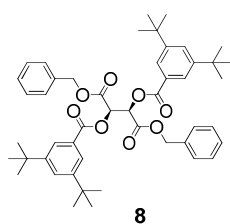
ⁱ Thank Chandranouli Nagula (postdoctor) for synthesizing the compound NH₂-PN₂-Boc **4**.

1H), 8.12 (d, $J(\text{H}, \text{H}) = 7.8$, 1H), 8.01 (d, $J(\text{H}, \text{H}) = 8.1$, 1H), 7.94 (br, 1H), 7.81-7.76 (m, 2H), 7.63 (s, 1H), 6.86 (d, $J(\text{H}, \text{H}) = 8.7$, 1H), 5.28 (br, 2H) 4.14 (d, $J(\text{H}, \text{H}) = 6.6$, 2H), 4.08 (d, $J(\text{H}, \text{H}) = 6.6$, 2H), 2.36-2.22 (m, 2H), 1.36 (s, 9H), 1.17 (d, $J(\text{H}, \text{H}) = 6.6$, 6H), 1.13 (d, $J(\text{H}, \text{H}) = 6.6$, 6H). ^{13}C NMR (CDCl_3 , 75 MHz): δ 177.2, 164.1, 164.0, 163.8, 162.5, 160.7, 156.2, 154.9, 154.4, 153.6, 151.8, 150.2, 149.3, 140.7, 134.4, 133.0, 115.1, 115.0, 113.2, 111.4, 109.7, 109.5, 98.9, 97.7, 75.9, 75.5, 39.9, 28.7, 28.3, 27.6, 19.3. HRMS (TOF-ES⁺): m/z calcd for $\text{C}_{36}\text{H}_{42}\text{N}_9\text{O}_5$ $[\text{M}+\text{H}]^+$ 680.3309; found 680.3298.



Piv-PN₂PyzPyrN₂P-Piv 2. To a solution of diacid of pyr-pyz-pyr **7**ⁱⁱ (93 mg, 0.29 mmol) and Piv-PN₂ **6** (0.39g, 0.57mmol) in CHCl_3 (20 mL) was added Et_3N (0.2 mL, 1.4 mmol) and PyBOP (0.75g, 1.4 mmol). Then the reaction mixture was heated at 45 °C for 12 h. The solution was evaporated, and the residue was purified by flash chromatography (SiO_2) eluting with EtOAc/cyclohexane (10:90 to 30:70) to obtain product **2** as white solid (0.42 g, 88% yield). ^1H NMR (CDCl_3 , 16 mM, 300 MHz): δ 10.57 (s, 2H), 10.07 (s, 2H), 9.55 (s, 2H), 9.32 (s, 2H), 8.45 (d, $J(\text{H}, \text{H}) = 7.2$, 2H), 8.25 (d, $J(\text{H}, \text{H}) = 9.0$, 2H), 8.02 (d, $J(\text{H}, \text{H}) = 9.0$, 4H), 7.89 (d, $J(\text{H}, \text{H}) = 9.0$, 2H), 7.61-7.53 (m, 4H), 7.48 (br, 2H), 7.45-7.38 (m, 4H), 7.29-7.24 (m, 2H), 7.22 (s, 2H), 6.72 (s, 2H), 3.86-3.69 (m, 8H), 2.32-2.19 (m, 4H), 1.29-1.26 (m, 12H), 1.18-1.13 (m, 12H), 0.69 (s, 18H). ^{13}C NMR (CDCl_3 , 16 mM, 75 MHz): δ 177.1, 162.9, 162.7, 162.1, 161.2, 160.9, 156.2, 153.8, 153.6, 153.3, 153.2, 152.6, 151.8, 151.5, 149.7, 148.2, 146.9, 139.4, 137.0, 134.6, 133.3, 127.7, 124.1, 121.7, 115.0, 114.7, 113.7, 113.5, 109.1, 108.4, 98.5, 97.9, 75.5, 75.3, 39.4, 28.4, 28.3, 26.9, 19.6, 19.5, 19.5, 19.4. HRMS (TOF-ES⁺): m/z calcd for $\text{C}_{88}\text{H}_{89}\text{N}_{22}\text{O}_{12}$ $[\text{M}+\text{H}]^+$ 1645.7030; found 1645.7010.

5.5.2 Synthesis of guests

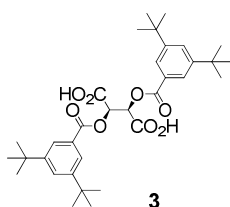


(*R,R*)-Dibenzyl tartrate di-3,5-di-*tert*-butylbenzoate 8. 3,5-Di-*tert*-butylbenzoic acid (0.7 g, 3 mmol) was dissolved in dry CH_2Cl_2 (10 mL). Oxalyl chloride (1.3 mL, 15 mmol) was added, and the reaction was allowed to stir at room temperature for 3 h. The solvent and excess reagents were removed under vacuum and the residue was dried under vacuum for at least 2 h to yield 3,5-di-*tert*-butylbenzoyl chloride as a white solid.

To a solution of (*R,R*)-dibenzyl tartrate (0.49 g, 1.5 mmol), Et_3N (2.5 mL, 18 mmol) and 4-dimethylamino-pyridine (DMAP) (7.3 mg, 0.06 mmol) in dry CH_2Cl_2 (10 mL) was added dropwise a solution of freshly prepared 3,5-di-*tert*-butylbenzoyl chloride in dry CH_2Cl_2 (5 mL) at 0 °C. Then the reaction mixture was allowed to proceed at room temperature for 24 h. The solution was evaporated, and the residue was purified by flash chromatography (SiO_2) eluting with DCM/cyclohexane/ether (5:90:5 to 25:70:5) to obtain product **8** as white solid (0.88 g, 78% yield). ^1H NMR (CDCl_3 , 300 MHz): δ 7.93 (d, $J(\text{H}, \text{H}) = 1.8$, 4H), 7.68 (t, $J(\text{H}, \text{H}) = 1.8$, 2H), 7.28-7.09 (m, 10H), 6.08 (s, 2H), 5.27 (d, $J(\text{H}, \text{H}) = 12$, 2H), 5.15 (d, $J(\text{H}, \text{H}) = 12$, 2H), 1.35 (s, 36H). ^{13}C NMR

ii Thank Didier Dubreuil group (Université de Nantes) for providing the compound pry-prz-pry **7**.

(CDCl₃, 75 MHz): δ 165.9, 165.9, 151.3, 134.9, 128.6, 128.4, 128.2, 128.0, 124.5, 71.6, 67.8, 35.0, 31.5. HRMS (TOF-ES⁺): m/z calcd for C₄₈H₅₈O₈Na [M+Na]⁺ 785.4029; found 785.4050. mp 140.6-141.3 °C.



(*R,R*)-Tartaric acid di-3,5-di-*tert*-butylbenzoate (3-*L*). A suspension of (*R,R*)-dibenzyl tartrate di-3,5-di-*tert*-butylbenzoate **8** (0.4 g, 0.52 mmol) and 10% Pd/C (40 mg) in ethyl acetate (20 mL) was vigorously stirred under hydrogen atmosphere at room temperature for 12 h. The mixture was filtered through a pad of Celite with ethyl acetate and concentrated under vacuum to give product **3** (0.3 g, quant.). ¹H NMR (CDCl₃, 300 MHz): δ 9.14 (br, 2H), 7.90 (d, J (H, H) = 1.8, 4H), 7.61 (t, J (H, H) = 1.8, 2H), 5.95 (s, 2H), 1.25 (s, 36H). ¹³C NMR (CDCl₃, 75 MHz): δ 171.5, 166.1, 151.3, 128.2, 127.9, 124.5, 71.4, 35.0, 31.4. HRMS (TOF-ES⁻): m/z calcd for C₃₄H₄₅O₈ [M-H]⁻ 581.3114 found 581.3117. mp 152.0-153.1 °C.

(*S,S*)-Tartaric acid di-3,5-di-*tert*-butylbenzoate (3-*D*) was synthesised using a similar procedure than for (**3-*L***) : see above.

6. References

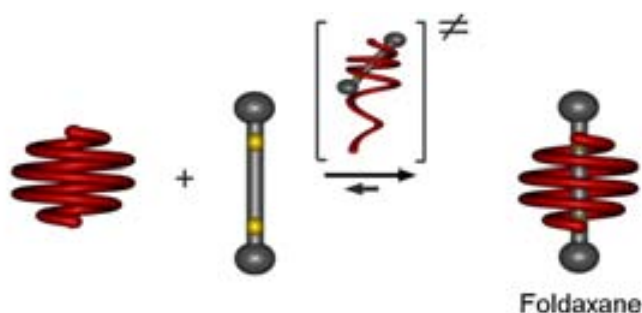
- 1 G. M. Whitesides, M. Boncheva, Beyond molecules: self-assembly of mesoscopic and macroscopic components. *Proc. Natl. Acad. Sci. USA*, **2002**, *99*, 4769–4774.
- 2 V. Percec, et al. Self-organization of supramolecular helical dendrimers into complex electronic materials. *Nature*, **2002**, *417*, 384–387.
- 3 P. Y. W. Dankers, M. C. Harmsen, L. A. Brouwer, M. J. A. Van Luyn, E. W. Meijer, A modular and supramolecular approach to bioactive scaffolds for tissue engineering. *Nature Mater.*, **2005**, *4*, 568–574 (2005).
- 4 C. Mao, W. Sun, N. C. Seeman, Assembly of borromean rings from DNA. *Nature*, **1997**, *386*, 137–138.
- 5 G. M. Whitesides, B. Grzybowski. Self-assembly at all scales. *Science*, **2002**, *295*, 2418–2421.
- 6 J.-M. Lehn, Toward self-organization and complex matter. *Science*, **2002**, *295*, 2400–2403.
- 7 S. Sato, Y. Ishido, M. Fujita, Remarkable stabilization of $M_{12}L_{24}$ spherical frameworks through the cooperation of 48 Pd(II)-pyridine interactions. *J. Am. Chem. Soc.*, **2009**, *131*, 6064–6065.
- 8 J. P. Mathias, E. E. Simanek, C. T. Seto, G. M. Whitesides, Molecular self-assembly through hydrogen bonding: aggregation of five molecules to form a discrete supramolecular structure. *Angew. Chem. Int. Ed.*, **1993**, *32*, 1766–1769.
- 9 V. Paraschiv, V. Crego-Calama, T. Ishi-I, C. J. Padberg, P. Timmerman, D. N. Reinhoudt, Molecular “chaperones” guide the spontaneous formation of a 15-component hydrogen-bonded assembly. *J. Am. Chem. Soc.*, **2002**, *124*, 7638–7639.
- 10 P. A. Korevaar, S. J. George, A. J. Markvoort, M. M. J. Smulders, P. A. J., Hilbers, A. P. H. J. Schenning, T. F. A. De Greef, E. W. Meijer, *Nature*, **2012**, *481*, 492–496.
- 11 B. Hasenknopf, J.-M. Lehn, N. Boumediene, E. Leize, A. Van Dorsselaer, Kinetic and thermodynamic control in self-assembly: sequential formation of linear and circular helicates. *Angew. Chem. Int. Ed.*, **1998**, *37*, 3265–3268.
- 12 M. D. Levin, P. J. Stang, Insights into the mechanism of coordination-directed self-assembly. *J. Am. Chem. Soc.*, **2000**, *122*, 7428–7429.
- 13 V. M. Cangelosi, T. G. Carter, L. N. Zakharov, D.W. Johnson, Observation of reaction intermediates and kinetic mistakes in a remarkably slow self-assembly reaction. *Chem. Commun.*, **2009**, 5606–5608.
- 14 K. Kinbara, T. Aida, Toward intelligent molecular machines: directed motions of biological and artificial molecules and assemblies. *Chem. Rev.*, 2005, *105*, 1377–1400.
- 15 E. R. Kay, D. A. Leigh, F. Zerbetto, Synthetic molecular motors and mechanical machines. *Angew. Chem. Int. Ed.*, **2007**, *46*, 72–191.
- 16 N. Takeda, K. Umamoto, K. Yamaguchi, M. Fujita, A nanometre-sized hexahedral coordination capsule assembled from 24 components. *Nature*, **1999**, *398*, 794–796.
- 17 Y. Ferrand, A. M. Kendhale, B. Kauffmann, A. Grélard, C. Marie, V. Blot, M. Pipelier, D. Dubreuil, I. Huc, Diastereoselective encapsulation of tartaric acid by a helical aromatic oligoamide. *J. Am. Chem. Soc.*, **2010**, *132*, 7858–7859.
- 18 Y. Ferrand, N. Chandramouli, A. M. Kendhale, C. Aube, B. Kauffmann, A. Grélard, M. Laguerre, D. Dubreuil, I. Huc, Long-range effects on the capture and release of a chiral guest by a helical molecular capsule. *J. Am. Chem. Soc.*, **2012**, *134*, 11282–11288.
- 19 Q. Gan, Y. Ferrand, C. Bao, B. Kauffmann, A. Grélard, H. Jiang, I. Huc, Helix-rod host-guest complexes with shuttling rates much faster than disassembly. *Science*, **2011**, *331*, 1172–1175.
- 20 Y. Ferrand, Q. Gan, B. Kauffmann, H. Jiang, I. Huc, Template-induced screw motions within an aromatic amide foldamer double helix. *Angew. Chem. Int. Ed.*, **2011**, *50*, 7572–7575.

- 21 V. Berl, R. G. Khoury, I. Huc, M. J. Krische, J.-M. Lehn, Interconversion of single and double helices formed from synthetic molecular strands. *Nature*, **2000**, *407*, 720–723.
- 22 Q. Gan, C. Bao, B. Kauffmann, A. Grélard, J. Xiang, S. Liu, I. Huc, H. Jiang, Quadruple and double helices of 8-fluoroquinoline oligoamides. *Angew. Chem. Int. Ed.*, **2008**, *47*, 1715–1718.
- 23 B. Baptiste, J. Zhu, D. Haldar, B. Kauffmann, J.-M. Léger, I. Huc, Hybridization of long pyridine-dicarboxamide oligomers into multi-turn double helices: slow strand association and dissociation, solvent dependence, and solid state structures. *Chem. Asian J.*, **2010**, *5*, 1364–1375.
- 24 H. Jiang, J.-M. Léger, I. Huc, Aromatic δ -peptides. *J. Am. Chem. Soc.*, **2003**, *125*, 3448–3449.
- 25 E. Berni, J. Garric, C. Lamit, B. Kauffmann, J.-M. Léger, I. Huc, Interpenetrating single helical capsules. *Chem. Comm.*, **2008**, 1968–1970.
- 26 N. Delsuc, T. Kawanami, J. Lefeuvre, A. Shundo, H. Ihara, M. Takafuji, Ivan Huc, Kinetics of helix handedness inversion: folding and unfolding in aromatic amide oligomers. *ChemPhysChem*, **2008**, *9*, 1882–1890.
- 27 W. J. Kabsch, Automatic processing of rotation diffraction data from crystals of initially unknown symmetry and cell constants. *J. Appl. Crystallogr.*, **1993**, *26*, 795–800
- 28 SAINT Software Reference Manual, Version 4, Bruker AXS, Madison (USA), 1994-1996.
- 29 L. Palatinus, G. Chapuis, SUPERFLIP—a computer program for the solution of crystal structures by charge flipping in arbitrary dimensions. *Appl. Crystallogr.*, **2007**, *40*, 786–790.
- 30 G. M. Sheldrick, A short history of SHELX. *Acta Cryst.*, **2008**, *A64*, 112–122.
- 31 P. van der Sluis, A. L. Spek, BYPASS: an effective method for the refinement of crystal structures containing disordered solvent regions. *Acta Cryst.*, **1990**, *A46*, 194–201.

CONCLUSION AND PERSPECTIVES

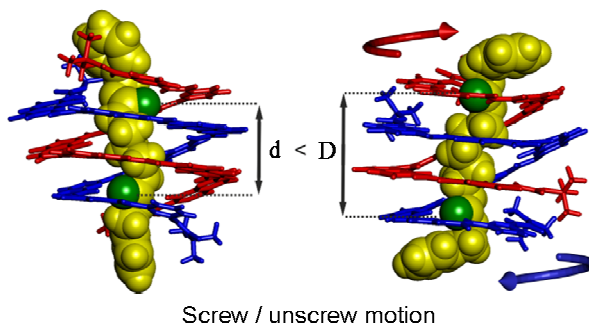
Design of molecules with self-assembled functions is a challenging research in the field of supramolecular chemistry, chemical biology and materials science. Among these studies, one particularly interesting topic is to design artificial foldamers that can self-assemble into a helical structure, for the purpose of not only mimicking the structure and function of living matter, such as DNA and proteins, to facilitate one to understand the nature of life, of but also creating new artificial structures and functions.

A new series of single helical pseudorotaxanes, termed as foldaxanes, have been designed and synthesized. In this system, helical molecular tapes can slowly wind around rod-like guests to form host-guest complexes. The winding process only requires unfolding and refolding of helices, and no longer needs them irreversibly fixed with guests. At the same time, the length of helices and anchor points on the rods must be strictly matched in the complexes. While the single helical foldaxanes form, the helices can shuttle along the guests without dissociating, because the timescale of helical unwinding is relatively slow. Furthermore, the regulation of sliding motion is achieved according to protonation and deprotonation of the rods.

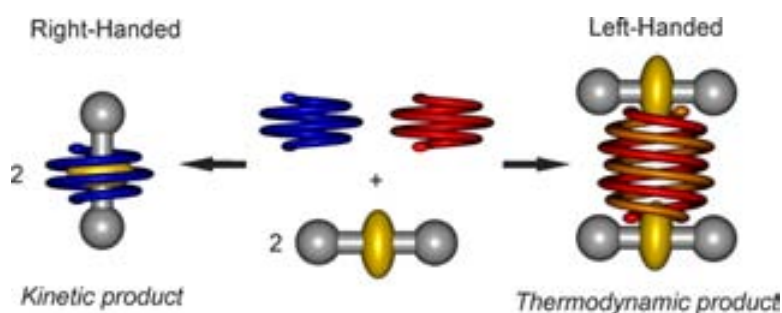


An anti-parallel double helical aromatic oligoamide foldamer is shown to bind to a series of rod-like guests of various lengths upon winding of the duplex around the guests. X-ray structures of the host-guest complexes show that the two strands of the duplex undergo a relative screw motion to adjust the distance between hydrogen bond donors located at the end of one of their extremities so that they bind to hydrogen bond acceptors of the guest. When the duplex binds to a long guest possessing two binding stations of different lengths, it is shown to shuttle between the

two stations without dissociating, implying a simultaneous screw motion to adjust to the length of the binding station where it resides.



An aromatic oligoamide sequence has been designed and synthesized to fold in a single helix having a large cavity and to behave as a host for a dumbbell-shaped guest derived from tartaric acid. NMR, molecular modeling and circular dichroism evidence demonstrated the rapid formation of this 1:1 host-guest complex and the induction of the helix handedness of the host by the guest. This complex was found to be a long-lived kinetic supramolecular by-product as it slowly transformed into a 2:2 host-guest complex in which two guest molecules are bound at the extremities of a double helix formed by the host, as shown by NMR, CD and by a solid state structure. The guest also induces the handedness of the double helical host, but with an opposite bias. The chiroptical properties of the system are thus found to revert with time as the 1:1 complex forms first, followed by the 2:2 complex.



All our efforts in the previous studies demonstrated that aromatic oligoamide foldamers could be good candidates for the elaboration of molecular machines and further steps of research should still be passed.

- In the studies presented herein, the control of chirality was transiently achieved upon trapping one enantiomer of tartaric acid. One can imagine a similar chirality transfer not from the cavity but from the terminus of the rod to form a stable chiral foldaxane.
- A step further into complexity would consist in decorating a long rod with several single, double or triple helices loaded on pre-designed stations. It would require that all the helices could strictly match their corresponding stations and simultaneously present high diastereoselectivities at their points of contact.
- Foldaxanes assembly proceeds through hydrogen bonding and fine kinetic control. A crucial question is: can we use other non-covalent interactions? In fact, hydrophobic effect could be particularly efficient as a driving force for the foldaxane formation. Water soluble helix with an apolar hollow (Q^f) would accommodate an alkyl chain in the cavity.
- A last aspect that could be envisaged is the control of the screw sense by polarized light. All of these new lines of development would push foldaxanes to be truly molecular machinery.